ABSORBED DOSE CALCULATION OF NUCLETRON HDR IRIDIUM-192 BRACHYTHERAPY SOURCE USING MONTE CARLO METHOD

VIYADA SANOESAN

**A THESIS SUBMITTED IN PARTIAL FULFILLMENT
OF THE REQUIREMENTS FOR
THE DEGREE OF MASTER OF SCIENCE
(RADIOLOGICAL TECHNOLOGY)
FACULTY OF GRADUATE STUDIES
MAHIDOL UNIVERSITY
2014**

Thesis
entitled

ABSORBED DOSE CALCULATION OF NUCLETRON HDR IRIDIUM-192 BRACHYTHERAPY SOURCE USING MONTE CARLO METHOD

.....
Miss Viyada Sanoesan
Candidate

.....
Assoc. Prof. Chiraporn Tocharoenchai,
Ph.D. (Biomedical Engineering)
Major advisor

.....
Asst. Prof. Yudthaphon Vichianin,
Ph.D. (Information Science)
Co-advisor

.....
Lect. Nuanpen Damrongkijudom,
Ph.D. (Medical Radiation Physics)
Co-advisor

.....
Prof. Banchong Mahaisavariya,
M.D., Dip Thai Board of Orthopedics
Dean
Faculty of Graduate Studies
Mahidol University

.....
Asst. Prof. Yudthaphon Vichianin,
Ph.D. (Information Science)
Program Director
Master of Science Program in
Radiological Technology
Faculty of Medical Technology
Mahidol University

Thesis
entitled

ABSORBED DOSE CALCULATION OF NUCLETRON HDR IRIDIUM-192 BRACHYTHERAPY SOURCE USING MONTE CARLO METHOD

was submitted to the Faculty of Graduate Studies, Mahidol University
for the degree of Master of Science (Radiological Technology)
on
March 26, 2014

.....
Miss Viyada Sanoesan
Candidate

.....
Lect. Puangpen Tangboonduangjit
Ph.D. (Medical Radiation Physics)
Chair

.....
Assoc. Prof. Chiraporn Tocharoenchai,
Ph.D. (Biomedical Engineering)
Member

.....
Asst. Prof. Yudthaphon Vichainin,
Ph.D. (Information Science)
Member

.....
Lect. Nuanpen Damrongkijudom
Ph.D. (Medical Radiation Physics)
Member

.....
Lect. Lakkana Apipanyasopon,
Ph.D. (Nuclear Engineering)
Member

.....
Prof. Banchong Mahaisavariya,
M.D., Dip Thai Board of Orthopedics
Dean
Faculty of Graduate Studies
Mahidol University

.....
Prof. Virapong Prachayasittikul,
Ph.D. (Microbiology)
Dean
Faculty of Medical Technology
Mahidol University

ACKNOWLEDGEMENTS

The success of this thesis can be attributed to assistance from my major advisor, Assoc. Prof. Chiraporn Tocharoenchai, Department of Radiological Technology, Faculty of Medical Technology, Mahidol University. She gave me all valuable advices and guidance in this thesis. She helped me to keep on track and beside me whenever I had a problem. During the entire course of study, she gave me the encouragement, care and understanding. Especially, she gave me any good chance for my life. I also thank my co-advisor, Asst. Prof. Yudthaphon Vichainin, for his training of the use Linux operating system. He helped me to install program for running Monte Carlo simulation in this study and I also thank my co-advisor, Lect. Nuanpen Damrongkijudom, for giving me suggestion and the good idea in this study.

I also express my deep appreciation to Asst. Prof. Chumpot Kakanaporn, Department of Radiology, Siriraj Hospital, for her kindness and allowance in the beginning time for my practice in Department of Radiology.

I would like to thank Lect. Lakkana Apipanyasophon, Radiation Oncology Unit, Chulabhorn Hospital, for her kind teaching me the first time using film measurements in brachytherapy, her advice and encouragement.

I also thank Asst. Prof. Chirapha Tannanonta, Radiation Oncology Unit, Chulabhorn Hospital for her suggestion in the use of Gafchromic EBT2 film.

I would like to deeply thank my sincere gratitude to Lect. Puangpen Tangboonduangjit, Program Director of Master of Science program in Medical Physics for her advice and comments in the research proposal and her suggestion for improvement of TLD and Gafchromic EBT2 film measurements in this study.

I am grateful to Ms Siwaporn Sakulsingharoj and Ms Supaporn Srisuwan, Department of Radiology, Ramathibodi Hospital, for their help in TLD and Gafchromic EBT2 film measurements in this study.

My special thanks also go to Siriraj and Ramathibodi Hospital for allowing me to use their machines and their instruments in this study. I would like to express my gratitude to all staffs for their help.

I would to thank my family and my friends for their endless love unconditional support and cheerfulness.

Finally, this thesis is partially supported by Graduate studies of Mahidol University Alumni Association.

Viyada Sanoesan

ABSORBED DOSE CALCULATION OF NUCLETRON HDR IRIDIUM-192 BRACHYTHERAPY SOURCE USING MONTE CARLO METHOD

VIYADA SANOESAN 5336729 MTRT/M

M.Sc. (RADIOLOGICAL TECHNOLOGY)

THESIS ADVISORY COMMITTEE: CHIRAPORN TOCHAROENCHAI, Ph.D., YUDTHAPHON VICHIANIN, Ph.D., NUANPEN DAMRONGKIJUDOM, Ph.D.

ABSTRACT

This research aimed to study the absorbed dose calculation of Nucletron HDR ^{192}Ir brachytherapy source using EGSnrc/DOSRZnrc version 4.r2.3.3.2 (Monte Carlo code). The ^{192}Ir source with the specification and geometry provided by the manufacturer was modeled at the center of the cylindrical water phantom with 40 cm in diameter and height in an effort to obtain full scatter condition recommended by AAPM TG-43. The validation of DOSRZnrc was performed using Oncentra Brachy TPS version 4.1. The absorbed doses were calculated at radial distances from 0.1 cm to 15 cm. The absorbed dose measurements, using LiF TLD-100 rods and Gafchromic EBT2-films, were performed in a 30 x 30 x 30 cm^3 cubic water phantom with similar conditions to the simulation. Each measurement was repeated three times, and the average doses were calculated. The relative doses of absorbed doses from simulation and measurements were then calculated by normalizing the dose at 1 cm from the source center and compared. The results showed that there were a good agreement (<5%) between TPS and DOSRZnrc except at radial distances near the source and the phantom boundaries due to the limitation of TPS. The differences of relative dose between DOSRZnrc and TLD were about 10% at radial distances from 0.5 cm to 15 cm, and 87.88% at 0.3 cm. The differences of relative dose between DOSRZnrc and EBT2-film were about 10% at radial distances from 0.3 cm to 5 cm, and more than 100% beyond 5 cm. This study found that the differences of relative dose between DOSRZnrc and TLD near the source were caused by the high dose gradients and the finite size of LiF TLD-100 rods. While the differences of relative dose between DOSRZnrc and EBT2-film were very high, beyond 5 cm due to the characteristics of EBT2-film to low dose. In summary, the EGSnrc/DOSRZnrc MC code can calculate the absorbed dose in brachytherapy for all radial distances, especially, at radial distances close to the source. The dosimetric parameter based on TG-43, radial dose function, was calculated by DOSRZnrc, and the results were good agreements (±3%) with previous studies. The absorbed doses using LiF TLD-100 rods were acceptable for radial distances from 0.5 cm to 15 cm. While those measured by EBT2-film were acceptable from 0.3 cm to 5 cm. The experimental measurement should be handled with meticulous cares, and requires repetition of the process to reduce measurement errors.

KEY WORDS: EGSnrc/DOSRZnrc/ MONTE CARLO SIMULATION/ NUCLETRON HDR IRIDIUM-192 BRACHYTHERAPY SOURCE/ ABSORBED DOSE CALCULATION

125 pages

การคำนวณปริมาณรังสีของแหล่งกำเนิดรังสีเออริเดียม-192 Nucletron HDR ด้วยวิธีมอนติคาร์โล

ABSORBED DOSE CALCULATION OF NUCLETRON HDR IRIDIUM-192 BRACHYTHERAPY SOURCE USING MONTE CARLO METHOD

วิยะดา เสนาะสันต์ 5336729 MTRT/M

วท.ม.(รังสีเทคนิค)

คณะกรรมการที่ปรึกษาวิทยานิพนธ์ : จิราภรณ์ โตเจริญชัย, Ph.D. ยุทธพล วิเชียรอินทร์, Ph.D. นวลเพ็ญ ดำรงกิจอุดม, Ph.D.

บทคัดย่อ

งานวิจัยนี้มีวัตถุประสงค์เพื่อศึกษาการคำนวณปริมาณรังสีของแหล่งกำเนิดรังสีเออริเดียม-192 Nucletron HDR ด้วยรหัสมอนติคาร์โล EGSnrc/DOSRZnrc รุ่น 4.r2.3.3.2 แหล่งกำเนิดรังสีเออริเดียม-192 ที่มีคุณลักษณะและรูปร่างตรงกับบริษัทผู้ผลิต ได้ถูกสร้างขึ้นที่กึ่งกลางหุ่นจำลองน้ำรูปทรงกระบอกที่มีเส้นผ่านศูนย์กลางและความสูง 40 เซนติเมตร เพื่อให้เกิดรังสีกระเจิงตามที่แนะนำโดย AAPM TG-43 การตรวจสอบความถูกต้องของ DOSRZnrc ทำโดยใช้โปรแกรม Oncentra Brachy TPS รุ่น 4.1 ปริมาณรังสีถูกคำนวณในแนวตามขวางที่ระยะห่างตั้งแต่ 0.1 – 15 เซนติเมตร การวัดปริมาณรังสีด้วย LiF TLD-100 และฟิล์ม Gafchromic EBT2 ทำในหุ่นจำลองน้ำที่มีรูปร่างเป็นลูกบาศก์ขนาด 30 x 30 x 30 ลูกบาศก์เซนติเมตร และมีสภาวะเหมือนกับทำในการจำลองด้วย DOSRZnrc การวัดแต่ละแบบจะวัด 3 ครั้ง และคำนวณหาค่าเฉลี่ย ต่อมาปริมาณรังสีสัมพัทธ์ที่ได้จาก DOSRZnrc และการทดลองจะถูกคำนวณโดยการปรับเทียบด้วยค่าปริมาณรังสีที่ระยะ 1 เซนติเมตรห่างจากจุดศูนย์กลางของแหล่งกำเนิด และนำมาเปรียบเทียบกัน ผลการทดลองแสดงว่า ค่าที่ได้จาก โปรแกรม TPS และ DOSRZnrc ไปในทางเดียวกัน (<5%) ยกเว้นที่ระยะใกล้แหล่งกำเนิดรังสีและที่ขอบของหุ่นจำลองเนื่องจากข้อจำกัดของโปรแกรม TPS ค่าแตกต่างของปริมาณรังสีสัมพัทธ์ที่ได้จาก DOSRZnrc และ TLD มีค่าประมาณ 10% ในแนวตามขวางที่ระยะจาก 0.5 – 15 เซนติเมตร และมีค่า 86.88 % ที่ 0.3 เซนติเมตร ค่าแตกต่างของปริมาณรังสีสัมพัทธ์ที่ได้จาก DOSRZnrc และฟิล์ม EBT2 มีค่าประมาณ 10 % ในแนวตามขวางที่ระยะจาก 0.3 – 5 เซนติเมตร และมีค่ามากกว่า 100 % ที่ระยะเลย 5 เซนติเมตร การศึกษาครั้งนี้พบว่า ค่าความแตกต่างของปริมาณรังสีสัมพัทธ์ระหว่าง DOSRZnrc และ TLD บริเวณใกล้แหล่งกำเนิดรังสีจะมีค่าสูงมากเกิดจากการลดลงของปริมาณรังสีอย่างมากมายและขนาดของ TLD ขณะที่ค่าแตกต่างระหว่าง DOSRZnrc และฟิล์ม EBT2 เมื่อเลย 5 เซนติเมตร เนื่องจากเป็นคุณสมบัติของฟิล์มที่มีต่อปริมาณรังสีต่ำ โดยสรุป รหัสมอนติคาร์โล EGSnrc/DOSRZnrc สามารถนำมาใช้คำนวณหาปริมาณรังสีในการรักษาด้วยรังสีรักษาระยะใกล้ได้ทุกระยะ โดยเฉพาะในระยะที่อยู่ใกล้แหล่งกำเนิดรังสีในแนวขวาง ค่าพารามิเตอร์ในการคำนวณปริมาณรังสีตามกำหนดไว้ใน TG-43 คือ radial dose function ถูกคำนวณโดยใช้ DOSRZnrc และผลการทดลองก็ไปในทางเดียวกันกับงานการศึกษาที่มีมาก่อน ปริมาณรังสีที่วัดด้วย TLD ยอมรับได้ที่ระยะจาก 0.5 – 15 เซนติเมตร ในขณะที่การวัดด้วยฟิล์มจะยอมรับได้ในช่วง 0.5 – 5 เซนติเมตร การวัดปริมาณรังสีควรจะทำด้วยความระมัดระวังและต้องทำซ้ำหลายๆครั้งเพื่อลดข้อผิดพลาดจากการวัด

125 หน้า

CONTENTS

		Page
ACKNOWLEDGEMENTS		**iii**
ABSTRACT (ENGLISH)		**iv**
ABSTRACT (THAI)		**v**
LIST OF TABLES		**vii**
LIST OF FIGURES		**xi**
LIST OF ABBREVIATIONS		**xv**
CHAPTER I	**INTRODUCTION**	**1**
CHAPTER II	**OBJECTIVES**	**3**
CHAPTER III	**BACKGROUND**	**4**
CHAPTER IV	**MATERIALS AND METHODS**	**23**
CHAPTER V	**RESULTS**	**58**
CHAPTER VI	**DISCUSSION**	**93**
CHAPTER VII	**CONCLUSION**	**100**
REFERENCES		**102**
APPENDIX		**108**
BIOGRAPHY		**125**

LIST OF TABLES

Table		Page
3.1	Physical characteristics of some radionuclide used in brachytherapy	5
4.1	The characteristic of Nucletron HDR ^{192}Ir source	28
4.2	Description of source number 3: Internal uniform isotropically radiating disk of finite size (Interior isotropic cylindrical source) and parameters	32
4.3	Compositions used in source and phantom modeling from 521icru_nucletron.pegs4 file	34
4.4	Photon spectra from Ir192_bare_1993.spectrum file	35
4.5	The photon and electron transport parameters using in the simulation	38
4.6	The individual element correction coefficient (ECC_{ci}) value for each TLD (Created on March 2013)	44
4.7	The individual element correction coefficient (ECC_{ci}) value for each TLD (Created on July 2013)	45
4.8	The Geometry function, $G_L(r, 90)$, for Nucletron HDR ^{192}Ir source	54
4.9	Fourth-degree polynomial coefficients of correction factors (CF) used to quantitatively compare bounded to unbounded g(r) for common phantom shapes and sizes. CF was fitted as $CF = C_0 + C_1r + C_2r^2 + C_3r^3 + C_4r^4$	55
4.10	Correction factors (CF) used to transform g(r) for cubic phantom into approximate g(r) values for unbounded conditions.	56
4.11	Correction factors (CF) used to transform g(r) for cylindrical phantom into approximate g(r) values for unbounded conditions	57
5.1	The relative absorbed doses at radial distances from 0.1 cm to 15 cm away from the source center calculated by Oncentra TPS and DOSRZnrc	59
5.2	The percentage differences of relative absorbed dose at radial distances from 0.2 cm to 5 cm away from longitudinal axis of the source obtained from DOSRZnrc and Oncentra TPS	66

LIST OF TABLES (cont.)

Table		Page
5.3	The absorbed doses (Gy per incident particle) at radial distances from 0.1 cm to 15 cm along the transverse axis of the source calculated by DOSRZnrc	74
5.4	The relative absorbed doses obtained from DOSRZnrc and LiF TLD-100 rods at radial distances from 0.3 cm to 15 cm along the transverse axis of the source	77
5.5	The relative absorbed dose obtained from DOSRZnrc and EBT2 film with dose of 400 cGy and 800 cGy at radial distances from 0.3 cm to 15 cm along the transverse axis of the source	79
5.6	The relative absorbed dose obtained from DOSRZnrc and EBT2 film with dose of 800 cGy at radial distances 0.3 cm to 15 cm along the transverse axis of the source	81
5.7	The radial dose functions, g(r), at radial distances from 0.3 cm to 15 cm obtained from DOSRZnrc and LiF TLD-100	84
5.8	The radial dose functions, g(r), at radial distances from 0.3 cm to 5 cm obtained from DOSRZnrc and EBT2 film with doses of 800 cGy	87
5.9	The radial dose functions, g(r), at radial distances from 0.3 cm to 5 cm obtained from DOSRZnrc and EBT2 film with doses of 800 cGy	88
5.10	The g(r) values for Nucletron HDR ^{192}Ir source obtained from DOSRZnrc, AAPM/ESTRO (2012), CLRP TG-43 database and the study of Devan et al. (2007)	92
A.1	The values of individual TL reading (Q_i) from three measurements	109
A.2	The pixel value (PV) from EBT2 film measurements with exposed dose 400 cGy	110
A.3	The pixel value (PV) from EBT2 film measurements with exposed dose 800 cGy	112

LIST OF TABLES (cont.)

Table		Page
A.4	The predicted dose from EBT2 film measurements using Equation 14 with exposed dose 400 cGy.	114
A.5	The predicted dose from EBT2 film measurements using Equation 14 with exposed dose 800 cGy.	116
A.6	The absorbed dose calculated from TLD reading using the two different equations from this study and the study of Uniyal et al. (2012)	118
A.7	The relative absorbed dose calculated from TLD reading using the two different equations from this study and the study of Uniyal et al. (2012)	119
A.8	The radial dose function under unbounded condition calculated from EBT2 film in this study compared with the study of Sellakuma et al. (2009)	120
A.9	The radial dose function under unbounded condition calculated from DOSRZnrc in this study compared with the study of Sellakuma et al. (2009)	121
A.10	The radial dose function under unbounded condition calculated from EBT2 film in our study compared with the study of Uniyal et al. (2012)	122
A.11	The radial dose function under unbounded condition calculated from DOSRZnrc in our study compared with the study of Uniyal et al. (2012)	122
A.12	The radial dose function under unbounded condition calculated from EBT2 film in our study compared with the study of Uniyal et al. (2012)	123

LIST OF TABLES (cont.)

Table		Page
A.13	The radial dose function under unbounded condition calculated from DOSRZnrc in our study compared with the study of of Uniyal et al. (2012)	123
A.14	The radial dose function under unbounded condition calculated from EBT2 film in our study compared with the study of Uniyal et al. (2012)	124

LIST OF FIGURES

Figure		Page
3.1	Coordinate system used for brachytherapy dosimetry calculations	6
3.2	Schematic representation of the process involved in TL dosimetry	12
3.3	Configuration of Gafchromic EBT2 film	14
3.4	Absorption spectra of the active component in EBT2 film after irradiation, peak absorption at 636 nm with the secondary peak at about 585 nm	16
3.5	Steps of a typical radiation transport process in Monte Carlo simulation. The analogue transport samples every single event clearly. DETERMINE in block diagrams means that the quantities of interest are found by sampling from the relevant probability distribution using one or more random numbers	19
3.6	Flow chart of primary and secondary photons emitted by brachytherapy source in MC simulation	21
4.1	Front page of egs_inprz GUI	24
4.2	Front page of egs_gui GUI	24
4.3	LiF TLD 100 rods	26
4.4	Thermo Scientific Harshaw TLD Model 5500 reader	26
4.5	Annealing Oven (Harshaw)	26
4.6	The geometrical diagram of Nucletron HDR ^{192}Ir source	27
4.7	The Nucletron HDR remote afterloader (microSelectron v3)	28
4.8	The slabs of solid water phantom	29
4.9	The Vidar® Red LED Dosimetry Pro Advantage^{TM} scanner	30
4.10	ImageJ Software	31
4.11	Source position in a center of a cylindrical water phantom	33

LIST OF FIGURES (cont.)

Figure		Page
4.12	Geometry of DOSRZnrc-modeled (a) and the actual (b) Nucletron HDR ^{192}Ir source with RZ grid regions were indicated in (a). Red, yellow and orange colors represented ^{192}Ir active core source, encapsulation and source cable, respectively	33
4.13	DOSRZnrc modeled source with RZ regions. The red, yellow, orange and blue colors represented ^{192}Ir active core source, encapsulation, source cable and water phantom used in simulation, respectively	37
4.14	A virtual cylindrical water phantom created by Oncentra TPS	40
4.15	The linearity of all 46 TLD rods used in this study	43
4.16	A 30×30×30 cm^3 cubic water phantom from slabs of solid water phantom	47
4.17	The EBT2 film predetermined the source position	47
4.18	Top view of LiF TLD-100 and EBT2 film measurements. The center of a 30 cm x 30 cm x 30 cm represented Nucletron HDR ^{192}Ir source inside the flexible implant catheter connected to transfer tube	47
4.19	The dose measurement set up in TLD and EBT2 measurements	48
4.20	A 8"×10" original EBT2 film with a small slit at the top right corner when EBT2 film was viewed in landscape orientation. This small slit indicated that the side of the EBT2 film with the polyester laminate was faced to the observer	49
4.21	A 3 ×4 cm^2 EBT2 film using in the calibrations and measurements with a handle (white paper) and marker at top right corner corresponding to original film	49
4.22	The diagram of EBT2 film calibration using ^{192}Irsource. A film was placed at 1 cm and was separately exposed with dose range from 0 cGy (unexposed) to 1000 cGy	50

LIST OF FIGURES (cont.)

Figure		Page
4.23	An irradiated EBT2 film with holder for scanning	51
4.24	A digital image of EBT2 film after scanning. This TIFF image was the image of EBT2 film exposed with dose of 400 cGy at radial distance 0.3 cm	52
4.25	Calibration curve of Gafchromic EBT2 film using ^{192}Ir source	52
5.1	The relative absorbed dose profile curves at radial distances 0.1 cm to 0.9 cm obtained from DOSRZnrc and Oncentra TPS	61
5.2	The relative absorbed dose profile curves at radial distances from 1 cm to 3 cm obtained from DOSRZnrc and Oncentra TPS	61
5.3	The relative absorbed dose profile curves at radial distances from 3.5 cm to 15 cm obtained from DOSRZnrc and Oncentra TPS	62
5.4	The percentage differences of relative absorbed dose obtained from DOSRZnrc and Oncentra TPS at radial distances of 0.2 cm to 5 cm along the transverse axis of the source	62
5.5	The percentage differences of relative absorbed dose obtained from DOSRZnrc and Oncentra TPS at radial distances of 5 cm to 15 cm along the transverse axis of the source.	63
5.6	The relative absorbed dose profile curves at radial distances 0.2 cm and 0.3 cm obtained from DOSRZnrc and Oncentra TPS	64
5.7	The percentage differences of relative absorbed dose at radial distance 0.2 cm obtained from DOSRZnrc and Oncentra TPS	65
5.8	The percentage differences of relative absorbed dose at radial distance 0.3 cm obtained from DOSRZnrc and Oncentra TPS	65
5.9	The relative absorbed dose profile curves at radial distances 0.5 cm to 0.9 cm obtained from DOSRZnrc and Oncentra TPS	67
5.10	The percentage differences of relative absorbed dose at radial distance 0.5 cm obtained from DOSRZnrc and Oncentra TPS	68

LIST OF FIGURES (cont.)

Figure		Page
5.11	The percentage differences of relative absorbed dose at radial distance 0.7 cm obtained from DOSRZnrc and Oncentra TPS	68
5.12	The percentage differences of relative absorbed dose at radial distance 0.9 cm obtained from DOSRZnrc and Oncentra TPS	69
5.13	The relative absorbed dose profile curves at radial distances 1 cm to 5 cm obtained from DOSRZnrc and Oncentra TPS	70
5.14	The percentage differences of relative absorbed dose at radial distance 1 cm obtained from DOSRZnrc and Oncentra TPS	71
5.15	The percentage differences of relative absorbed dose at radial distance 2 cm obtained from DOSRZnrc and Oncentra TPS	71
5.16	The percentage differences of relative absorbed dose at radial distance 3 cm obtained from DOSRZnrc and Oncentra TPS	72
5.17	The percentage differences of relative absorbed dose at radial distance 4 cm obtained from DOSRZnrc and Oncentra TPS	72
5.18	The percentage differences of relative absorbed dose at radial distance 5 cm obtained from DOSRZnrc and Oncentra TPS	73
5.19	The g(r) values obtained from DOSRZnrc and TLD at radial distances from 0.3 cm to 1 cm	85
5.20	The g(r) values obtained from DOSRZnrc and TLD at radial distances from 1 cm to 15 cm	85
5.21	The g(r) values obtained from DOSRZnrc and EBT2 film with the dose 400 cGy and 800 cGy at radial distances 0.3 cm to 5 cm	89
5.22	The g(r) values for Nucletron HDR ^{192}Ir source obtained from DOSRZnrc compared to other studies	91

LIST OF ABBREVIATIONS

Abbreviation	Term
AE	Upper electron cutoff energy
AP	Upper photon cutoff energy
^{198}Au	Gold-198
CF	Correction factor
cGy	Centigray
^{60}Co	Cobalt-60
CPE	Charge particle equilibrium
^{137}Cs	Cesium-137
d	distance
D	Dose
D_u	Unknown dose
$\dot{D}$	Dose rate
ECC_{ci}	Individual element correction coefficient
ECC_i	Element correction coefficient
ECUT	Electron transport cutoff energy
$F(r, \theta)$	Anisotropy function
g/cm^3	gram per cubic centimeter
g(r)	Radial dose function
$G(r, \theta)$	Geometry function
GUI	Graphic user interface
Gy	Gray
HDR	High dose rate
^{125}I	Iodine-125
^{192}Ir	Iridium-192
keV	kiloelectron volt
K_δ	Air-kerma rate in vacuo

LIST OF ABBREVIATIONS (cont.)

Abbreviation	Term
LDR	Low dose rate
LiF	Lithium fluoride
MC	Monte Carlo
MDR	Medium dose rate
MV	Megavolt
nC	Nanocoulomb
PCUT	Photon transport cutoff energy
^{103}Pd	Palladium-103
PDF	Probability density function
PV	Pixel value
$\overline{Q}$	Average charge for TLD
$\overline{Q}_c$	Average charge for standard TLD
Q_{ci}	Corrected charge integral of standard TLD
Q_i	Charge of individual TLD
r	Radial distance
RCF	Reader calibration factor
RNG	Random number generator
ROI	Region of interest
SD	Standard deviation
S_k	Air-kerma strength
^{226}Ra	Radium-226
^{222}Rn	Radon-222
TG-43	Task Group Number 43
TLD	Thermoluminescence dosimeter
TPS	Treatment planning system
Z	Atomic number
μGy	microgray

CHAPTER I
INTRODUCTION

The clinical brachytherapy is the placement of small encapsulated radioactive sources at the short distances from the tumor volume in order to maximize the dose delivered to the tumor and minimize the dose delivered to the surrounding normal tissues. Nowadays, high dose rate (HDR) brachytherapy sources of various designs are used. The accuracy of absorbed dose calculations around the sources is crucial to dose delivery to patient and is restricted by the accuracy of the dosimetric parameters of the sources (1). In general, two dimensional dose calculation Task Group No.43 (TG-43) formalism recommended by the American Association of Physicists in Medicine (AAPM) is used to calculate the absorbed dose distribution and determine the dosimetric parameters of HDR brachytherapy source in treatment planning system (TPS) (2).

To measure absorbed dose around the source, TLD dosimetry is recommended dosimeter because of its small size, flat energy response and high sensitivity. However, its use is labor intensive, time consuming and associated with their uncertainties (3). Thus, Gafchromic EBT2 radiochromic film has been increasingly used in brachytherapy applications due to its high spatial resolution and lower sensitivity to the high dose gradient area compared to other detectors such as TLD that make it ideal to determine the absorbed dose distribution at distance very close to the source (4). However, these experimental measurements for dose distribution around the source are complicated and difficult to perform due to high dose gradients near the source and the shift of the photon spectrum to lower energies with increasing depths in phantom (5).

To improve the accuracy of absorbed dose calculation, the clinical use of Monte Carlo (MC) method in brachytherapy has been significantly increased as an accepted dose calculation algorithm in the last decade (6, 7, 8). The advantages of MC are not affected by the uncertainties in detector positioning, energy independence, and high dose gradients near the sources. Nowadays, MC method is not only used for dose

calculations around brachytherapy sources but also for benchmarking TPS which is an important component of brachytherapy dose calculations to ensure accurate dose delivery to patients (9).

The study of Georgi M. Daskalov et al. (10) used a Monte Carlo transport (MCPT) code for calculating the dose rate distribution included all dosimetric parameters of new design microSelectron-HDR source at distance of 0.1 cm to 7 cm. This study showed that the algorithm used on the vendor's planning system lead to large calculation error at distance less than 5 mm compared to MC calculation. And the study of A. Angelopoulos et al. (11) also used MCPT code to derive accurate calculations of all necessary dosimetric parameters for the new Varian ^{192}Ir source. This study mentioned that there were significant differences of dose rate distribution included some dosimetric parameters for the sources such as anisotropy function due to the differences of geometric characteristics of the sources.

The study of Alireza Naseri and Asghar Mesbahi (9) used MCNP4C MC code to validate the accuracy of treatment planning system (TPS) before clinical use in brachytherpy. They modeled three sources of a new HDR ^{60}Co brachytherapy unit and compared the radial dose functions and the isodoses of three sources calculated from MC calculations with a dedicated TPS. And they mentioned that there was a good agreement (< 2%) between TPS and MC calculated dose distributions. Except at the point near the sources (< 1cm) and beyond the tip of sources because the algorithm used in the TPS cannot consider the photon attenuation. Furthermore, MC method was used to characterize shielding effects and relevant factors to clinical brachytherapy dose calculation (12, 13).

According to several studies, MC method already plays an important role in several aspects of brachytherapy dose calculation. Due to these applications in brachytherapy and more MC codes are now available for researchers, this research aimed to study absorbed dose calculation of the Nucletron HDR ^{192}Ir brachytherapy source using DOSRZnrc MC code and compare the results with TLD and EBT2 film measurements. Furthermore, the values of radial dose function, which was AAPM TG-43 dosimetric parameter accounted for dose fall-off on transverse-plane due to photon scattering and attenuation, obtained from MC calculation, TLD and EBT2 film measurements were studied and compared.

CHAPTER II
OBJECTIVE

The objective of this study is to study the absorbed dose calculation of the Nucletron HDR ^{192}Ir brachytherapy source using the Monte Carlo method.

CHAPTER III
BACKGROUND

3.1 Brachytherapy

Brachytherapy is one type of radiotherapy modality which has been applied for over a century using a small encapsulated radioactive source to deliver radiation by placing the source directly into or near the tumor. Compared to external beam radiotherapy, the main advantage of brachytherapy is a locally delivered dose, sharp dose fall-off the target and the sparing of surrounding normal tissue (14).

3.1.1 Brachytherapy source

The use of radionuclide in brachytherapy started after the discovery of radium (^{226}Ra) by Madame Curie in 1898. Traditionally, it was used as the first radionuclide with the advantages of its very long half life and its daughter element radon (^{222}Rn) which was later used. Subsequently, both radium and radon have been replaced in the early 1950s because there was the production of alpha-emitting gaseous daughter product from radium and the alternative artificially radionuclide became available from producing of nuclear reactors during the Second World War (15). Nowadays, there are various types of radionuclide that have been used for brachytherapy as shown in Table 3.1.

According to the definition of dose rate from ICRU Report 38 (16), brachytherapy sources can be classified with respect to the dose rate in three categories: high dose rate (HDR) sources (>12 Gy/h) such as ^{60}Co and ^{192}Ir, medium dose rate (MDR) source (2-12 Gy/h) such as ^{198}Au and low dose rate (LDR) sources (0.4-2 Gy/h) such as ^{125}I, ^{137}Cs and ^{103}Pd. Currently, ^{192}Ir HDR brachytherapy source is the most commonly used in clinical brachytherapy. The photon-emitting brachytherapy sources are available in various forms such as needles, seeds, wire, pellets that are generally used as sealed sources. They usually are encapsulated for

containing the radionuclide, providing source rigidity and as well absorbing any alpha and beta radiation produced through the radioactive decay (17).

Table 3.1 Physical characteristics of some radionuclide used in brachytherapy (15).

Radionuclide	Symbol	Half-life	Average photon energy (MeV)
Cesium	^{137}Cs	30 years	0.662
Cobalt	^{60}Co	5.26 years	1.250
Iridium	^{192}Ir	73.83 days	0.380
Iodine	^{125}I	59.7 days	0.028
Palladium	^{103}Pd	17 days	0.021
Gold	^{198}Au	2.7 days	0.412

3.1.2 Brachytherapy dosimetry

The dosimetry of brachyherapy in this study refers to the methodology of calculating absorbed dose at the point of interest from a brachytherapy source in a given medium that usually is significant on evaluations of dose distributions and shielding considerations for brachytherapy sources (18). The accuracy of brachytherapy dose calculations is very important to the quality of treatment planning and to dose delivery to patients undergoing radiotherapy. The clinical HDR brachytherapy sources currently have a cylindrical geometry and are encapsulated in a metal shell of stainless steel, platinum, or titanium. Thus, dose distributions around such a source depend significantly on source and encapsulation geometric characteristics (19).

In general, brachytherapy dosimetry can be performed by experimental dosimetry method or fundamental theoretical method. In experimental dosimetry method, thermoluminescent dosimeter (TLD), diode and radiochromic film (RCF) have commonly been used (8). As the dose measurements around brachytherapy source are very complicated due to high dose gradients near the sources, low dose rate further away from sources and the shift of the photon spectrum to lower energies with increasing depths in phantom, MC method has become a powerful tool as a theoretical

method for dose calculation around brachytherapy sources, validation of treatment planning system (TPS) and calculation of datasets used as input in the new TPS algorithms. However, all other theoretical methods must be validated against measurements as recommendation of AAPM Task Group No. 43 reports (2, 20).

3.2 The TG-43 Formalism (2, 20)

The AAPM Task Group No. 43 formalism is a current standard of brachytherapy dose calculations which was published in 1995 by the Radiation Therapy Committee of the American Association of Physicists in Medicine (AAPM). The TG-43 formalism relied on superposition of a single brachytherapy source dose distributions obtained in a homogeneous liquid water phantom with a fixed volume for radiation scattering. In principle, the TG-43 formalism established for two-dimensional dose distribution around cylindrically symmetric sources and the dose distribution of such sources were described in term of a polar coordinate system along the long axis (z-axis) of source with its origin located at source center. From the origin to the point of interest, P(r, θ), dose distribution were obtained with radial distance r and polar angle θ with respect to the long axis of the source as shown in Figure 3.1. The reference point, P(r_0, θ_0) of dose calculation lay on the transverse bisector of the source at a distance of 1 cm and polar angle of 90 degree.

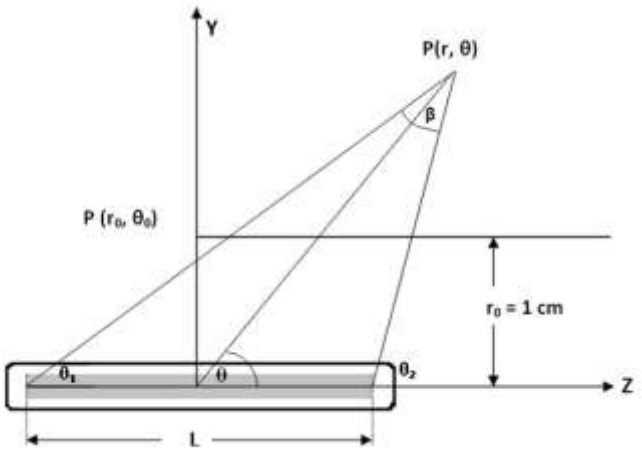

Figure 3.1 Coordinate system used for brachytherapy dosimetry calculations

The TG-43 formalism was clearly defined and expressed in mathematical formulas and incorporated quantities for calculating dose rate to water at the point of interest, P(r, θ) in water medium. This formalism introduced air-kerma strength, dose rate constant, geometry function, radial dose function and anisotropy function that depended on the specific source design. In addition, these parameters used to calculate absorbed dose distributions around sources. Two-dimensional dose rate at the point of P(r, θ) can be written as Equation 1.

$$\dot{D}(r,\theta) = S_k \Lambda \frac{G(r,\theta)}{G(r_0,\theta_0)} g(r) F(r,\theta) \quad (1)$$

Where S_k = Air-kerma strength
Λ = Dose rate constant
$G(r, \theta)$ = Geometry function
$g(r)$ = Radial dose function
$F(r, \theta)$ = Anisotropy function

3.2.1 Air-kerma strength

Air-kerma strength, S_k, was used to describe the strength of brachytherapy sources. It was defined as the product of air kerma rate, $K_\delta(d)$, in free space at a measurement distance d along the transverse axis of the source and a square of this distance d, d^2, as Equation 2 and $K_\delta(d)$ is air-kerma rate in vacuo.

$$S_k = K_\delta(d) \cdot d^2 \quad (2)$$

For photon energy greater than a certain cutoff value of δ which typically was 5 keV for low-energy photon emitting brachytherapy source. $K_\delta(d)$ was inferred from air-kerma measurement in a free-air space at distance of 1 m along the transverse axis of the source. It was corrected for attenuation and scattering in air and any other medium interposed between the source and detector. The distance from the source center to the point of $K_\delta(d)$, located on the transverse axis of the source was represented as d. It can be any distance that was large enough to find independent

air-kerma strength of distance. The unit for air-kerma strength was denoted by the symbol U, where 1 U was equal to 1 μGy m^2 h^{-1} and also was equal to 1 cGy cm^2 h^{-1}.

3.2.2 Dose rate constant

The dose rate constant, Λ, was defined as the dose rate at the reference point per unit air-kerma strength in a water phantom as shown in Equation 3. The dose rate constant was the absolute quantity that depended on both the radionuclide and source model and was influenced by source geometry, the spatial distribution of the radioactivity within the source, encapsulation, and self-filtration within the source, scattering in water surrounding the source and the experimental methodology used to determine air-kerma strength.

$$\Lambda = \frac{\dot{D}(r_0,\theta_0)}{S_k} \tag{3}$$

3.2.3 Geometry function

The geometry function, $G_X(r, \theta)$, accounted for the variation of relative dose due to only the spatial distribution of radioactivity within the source and distance between the source and point of interest. Physically, the geometry function provided an effective inverse square law correction and neglected the effects of scattering and attenuation in the source or the surrounding medium. The accuracy in the calculation of the geometry function resulted in the accuracy in the interpolation and extrapolation of the radial dose function and the anisotropy function. The geometry function has been performed by considering point and line models of source. For point source approximation, the activity distribution was considered as a dimensionless point with an isotropic dose distribution around the source, so the geometry function was calculated using Equation 4. For line source approximation, radioactivity was assumed to be uniformly distributed along a one dimensional line segment with active length L (Figure 3.1). The geometry function was calculated using Equation 5, where β was the angle, in radians, subtended by the tips of the line source with respect to the point of interest, P(r, θ), as shown in Equation 6. The symbol of X was equal to r cos θ and y was equal to r sin θ.

3.2.3.1 For point source approximation

$$G_P(r,\theta) = r^{-2} \tag{4}$$

3.2.3.2 For line source approximation

$$G_L(r,\theta) = \begin{cases} \frac{\beta}{L r \sin\theta} & \text{if } \theta = 0 \\ (r^2 - \frac{L^2}{4})^{-1} & \text{if } \theta \neq 0 \end{cases} \tag{5}$$

$$\beta = \theta_2 - \theta_1 = \tan^{-1}\left(\frac{x+\frac{L}{2}}{y}\right) - \tan^{-1}\left(\frac{x-\frac{L}{2}}{y}\right) \tag{6}$$

3.2.4 Radial dose function

The radial dose function, $g_x(r)$, accounted for the dose fall-off on the transverse axis of the source due to photon scattering and attenuation and can also be affected by filtration of photons by the encapsulation and source material. This quantity applied only to transverse axis that meant only for points with the angle of θ_0 which was equal to 90°.The radial dose function can be written in mathematic form as in Equation 7 where the subscribed "x" to the radial dose function and geometry function to indicate a point source "P" and a line source "L".

$$g_x(r) = \frac{\dot{D}(r,\theta_0)}{\dot{D}(r_0,\theta_0)} \frac{G_x(r_0,\theta_0)}{G_x(r,\theta_0)} \tag{7}$$

3.2.5 Anisotropy function

The anisotropy function, $F(r, \theta)$, accounted for the anisotropy of dose distribution around the source by describing the variation in dose as the function of the polar angle relative to the transverse plane. This variation was due to the distribution of radioactivity within the source, self-absorption and oblique filtration of the radiation in the encapsulated material. The anisotropy function was defined as Equation 8.

$$F(r) = \frac{\dot{D}(r,\theta)}{\dot{D}(r,\theta_0)} \frac{G_x(r,\theta_0)}{G_x(r,\theta)} \quad (8)$$

Since all dosimetric parameters used in TG-43 formalism were obtained for a single brachytherapy source located at the center of a fixed volume and homogeneous liquid water phantom. So this formalism had limitation that was not account for the effects of radiation scattering and patient heterogeneity (8).

3.3 Experimental method

According to AAPM TG-43 report, the exact dose delivery to patient by brachytherapy treatment should be obtained dose distribution data such as dose rate constant, geometry function, radial dose function and anisotropy function by either experimental or Monte Carlo methods. Then, these dosimetric parameters were used as input data in HDR brachytherapy TPS. In principle, the dose distributions around brachytherapy source were characterized by high dose gradients near source, low dose rate further away from source. An energy spectrum varied rapidly with depth around source. The accurate dose measurements in the vicinity of brachytherapy source were difficult to perform because of these characteristics. Moreover, there were large uncertainties caused by volume averaging and self-attenuation that influenced by source to detector distance and detector size. For this reason, the suitable detectors were very important in experimental measurements around brachytherapy source. They should have a wide dynamic range, flat energy response, small active volume, high sensitivity and high spatial resolution (21). In brachytherapy, a variety of detectors in general use were thermoluminescence dosimeter (TLD), ionization chamber, semiconductor diode, metal oxide semiconductor field effect transistor (MOSFET), radiochromic film and polymer or Fricke gel dosimetry (22) and the most popular detectors in brachytherapy were TLD and radiochromic film (23).

3.3.1 Thermoluminescence dosimetry (TLD)

In clinical brachytherapy, TLD has been used the most frequently because of a good compromise between flat energy dependence, small size and detector

dynamic range for both high and low energy brachytherapy sources. According to AAPM TG-43 report, Lithium fluoride (LiF) thermoluminescence dosimetry was the recommended method for experimental measurements of dose distribution around brachytherapy sources. They were used to map the dose distribution in the water equivalent medium and they also played a major role in the assessment of various TG-43 dosimetric parameters for a given brachytherapy source.

3.3.1.1 Principles of TLD

Thermoluminescence (TL) dosimetry was based on the ability of the materials (imperfect crystals) to absorb and store energy of ionizing radiation inside their structures. When TL material was irradiated to ionizing radiation, free electron and holes were produced. The excitation by ionizing radiation raised the energy level of electrons from the valence band to the conduction band in TL material. Concurrently, an electron hole was created. Electrons are free to travel through the conduction band in short time until they are trapped in a metastable energy state as shown in Figure 3.2. When TL material was heated, the electrons trapped in the metastable energy states were given sufficient thermal energy to escape from the traps into the valence band again and recombining, then resulting in the emission of visible light that is called thermoluminescence (TL). And these thermoluminescence phenomenon referred to band theory. The importance of thermoluminescence phenomenon for dose measurement is due to the fact that the amount of visible light emitting from TL material was proportional to the absorbed dose previously received from ionizing radiation.

3.3.1.2 Detector (24)

The used TLD were commonly obtained by doping phosphors such as lithium fluoride (LiF) and lithium borate ($Li_2B_4O_7$) with suitable chemical impurities called activators. Due to their tissue equivalences and low rate of fading, the most commonly used TL materials in medical application were LiF:Mg,Ti (lithium fluoride doped with magnesium and titanium), LiF:Mg,Cu,P (lithium fluoride doped with magnesium, copper and titanium), and $Li_2B_4O_7$:Mn (lithium borate doped with manganese). All TL materials were available in various forms, either in form of power or in form of solid dosimeter that maybe made of phosphor as single crystal or polycrystalline extrusions such as rods, chips and ribbons. Moreover, the

characteristics of the pure phosphor dosimeters should be noted that they may be considerably different from those of the composites and depend widely on the percent of activators.

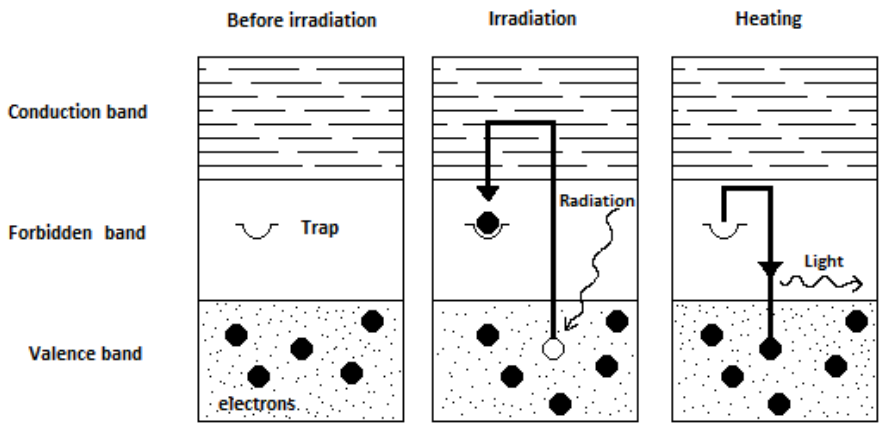

Figure 3.2 Schematic representation of the process involved in TL dosimetry.

3.3.1.3 TLD Reader (24)

The basic TLD reader system consists of a planchet, photomultiplier tube (PMT) and an electrometer. In the principle of TLD reader, the irradiated TLD were placed on a planchet inside a readout chamber and were gradually heated to temperature of the trap and light was emitted. Then an emitted light was detected and converted into an electronic signal linearly proportional to the detected photon fluence by PMT. Finally, an electrometer recorded the signal from PMT as a charge or current correlating to absorbed dose that were either readout or stored by the operator, or automatically saved on a computer. Normally, two different temperatures included preheating temperature for clearing unstable peaks and readout temperature for correcting the information from dosimetric peaks were used in TLD reader. These temperatures must be carefully controlled in stability and reproducibility which were important in the accuracy of dosimetry. In addition, the close contacts between TLD, planchet and heating system were necessary to obtain a good reproducibility. The readout chamber must be continuously flushed with nitrogen gas in order to reduce the signal produced from impurities in the air as well as decrease the background.

In clinical brachytherapy, LiF was commonly used as TL material because of the almost constant response of TL over the large range of photon energies, and its atomic number of approximately 8.3 that was almost equivalent to tissue (atomic number 7.3). Although TLD in clinical brachytherapy offered the best compromise between relatively small size, flat energy response and high sensitivity, it had volume averaging, inter-detector and self attenuation, positioning errors in vicinity of brachytherapy sources and higher total uncertainty in dose determination. Moreover, TLD was labor intensive and time consuming. For this reason, radiochromic film had been introduced in experimental brachytherapy dosimetry method (8).

3.3.2 Radiochromic film dosimetry

Film dosimetry has been developed into a powerful high resolution tool in radiotherapy. Since radiochromic films had all the advantages of conventional radiographic film systems without requiring chemical processing and darkroom facilities. The quality of radiochromic film has improved over the last decade in both accuracy and handle (22). They had lower sensitivity to visible light that allows them to be handled in ambient light and also had a wider useful dose range and greater sensitivity compared to radiographic films. These made radiochromic films a very important dosimetric tool in radiotherapy (25). Due to the high dose gradients in the vicinity of brachytherapy source, the high spatial resolution of radiochromic film dosimetry was an advantage over other detectors such as TLD (4). Prior to use, the radiochromic films need to be calibrated.

In this study, Gafchromic EBT2 radiochromic film was used. It has been mainly used to quantitative dose measurement applications in external beam radiotherapy, in particular intensity modulated radiation therapy (IMRT) and increasingly in brachytherapy dosimetry as a two-dimensional detector (26).

3.3.2.1 Configuration and structure of EBT2 film (27)

The configuration of EBT2 film was shown in Figure 3.3. The active part of film was a single sensitive layer about 30 microns in thickness with a thin topcoat made on a clear polyester substrate of thickness 175 microns. The active layer was covered by a 50 microns thickness polyester over-laminate with an adhesive layer of thickness 25 microns. Thus, the total nominal thickness of EBT2 film was approximately 285 microns (0.285 mm) and the structure of EBT2 film did not symmetrical cross section**.**

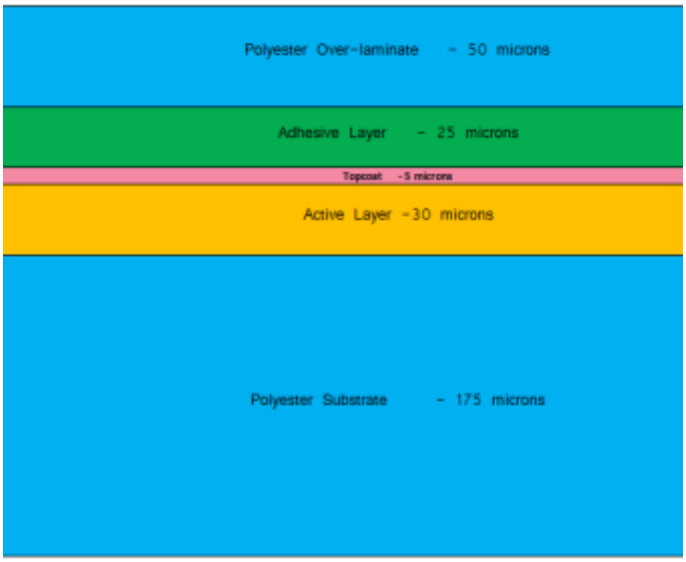

Figure 3.3 Configuration of Gafchromic EBT2 film (27).

From the configuration of EBT2 film, the polyester over-laminate and substrate were designed as a protective coating for the active layer film from mechanical damage as well as from the effects of water and other liquid. This allowed EBT2 film can be immersed in water for short period of time. Between the active layer and topcoat in EBT2 film, there was a synthetic polymer binder. Moreover, the EBT2 film contained a yellow marker dye that provides two benefits. Firstly, the yellow dye protected the active layer from ambient light. Secondly, the yellow dye made the response of EBT2 film independent of small differences in the thickness of the active layer. A yellow marker dye in EBT2 film also enabled the benefits of multi-channel dosimetry due to an available RGB film scanner.

Additionally, the presence of a dye incorporated in the active layer made the yellow color of EBT2 film.

3.3.2.2 The EBT2 film properties (27)

The EBT 2 film has been designed for absorbed dose measurement of high-energy photons. The usage of EBT2 film was related to the clinical dose range from 0.01 to 40 Gy with measuring dose of 0.01 to 10 Gy in red color channel and 10 to 40 Gy in green color channel of film scanner. The EBT2 film also has been designed to have a photon response nearly energy independent from 60 keV into the MV range due to the atomic composition in each layer of EBT2 film. It was composed almost entirely of hydrogen (H), carbon (C), oxygen (O) and nitrogen (N). And the EBT2 film was near tissue equivalence with effective atomic number 6.84, which was very close to the effective atomic number of tissue 7.3. Nowadays, film dosimetry has been generally developed into a powerful high resolution tools and EBT2 film also had a very high spatial resolution that can resolve features to at least 0.1 mm because of its grainless.

3.3.2.3 Principle of EBT2 film dosimetry (27)

When EBT2 film was exposed to radiation, a radiation-sensitive dye organized into microcrystals and embedded in a binder was used to measure the dose of radiations. A solid-state polymerization originated in EBT2 film and its color continuously changed from a light yellow color to a strong yellow color and following by dark green as dose increases. As mentioned previously, the advantage of EBT2 film was self-developing in real time with no chemical developing processing was required. Thus, an irradiated EBT2 film responded to radiation by immediately developing a blue-colored image, in which the optical density at any point represented the dose of radiation absorbed by film at that point. These required a suitable transmission dosimeters, film scanners or spectrophotometers for measurement and evaluation. Since the absorption spectrum of the active component in EBT2 film after irradiation exhibited a maximum in red region (peak at 636 nm) of visible spectrum as shown in Figure 3.4. Thus, the response of EBT2 film was enhanced by measurement with the red light of the film scanners.

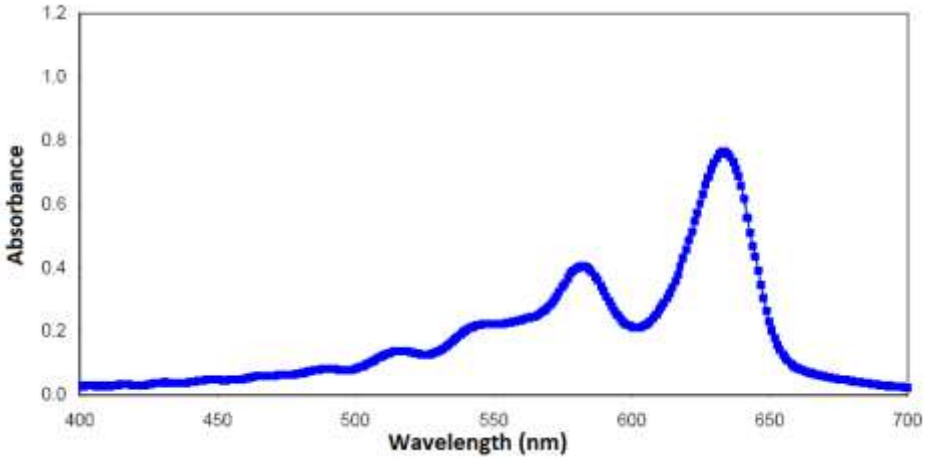

Figure 3.4 Absorption spectra of the active component in EBT2 film after irradiation, peak absorption at 636 nm with the secondary peak at about 585 nm (27).

In EBT2 film measurement, it was important to recognize the effect of post-exposure density growth. Since EBT2 film response changed with time, this effect was proportional to logarithmic of time after exposure. In principle, the measurement and scanning of EBT2 film should not be performed immediately after exposure because the uncertainties of that time can be significantly effect on the accuracy of dose. According to AAPM TG-55 report, the recommendation of appropriate time between irradiation and scanning was at least 24 hours and preferably 48 hours. In addition, EBT2 film was a two dimensional relative dosimetry, it required the characterization of film response with absorbed dose to film. Thus, the calibration curve should be constructed and was generally plotted as a relationship between absorbed dose and film response while the slope of curve gradually decreases as dose increases. It provided information for conversion of film response to absorbed dose and conversely conversion of absorbed dose to film response (4).

3.3.2.4 Film analysis

The measurement of absorbed dose in EBT2 film dosimetry involved the measurement by a suitable film scanner or digitizer. Currently, Epson scanner either Epson Perfection V700 Photo flatbed scanner (28) or Epson Expression 10000XL Photo scanner (29), and Vidar film scanner (30) were widely used for the radiochromic film dosimetry. In addition, both were charge-coupled device (CCD) film scanners that used long and diffuse light source such as a fluorescent tube to

broadly illuminate the film and projected an image of the film on linear or a two-dimensional CCD array. As EBT2 film had absorption spectrum with peaks in red light wavelengths (636 nm), measuring light transmission of film by scanner generally using the red color channel. Furthermore, the response of EBT2 film depended on the orientation of the film on the scanner because of an asymmetrical cross section of EBT2 film (Figure 3.3). For this reason, all film must be scanned in the same orientation (27).

After scanning, a digital image which essentially described lightness or darkness of film was produced and can be evaluated with a number of image analysis software packages such as OmniPro-I'mRT software (31) or ImageJ software (32). However, the influence of film orientation, film position, spatial resolution of scanner and region of interest (ROI) should be considered, these can be effected to the value of pixel and absorbed dose extract from EBT2 film.

3.4 Monte Carlo (MC) method

Monte Carlo (MC) method provided approximate solutions to a variety of mathematical problems by performing statistical sampling experiments on a computer. The applications of MC simulation increased in various areas of science and technology by using random sampling and statistical modeling to estimate mathematical functions and then imitate the operations of complex processes or systems (33). Although MC method based on random sampling was originally used for solving the mathematical problem by Comte de Buffon in 1777, the first developed and systematically used of MC simulation occurred during the Manhattan Project for developing of atomic bombs as a nuclear weapon using in the Second World War by Stanislaw Ulam and John von Neumann. They suggested MC method to investigate the properties of neutron travel through radiation shielding. Furthermore, they used MC method for many nuclear weapon problems along with others. The name of MC was coined during the Manhattan Project from MC Casino in Monaco, a center of gambling, due to the similarity of statistical simulation to games of chance (34).

The basis component of MC method for using in simulation was a random number generator (RNG) and probability density function (PDF). The RNG was a

computer algorithm for producing of uniformly distributed random numbers while PDF described the physical or mathematical system. The simulation began by random sampling from PDFs and subsequently determining the desired properties of some phenomenon or behavior. The outcomes were decided based on some reasonable mathematical and/or physical theory and then they were recorded. In the final step, the behavior of the overall system was obtained by computing the average of outcomes (35).

Monte Carlo (MC) simulation has become extensively in various fields because of the decreasing of the cost of computer while increasing in speed and increasing of many powerful software tools (36). Nowadays, MC simulation is one of the most important scientific tools for studying a wide range of problems by obtaining numerical solutions to problems which are too complicated, time-consuming, costly or impractical to solve analytically. In radiotherapy, MC simulation was widely used as research tools over the last 50 years especially in medical physics applications. One of widely used of MC method for simulation was solving radiation transport problems. In addition, the use of MC methods in radiotherapy has increased dramatically due to the available general-purpose software packages and the massive increase in computing power while decrease in cost (37).

3.4.1 Monte Carlo (MC) Photon Transport Simulations

In general, MC method in radiotherapy mainly used for the simulation of all processes associated with radiation transport by using random numbers and the knowledge of appropriate probability distributions to simulate the tracks of individual interaction for electrons and photons transport within a medium. Figure 3.5 showed steps of a typical analogue transport process of primary and secondary particles (36). The simulation of the particle transport was the same principle as different in the details.

The simulation of radiation transport processes by MC method was a simulation of physical interaction. It had an ability to simulate the tracks of individual particles such as electrons and photons through an idealized geometry by sampling quantities of interest from an appropriate probability distribution of the individual physical processes. The particles traveled with the certain distances until they were

absorbed or left the geometry of simulation. These quantities of interest can be calculated by simulating a large number of particle histories that were known as a set of MC particles. In addition, the complete simulation occurred when the quantities of interest were scored (38). The photon interactions were simulated by MC such as photoelectric effect, Compton scattering, pair production, characteristic x-rays and coherent scattering.

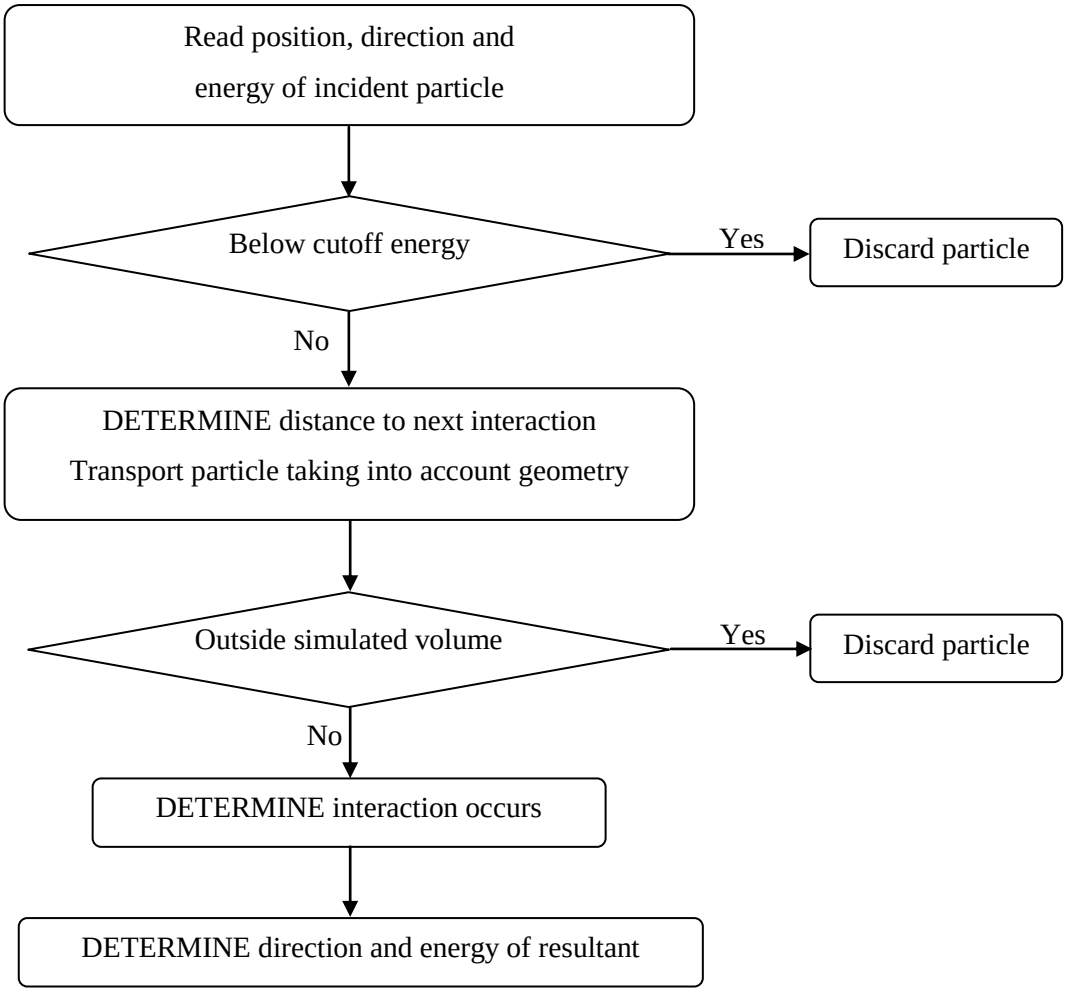

Figure 3.5 Steps of a typical radiation transport process in Monte Carlo simulation. The analogue transport samples every single event clearly. DETERMINE in block diagrams means that the quantities of interest are found by sampling from the relevant probability distribution using one or more random numbers.

3.4.2 Monte Carlo (MC) Code

A program using MC method to simulate for any applications was called MC code. Several MC programs have been used for simulating radiation transport in radiotherapy such as Monte Carlo N-Particle (MCNP), Geometry and Tracking (GEANT), Penetration and Energy loss of positrons and Electrons (PENELOPE) and Electron Gamma Shower (EGSnrc).

3.4.3 Monte Carlo (MC) in Brachytherapy

As mentioned previously, brachytherapy dosimetry using experimental method was very complicated or even in small distance was impractical and higher degree of uncertainties. To improve the accuracy of calculation and to improve the understanding of all processes associated with radiation emission from source and radiation transport in brachytherapy, MC method has been used. The most important application of MC method in brachytherapy was to obtain dose rate distribution in water around brachytherapy sources in order to obtain the dosimetric parameters of brachytherapy sources (39).

In brachytherapy, there were three main steps for dose calculation in a medium using MC method. First, the energy fluence of photons emitted by the brachytherapy source was simulated. Second, these photons must be transported through the active source core and encapsulation materials. Thus, the sampling of photon interaction points and the simulation of photon interactions were simulated in order to define the energy fluence of photons emerging from the source. Third, photon transports in the medium surrounding brachytherapy source were simulated in order to estimate the energy deposited in scoring volume (21). A simplified flow chart of MC method of sampling primary and secondary photons emitted by brachytherapy source was given in Figure 3.6.

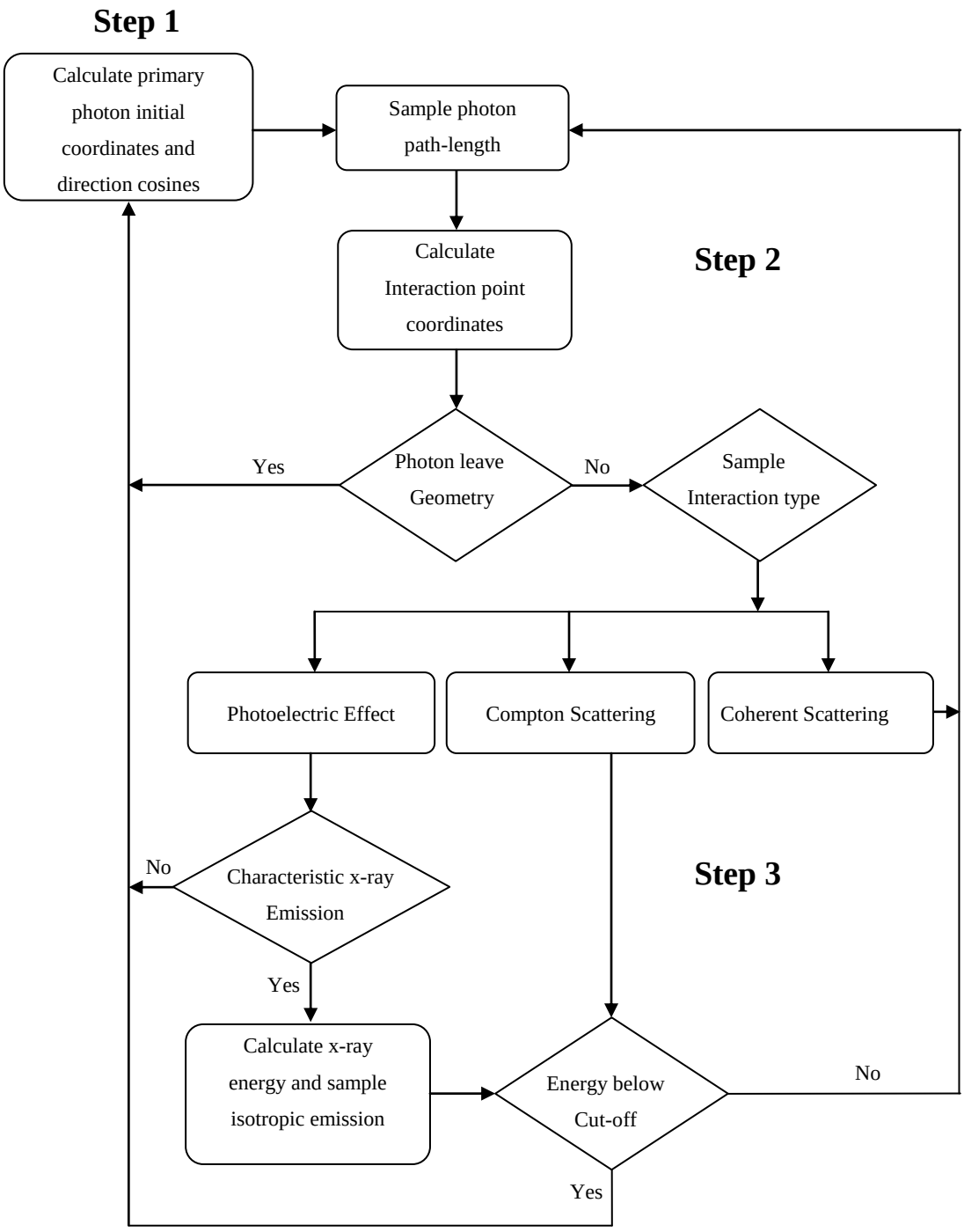

Figure 3.6 Flow chart of primary and secondary photons emitted by brachytherapy source in MC simulation (21).

3.5 Brachytherapy treatment planning calculation algorithm.

Brachytherapy treatment planning has advanced from simple look-up tables to computer-based dose calculation algorithms. Previously, computer algorithms have been based on the use of tabulated data in Cartesian or polar coordinates, or the use of dose rate table performed by the Sievert integral in dose calculation algorithms. The current computerized TPS for brachytherapy dose calculation, most are based on the recommendations of AAPM TG-43 dose calculation formalism (12). The tabulated data of TG-43 parameters were used as input data for the treatment planning software for brachytherapy sources. In general, the TG-43 dose calculation formalism was based on the principle of a single brachytherapy source superposition which obtained in a homogeneous liquid water phantom with a fixed volume for radiation scattering. As mention previously, the influence of tissue and applicator heterogeneities, inter-seed attenuation and the patient finite dimensions were not accounted in TG-43 dose calculation in TPS clinical dosimetry. For this reason, new algorithms are currently become in commercial TPS which are early adopters of model-based dose calculation algorithms (MBDCAs) for brachytherapy dose calculations such as MC methods, collapsed-cone (CC) convolution, and solving linear Boltzmann transport equation. They have been developed to address the limitations of TG-43 formalism for brachytherapy and also improve dose calculation tools and TPS. However, most of current brachytherapy TPS have used AAPM TG-43 dose calculation formalism as an important part of clinical brachytherapy TPS. Presently, a single commercial MBDCA-based TPS is only available namely Acuros® (13).

CHAPTER IV
MATERIALS AND METHODS

4.1 Materials

4.1.1 Monte Carlo (MC) code

In this study, MC code was used to calculate the absorbed dose distribution around the brachytherapy source which currently has a cylindrical geometry and DOSRZnrc MC code is a program that uses MC method for modeling the passage of an electron or photon transport in a cylindrical geometry to calculate the dose distribution (38). Furthermore, DOSRZnrc works with EGSnrc MC code system that is well benchmarked for modeling brachytherapy source as recommended in AAPM TG-43 report.

EGSnrc is an acronym for Electron Gamma Shower that developed by the group of National Research Council of Canada. The EGSnrc code system is a general purpose software toolkit for MC simulation of the coupled transport of electrons and photons for particle energies ranging from 1 keV to 10 GeV. The original version of the EGSnrc code system was developed during 1972-1978 by R.L. Ford and W.R. Nelson for simulating high-energy particle physics at Stanford Linear Accelerator Center (SLAC). In this study, EGSnrcMP version 4.r2.3.2 was used for running DOSRZnrc MC code which can work on GNU/Linux, Unix, Mac OS X and Windows and is freely available on National Research Council Canada webpage (39).

The EGSnrc code system consists of egs_inprz (40) and egs_gui (41) graphic user interfaces (GUIs) as shown in Figure 4.1 and Figure 4.2 for any users can do simulation easily. The egs_inprz is a GUI for the EGSnrc user codes as known in RZ user codes due to the RZ geometry simulated by each user code. These user codes are DOSRZnrc, CAVRZnrc, SPRRZnrc and FLURZnrc code. For egs_gui, it is a GUI that allows any users to create a new input data set for RZ user codes which namely is PEGS4 cross-section data set.

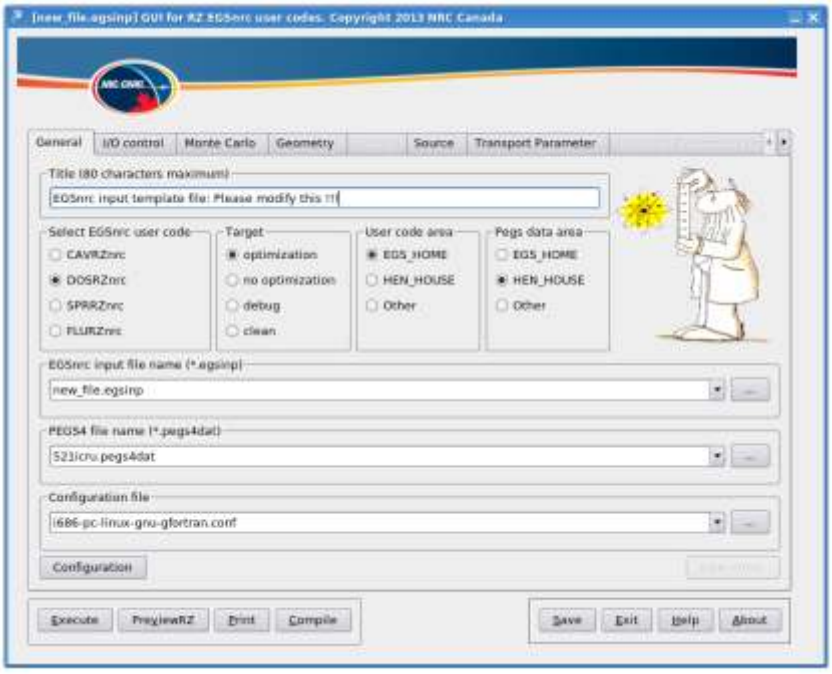

Figure 4.1 Front page of egs_inprz GUI.

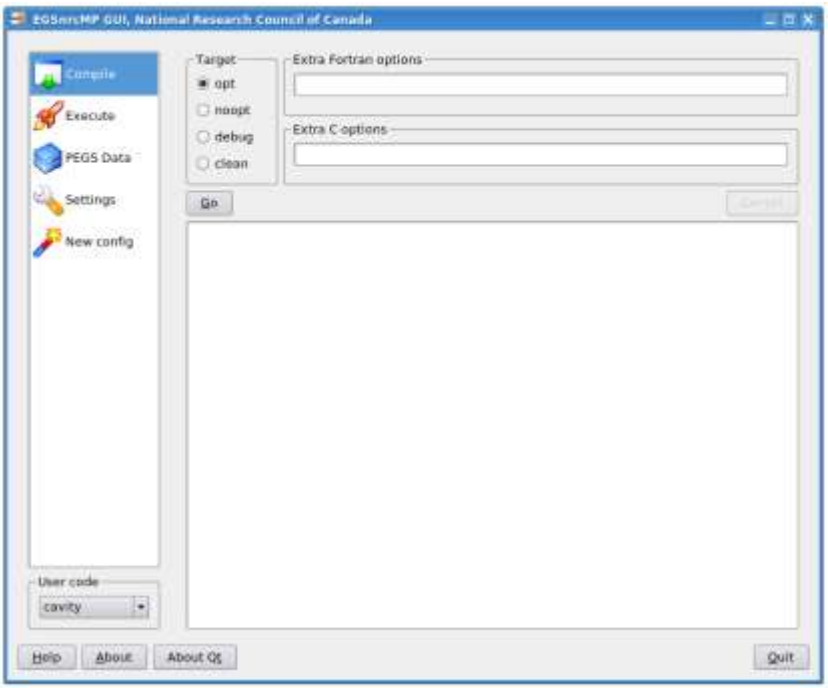

Figure 4.2 Front page of egs_gui GUI.

4.1.2 Thermoluminescence dosimeter (TLD) system

4.1.2.1 Thermoluminescence dosimeter (LiF TLD-100)

The LiF TLD-100 rod with 1 mm in diameter and 6 mm in length (Harshaw Chemical Company) was used in this study as shown in Figure 4.3 because it was near tissue equivalence with effective atomic number of 8.3. It had the almost constant response over the large range of photon energies. Furthermore, LiF TLD-100 offers relatively small size to resolve the steep dose gradients around brachytherapy source and had high sensitivity to allow measurements at both low dose and low dose rate with high precision in brachytherapy. It is lithium fluoride (LiF) crystal doped with magnesium and titanium (LiF:Mg,Ti). The dosimeter contained a natural abundance of 92.5% ^{7}Li and 7.5% ^{6}Li (10).

4.1.2.2 Thermoluminescence reader

Figure 4.4 shows a Thermo Scientific Harshaw TLD Model 5500 reader with WinREMS operating software. The reader uses hot nitrogen gas for heating with a close loop feedback system to reduce non-irradiation-induced thermoluminescence.

4.1.2.3 Annealing oven

The use of annealing oven as shown in Figure 4.5 for thermal treatment of TLD has two different programs. Program 1 is annealing that used for annealing of TLD before irradiation and program 2 is preheating that used for preheating of TLD after irradiation and before reading.

4.1.3 The Gafchromic EBT2 dosimetry film

The Gafchromic EBT2 film produced by International Specialty Products (ISP Technologies, Wayne, NJ) was used. All films in this study were in size of 8"×10" from lot number A08111102. The configuration and structure of EBT2 film were described in section 3.3.2.1 in Chapter 3 as shown in Figure 3.3.

According to the manufacturer, the photon response of the EBT2 film was nearly energy independent from 60 keV to MV range that included energies emitted from the Nucletron HDR ^{192}Ir source used in this study. The EBT2 film has been designed for usage dose range of 1 cGy to 10 cGy in red color channel and wider dose range up to 40 cGy in green color channel. The use of EBT2 film for Nucletron HDR

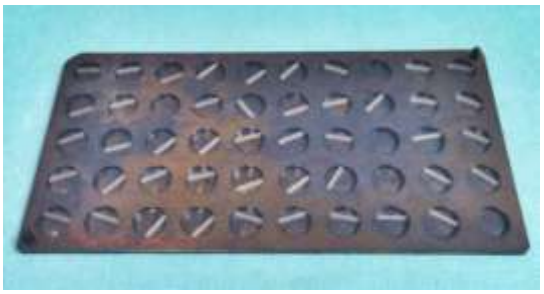

Figure 4.3 LiF TLD-100 rods.

Figure 4.4 Thermo Scientific Harshaw TLD Model 5500 reader.

Figure 4.5 Annealing Oven (Harshaw).

^{192}Ir brachytherapy source in this study because its high spatial resolution required to assess doses in a very high dose gradient regions near the source. For Gafchromic EBT2 film, its spatial resolution was at least 0.01 mm due to its grainless. Moreover, its effective atomic number was 6.84, which made it near tissue equivalent.

4.1.4 High Dose Rate (HDR) Remote Afterloading System

The HDR remote afterloading system consists of brachytheapy source, the remote afterloader, catheter and transfer tube.

4.1.4.1 Brachytherapy source

The Nucletron HDR Iridium-192 brachytherapy source as known in microSelectron v2 (mHDRv2) source was used. The internal construction and geometric dimensions were derived from manufacturer and previous study by Daskalov et al (10) that are illustrated in Figure 4.6.

The source has an active core made of a pure iridium metal cylinder with effective density of 22.42 g/cm^3 and active length of 3.6 mm with active diameter of 0.65 mm. The radioactive ^{192}Ir is uniformly distributed within active core with a half life of 73.83 days. It has a wide spectrum of photon energies ranging from 0.065 to 0.885 MeV with average energy of 0.38 MeV. The active core is surrounded by the stainless steel AISI 316L encapsulation of density 8.02 g/cm^3 with elemental composition by weight, Iron (Fe) 68%, Chromium (Cr) 17%, Nickel (Ni) 12%, Manganese (Mn) 2% and Silicon (Si) 1%. This encapsulation has a total length of 4.5 mm with total diameter of 0.9 mm. In addition, the source is welded on a flexible stainless steel AISI 304 cable with a diameter of 0.7 mm and length of 2 mm cylinder and its effective density of 4.81 g/cm^3 as shown in Table 4.1.

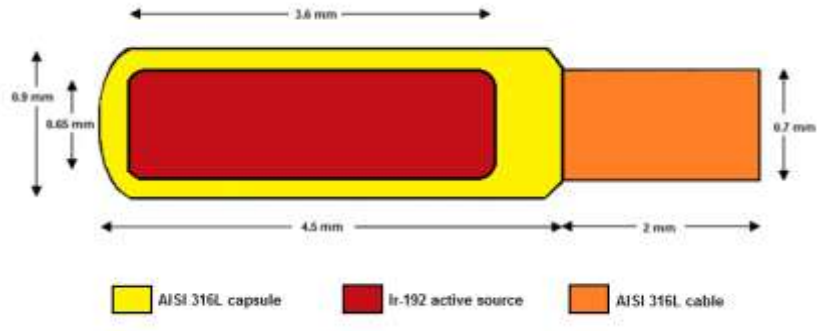

Figure 4.6 The geometrical diagram of Nucletron HDR ^{192}Ir source.

Table 4.1 The characteristics of Nucletron HDR ^{192}Ir source.

Characteristic	Active core	Encapsulation	Cable
Length (mm)	3.60	4.5	2.0
Diameter (mm)	0.65	0.9	0.7
Material	Iridium-192	Stainless steel (AISI316L)	Stainless steel (AISI316L)
Density (g/cm^3)	22.42	8.02	4.81

4.1.4.2 High Dose Rate (HDR) Remote Afterloader

The HDR remote afterloader used in this study as shown in Figure 4.7 was Nucletron HDR remote afterloader (microSelectron v3).

4.1.4.3 Catheter and Transfer tube

The flexible implant tube was used as catheter in this study. It has a length of 1290 mm with diameter of 6F and transfer tube number 7.

Figure 4.7 The Nucletron HDR remote afterloader (microSelectron v3).

4.1.5 Oncentra Treatment Planning System (TPS)

Oncentra Brachy TPS **(**version 4.1) was used in this study for MC validation. This TPS is a computer based dose calculation algorithm that is based on AAPM TG-43 dose calculation formalism to calculate the dose distribution around the source.

4.1.6 C-arm machine

The OEC 9900 Elite C-arm machine was used to produce the x-ray images of dummy source and catheter for checking their positions and then exported these x-ray images to TPS for planning.

4.1.7 Solid Water phantom

In this study, the slabs of Gammex RMI (Middleton, WI 53562) were used as solid water-equivalent phantom as shown in Figure 4.8. The slabs of solid water are water-equivalent materials. They have the physical density of 1.03 g/cm^3 and mean atomic number (Z) of 5.96. All slabs are 30 × 30 cm^2 in size with different thickness of 0.2, 0.5, 1, 2 and 5 cm.

Figure 4.8 The slabs of solid water phantom.

4.1.8 Bolus

The bolus 30 x 30^2 cm in size with the thickness of 0.3 cm was used in this study for reducing air gap between source and slab of solid water phantom. The material of bolus is tissue equivalent and sufficiently flexible to patient surface.

4.1.9 Vidar® Red LED Dosimetry Pro Advantage™ scanner

The Vidar® Red LED Dosimetry Pro Advantage™ scanner was used in this study as shown in Figure 4.9. It is charged-coupled device (CCD) scanner designed for use with radiochromic film. In principle, CCD scanner employs a long, diffuse light source as fluorescent tube to broadly illuminate the film and project an image of the film on a linear CCD array. The vidar scanner in this study employs a LED light source with nominal maximum emission at 627 nm which is very closely matched to the peak absorption of Gafchromic EBT2 film at 636 nm.

Figure 4.9 The Vidar® Red LED Dosimetry Pro Advantage™ scanner.

4.1.10 ImageJ software

An ImageJ software version 1.35s (276 commands, 18 macros) is an image processing program that used to analyze TIFF images of EBT2 film scanning derived from vidar scanner as shown in Figure 4.10

4.1.11 Operating system and PC computer

The Community enterprise operating system, CentOS, version 5.8 has been used as an operating system with KDE (K Desktop Environment) for simulation in this study. The CentOS or community enterprise operating system is a Linux

distribution which is a free operating system. For PC computer, CPU used for the simulation was Intel Core i5 2400 with 3.1 GHz processors and DDR RAM 4 GB.

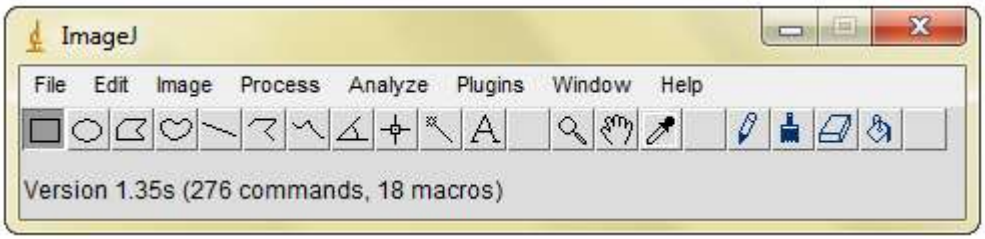

Figure 4.10 ImageJ software.

4.2 Methods

The procedures were divided into four major parts; MC simulation, validation of MC, measurements and comparison.

4.2.1 Monte Carlo (MC) simulation

In this study, EGSnrc/DOSRZnrc MC code was used to calculate absorbed dose distribution around Nucletron HDR ^{192}Ir source.

4.2.1.1 Source and phantom modeling

The DOSRZnrc modeled the Nucletron HDR ^{192}Ir source by using source type of internal uniform isotropically radiating disk of finite size in DOSRZnrc (source number 3). This source was defined by the parameters ZMIN and ZMAX for the length of the source in Z direction within the geometry and RMINBM and RBEAM for the inner and outer radii of the source, respectively as shown in Table 4.2 (41).

An ^{192}Ir active core source, encapsulation and source cable of Nucletron HDR ^{192}Ir source were modeled in DOSRZnrc code. The dimensions of ^{192}Ir active core source and encapsulation were described in Chapter 3 and the cable attached to the end of encapsulation was modeled 2 mm in length. After source modeling, the DOSRZnrc modeled a cylindrical water phantom with size of 40 cm in height and 40 cm in diameter to obtain full scatter condition (2). For dose calculation

Table 4.2 Description of source number 3: Internal uniform isotropically radiating disk of finite size (Interior isotropic cylindrical source) and parameters.

Parameters	Definition	In this study(cm)
RMINBM	Inner radius of active source	0.0325
RBEAM	Outer radius of encapsulation	0.045
ZSMIN	Minimum z-coordinate of active source	-0.18
ZSMAX	Maximum z-coordinate of active source	0.18

using MC in this study, the source was modeled at center of a water cylinder phantom due to recommendation of AAPM TG 43 report as shown in Figure 4.11

The source and phantom components used in the modeling were taken from PEGS4 data set of DOSRZnrc. The PEGS4 data used in this study was the 521icru_nucletron.pegs4 file with the compositions used in source and phantom modeling displayed in Table 4.3. However, some materials such as stainless steel and source cable were created using egs_gui program (40) and then were appended to 521icru_nucletron.pegs4 file for source modeling. The geometry of DOSRZnrc source model and real source were displayed in Figure 4.12. The DOSRZnrc had limitation in modeling of the tip of source which was modeled as a flat while the actual source was spherical. Due to high atomic number and density of iridium compared to stainless steel of the source, photon scattering and absorption in the source itself were dominated (42). Therefore, the errors of deviations from this actual geometry were small in absorbed dose calculation along the transverse axis from the source center in this study. This assumption was based on the low probability for photons to be scattered in a direction 180˚ (source tip) to the angle of incidence and back into the transverse axis with 90 degree.

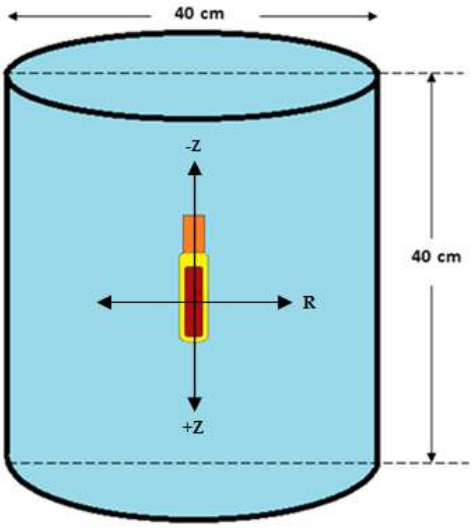

Figure 4.11 Source position in a center of a cylindrical water phantom.

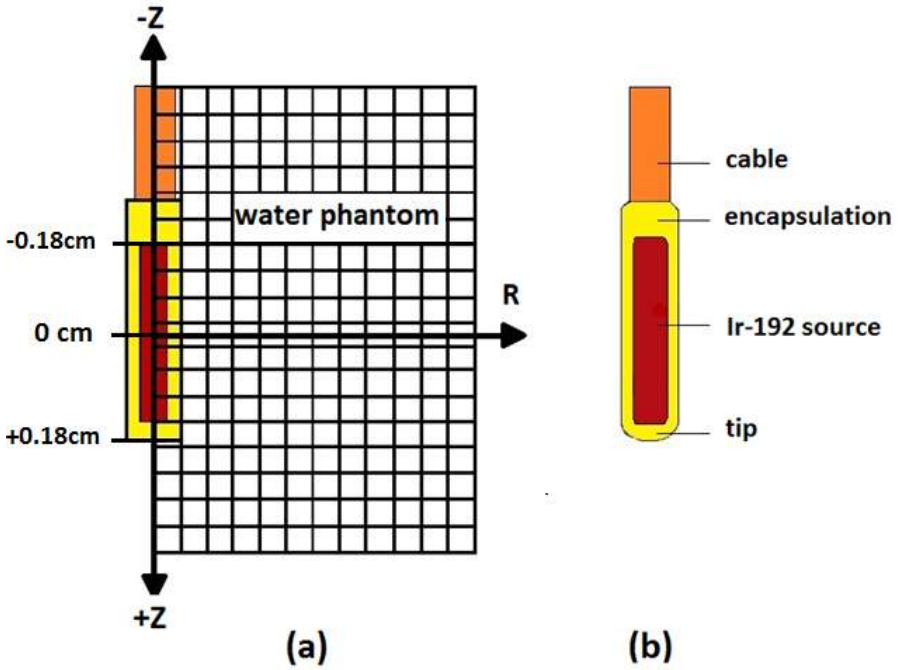

Figure 4.12 Geometry of DOSRZnrc-modeled (a) and the actual (b) Nucletron HDR ^{192}Ir source with RZ grid regions were indicated in (a). The red, yellow and orange colors represented ^{192}Ir active core source, encapsulation and source cable, respectively.

Table 4.3 Compositions used in source and phantom modeling from 521icru_nucletron.pegs4 file.

Structure	Material	Element	Composition (% by weight)	Density (g/cm^3)	AP (MeV)	AE (MeV)
Source	Iridium	Ir	100	22.42	0.001	0.521
Capsule	AISI316L Stainless steel	Fe	68	8.02	0.001	0.521
		Cr	17			
		Ni	12			
		Mn	2			
		Si	1			
Cable	AISI316L Stainless steel	Fe	68	4.81	0.001	0.521
		Cr	17			
		Ni	12			
		Mn	2			
		Si	1			
Phantom	Water	H	11.2	0.998	0.001	0.521
		O	88.8			
	Solid (RMI)	H	8.09	1.03	0.001	0.521
		C	67.22			
		N	2.40			
		O	19.84			
		Cl	0.13			
		Ca	2.32			

Table 4.4 Photon spectra from Ir192_bare_1993.spectrum file.

Energy interval or bin (keV)	Photon in bin per 100 decays (%)
7 - 14	5.8
61 - 67	10.72
71 - 79	2.892
136 - 137	0.181
201 - 202	0.485
205 - 206	3.33
283 - 284	0.266
295 - 296	28.85
308 - 309	30.05
316 - 317	82.8
374 - 375	0.721
416 - 417	0.664
468 - 469	47.8
484 - 485	3.16
489 - 490	0.427
588 - 589	4.48
604 - 605	8.16
612 - 613	5.26
884 - 885	0.288
Total (photon/ decay)	**2.363**

The ^{192}Ir spectrum employed in the simulations was spectrum of a bare ^{192}Ir source, Ir192_bare_1993.spectrum file, published by Duchemin & Coursol (1993) with an average photon energy of 345 keV (43). This spectrum has been employed by a number of authors for modeling a variety of HDR brachytherapy

sources. It included in HEN_HOUSE directory, home directory tree of EGSnrc system for modeling brachytherapy sources (40**)**. The components of this spectrum were shown in Table 4.4. An average one decay resulted in the emission of 2.636 photons with energy in the interval from a few keV to 855 keV.

4.2.1.2 RZ geometry of source

In this study, the source was modeled at the center of a water cylindrical phantom for simulation. Since the simulation of geometry in DOSRZnrc was based on RZ (radial-plane) coordinate. Thus, source and phantom were designed as coaxial in cylindrical coordinate system by planes cut all cylinders of source and phantom together as shown in Figure 4.12(a). The center of the active source was an origin of the RZ coordinate system and the negative and positive along the Z axis are equivalent to the distal ($\theta = 0°$) and the tip ($\theta = 180°$) of sources, respectively.

In this study, absorbed dose distribution around Nucletron HDR ^{192}Ir source were simulated in two densities of cylindrical water phantom. The first simulation was done in a cylindrical water phantom with density of 0.998 g/cm^3, these results were used for validated DOSRZnrc calculation in the same condition with treatment planning system based on AAPM TG-43 dose calculation formalism. As recommended by AAPM TG-43 report, the reference media with a mass density of 0.998 g/cm^3 was used in absorbed dose distribution. The second simulation was done in a cylindrical water phantom with density of 1.03 g/cm^3 that was similar to the density of experimental phantom used in this study because these results were used to compare with the experimental measurements.

The RZ grid regions were created as dose-scoring regions which stored the quantities of interest in RZ region (41). In principle, the quantities of interest such as the calculated dose and the spatial resolution are affected by the size of the scoring regions (33) which determines the resolution of dose distribution around brachytherapy source. In this study, high spatial resolution was achieved by reducing the RZ size. In the simulation, the size of Z was fixed as 0.05 cm while the size of R was 0.05 cm, 0.1 cm and 0.5 cm at distances of 0.1 cm to 2 cm, 2 cm to 3 cm and 3 cm to 20 cm, respectively as depicted in Figure 4.13. Due to high dose gradient near the source and low dose gradient at distance further away from the source, the size of R in

each scoring region was extended to 0.1 cm at distances of 2 cm to 3 cm and then 0.5 cm at distances of 3 cm to 20 cm to reduce the simulation time.

4.2.1.3 Radiation transport and MC parameters

The transport and interactions of primary and scattering photons for the processes of bound Compton scattering, Rayleigh scattering, photoelectric absorption and fluorescent emission of characteristic x-ray were all simulated as shown in Table 4.5. These interactions were simulated down to the global photon cutoff energy (PCUT) of 0.001 MeV (44, 45, 46) and the global electron cutoff energy (ECUT) of 0.521 MeV including rest mass of the electron.

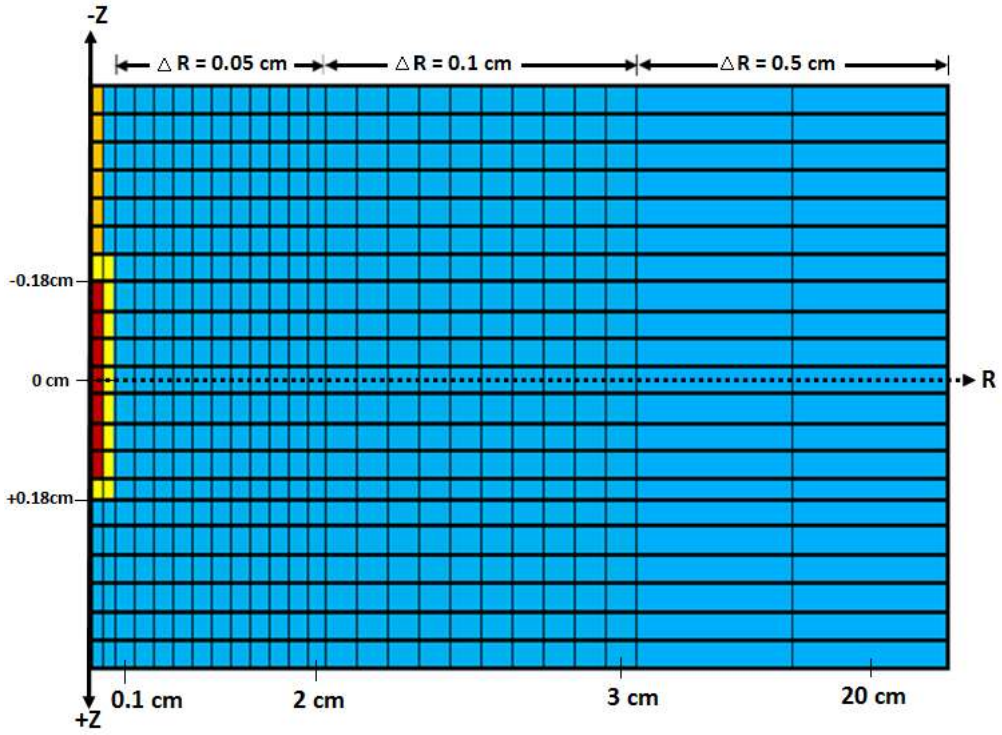

Figure 4.13 DOSRZnrc modeled source with RZ regions. Red, yellow, orange and blue colors represented ^{192}Ir active core source, encapsulation, source cable and water phantom used in simulation, respectively. This figure demonstrates the scoring geometry for the DOSRZnrc calculations but did not depict the true sizes and number of RZ regions as described above.

According to previous studies (44, 47), charge-particle equilibrium (CPE) existed for radial distance greater than 2 mm from the source axis of an ^{192}Ir source, so electron transport was negligible for all these distances and the collision kerma may be approximately equal to absorbed dose. In this study, the electron transport parameters and other parameters were set as default values as shown in Table 4.5.

A total of photon 500 million photon histories were set to run for both simulations in this study that took a total of approximately 9 hours to compute and provided 0.04 % statistic uncertainty.

Table 4.5 The photon and electron transport parameters using in the simulation.

	Transport parameters	**In the study**
Photon	Bound Compton scattering	On
	Rayleigh scattering	On
	PE angular sampling	On
	Atomic relaxations	On
	Pair angular sampling	Off
	Brems angular sampling	KM
	Brems cross section	BH
	Boundary crossing algorithm	EXACT
	Photon cross section library	XCOM
	PCUT	0.001 MeV
Electron	Electron-step algorithm	PRESTA-II
	Electron impact ionization	Off
	ECUT	0.521 MeV

After RZ geometry of source and phantom was carried out in DOSRZnrc. The appropriate radiation transport parameters, the size of dose scoring regions, the number of histories were defined. Consequently, the absorbed dose calculations were performed with Nucletron HDR ^{192}Ir source positioned at the center

of a cylindrical water phantom. In the simulation, the RZ grid regions were employed for the absorbed dose calculations and energy deposited in each region. In this study, the DOSRZnrc output was in gray per incident particles (Gy incident particles^{-1}) for each scoring region.

4.2.2 Dose calculation by Treatment Planning System (TPS)

To validate MC calculation of Nucletron HDR ^{192}Ir source, the Oncentra Brachy version 4.1 TPS (Oncentra TPS) was used as a reference in this study. The Oncentra TPS was not commissioning by any measurements as external beam TPS done. In general, the absorbed dose distribution around the source was based on the AAPM TG-43 dose calculation formalism which the TG-43 dosimetric parameters used to calculate dose delivery to patients supplied by the TPS manufacturer. Moreover, a measure of source strength as reference air-kerma rate was provided by manufacturer certificate. Therefore, the calibration of source was done in order to verify the value of reference air-kerma rate and ensure the accuracy of absorbed dose distribution calculated by Oncentra TPS. In this study, Nucletron HDR ^{192}Ir source was calibrated in well type chamber, in air and in phantom using ionization chamber and the values of reference air kerma rate obtained from three methods were in good agreement ($\pm$3%) with the reference air kerma rate from manufacturer certificate. For this reason, the absorbed dose calculation from Oncentra TPS was acceptable and used as a reference data in this study.

To validate DOSRZnrc, the Oncentra TPS was used to create a cylindrical water phantom with a height of 40 cm and diameter of 40 cm. The virtual phantom geometry and density (0.998 g/cm^3) were identical to a simulated phantom and was shown in Figure 4.14. The source was placed in the center of a homogeneous water phantom. Subsequently, the absorbed dose distributions at radial distance 0.1 cm to 15 cm along the transverse axis from the source center were calculated.

4.2.3 Validation of MC calculation

To validate MC calculation, the relative absorbed doses at distances from 0.1 cm to 15 cm obtained by Oncentra TPS were used to compare with those obtained

by MC calculation. To calculate relative absorbed dose, the absorbed dose at any distance was normalized with a reference point dose at 1 cm.

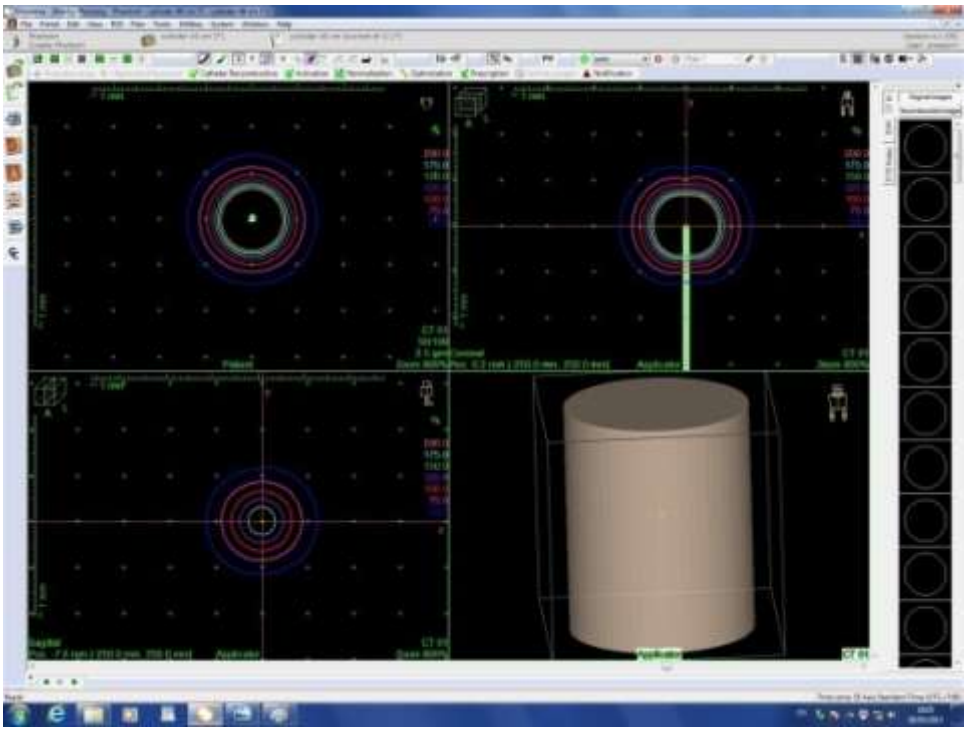

Figure 4.14 A virtual cylindrical water phantom created by Oncentra TPS.

4.2.4 TLD Measurement

4.2.4.1 TLD selection and calibration

The Cobalt-60 machine with output of 101.6141 cGy/min on 5th March, 2013 at the depth of maximum dose (0.5cm), 80 cm SSD for 10×10 cm^2 field size was used to calibrate TLD 50 rods with the dose 200 cGy.

For TLD selection, a total 50 TLD rods were selected with their uniform response to a dose of 200 cGy from Cobalt-60 machine (within ±10%). The process of TLD irradiation started with TLD annealing at 400°C for 1 hour and followed by 100°C for 2 hours to nullity the residual background. All 50 TLD rods were numbered. Then, placed TLD rods in a perspex phantom and exposed with Cobalt-60 machine to achieve a dose of 200 cGy. Before reading exposed TLD, they were preheated at 100 °C for 10 minutes to eliminate off-peak noise. In reading, the TLD rods were heated at 260°C for a rate of 10°C per second and the reading was

displayed in nanocoulomb (nC). In this step, the 4 TLD rods (1-2% of total TLD rods) having the element correction coefficient (ECC_i) closet to 1 were selected and used as standard TLD. The value of ECC_i is defined as following Equation 9 where $\bar{Q}$ is the average charge for all TLD rods and Q_i is the charge of individual TLD.

$$ECC_i = \frac{\bar{Q}}{Q_i} \quad (9)$$

In calibration of the TLD reader, these 4 standard TLD rods with ECC_i close to 1 (ranging from 0.9999 to 1.0002) were annealed and exposed with Cobalt-60 machine to achieve a dose of 200 cGy by placing TLD rods in a perspex phantom. Then, they were preheated at 100 °C for 10 minutes before reading and were heated at 260°C for a rate of 10°C per second in reading. The individual TL reading was calculated to the corrected charge integral (Q_{ci}) as shown in Equation 10

$$Q_{ci} = Q_i \times ECC_i \quad (10)$$

Then, the average of Q_{ci} represented in $\bar{Q}_c$ for 4 standard TLD rods was used to determine the reader calibration factor (RCF) using the Equation 11 where D is the dose of 200 cGy. In this study, the value of RCF for TLD reader was about 844.3609 nC/Gy.

$$RCF = \frac{Q_c}{D} \quad (11)$$

In calibration of individual TLD for unknown dose measurement, the rest of 46 TLD rods were annealed and exposed with Cobalt-60 machine to achieve a dose of 200 cGy by placing TLD rods in a perspex phantom. Then, they were preheated at 100°C for 10 minutes before reading and were heated at 260°C for a rate of 10°C per second in reading. These used to determine the individual element correction coefficient (ECC_{ci}) where D is the dose of 200 cGy, RCF is 844.3609 nC/Gy and Q_i is the TL reading for individual TLD.

$$ECC_{ci} = \frac{RCF \times D}{Q_i} \quad (12)$$

The value of ECC_{ci} for each 46 TLD rods was shown in Table 4.6 and Table 4.7 for the two sets of calibration because there was a gap of time between first and second measurements. To reduce the uncertainties of this time, the second TLD calibration was performed. In measurement of an unknown dose (D_u), the dose was calculated from individual TL reading (Q_i), ECC_{ci} and RCF according to Equation 13.

$$D_u = \frac{Q_i \times ECC_{ci}}{RCF} \quad (13)$$

4.2.4.2 Linearity test of TLD

After doing calibration, the linearity of 46 TLD rods were evaluated by exposing these TLD with doses 50, 100, 200, 300, 400 and 500 cGy with Co-60 machine. The reading from all rods of TLD for each dose were averaged and converted into the unit of dose and then plotted on a linear scale as a function of irradiated dose. And in this study, the linearity test was performed and plotted as shown in Figure 4.15 with R^2 of 0.998.

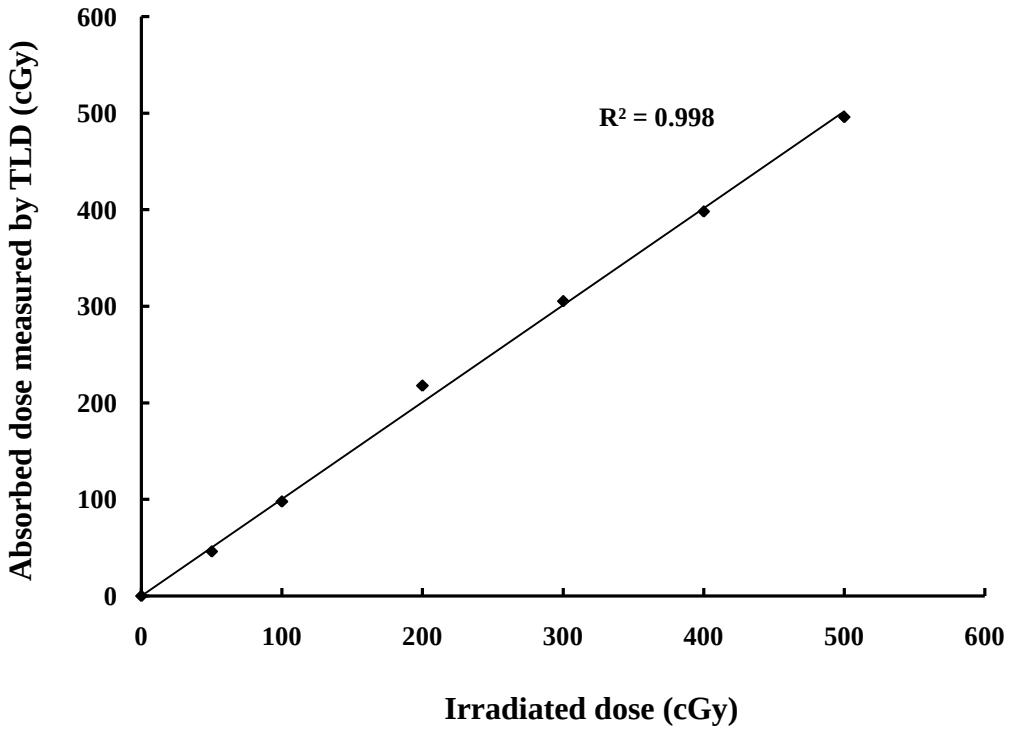

Figure 4.15 The linearity of all 46 TLD rods used in this study.

Table 4.6 The individual element correction coefficient (ECC_{ci}) value for each TLD (Calibrated on March 2013).

TLD No.	ECC_{ci}	TLD No.	ECC_{ci}
1	1.083250	24	1.047624
2	1.060770	25	1.033076
3	1.114346	26	1.034018
4	1.095869	27	1.066575
5	1.079785	28	1.055197
6	1.068557	29	1.061457
7	1.091754	30	1.030445
8	1.044454	31	1.149930
9	1.035036	32	1.116146
10	1.076225	33	1.076211
11	1.117431	34	1.067444
12	1.046627	35	1.056487
13	1.074932	36	1.021604
14	1.040828	37	1.021260
15	1.104946	38	1.033778
16	1.081567	39	1.007314
17	1.033487	40	1.097961
18	1.083197	41	1.081331
19	1.048830	42	1.077873
20	1.035449	43	1.088537
21	1.106743	44	1.070175
22	1.148449	45	1.097289
23	1.085985	46	1.016531

Table 4.7 The individual element correction coefficient (ECC_{ci}) value for each TLD (Calibrated on July 2013).

TLD No.	ECC_{ci}	TLD No.	ECC_{ci}
1	1.096280	24	0.938387
2	1.035994	25	0.910671
3	1.075163	26	0.981342
4	0.994350	27	0.958155
5	0.933336	28	-
6	0.959189	29	0.980244
7	0.961114	30	0.943191
8	-	31	1.136781
9	0.911011	32	1.056759
10	0.901126	33	1.030124
11	1.015388	34	0.957634
12	0.924779	35	0.949001
13	0.988998	36	0.941380
14	0.964274	37	1.000892
15	0.981810	38	-
16	0.951328	39	0.940665
17	0.929358	40	0.995998
18	0.966230	41	1.124701
19	0.945497	42	1.110944
20	0.963379	43	0.998793
21	1.150134	44	0.989214
22	1.087915	45	1.027208
23	1.064943	46	0.966379

4.2.4.3 TLD measurement

The absorbed dose measurement was obtained in a cubic water phantom as shown in Figure 4.16. The slabs of solid water phantom were formed into a 30 × 30 × 30 cm^3 cubic water phantom. Because of the limitation of our dedicated phantom, TLD holders were created by using the flexible and solid tubes. All holders were numbered for all rods. Before placing TLD rod in a cubic water phantom for measurements, the source position was first determined by using a 3 × 4 cm^2 EBT2 film as shown in Figure 4.17.

For measurement, two TLD rods with their holders were placed together at each 19 radial distances from 0.3 cm to 15 cm along the transverse axis from the source center and then each distances were exposed separately with a dose of 400 cGy. These separated measurements were made in each distance for avoiding inter-TLD rod attenuation effects. In this study, the 19 radial distances were 0.3, 0.5, 1, 1.5, 2, 2.5, 3, 4, 5, 6, 7, 8, 9, 10, 11, 12, 13, 14 and 15 cm, so a total number of 38 TLD rods were used in measurements. The diagram and the set up of TLD measurements were shown in Figure 4.18 and Figure 4.19.

After exposure, all 38 TLD rods were preheated at 100˚C for 10 minutes before reading. After reading, the two TL readings (Q_i) at each distance were derived and calculated to average TL reading for that distance. Then, the same procedure for measurement was repeated twice to reduce the uncertainty during the measurement, so there were three sets of the TLD measurements. And the TL reading (Q_i) from each set used to calculate the dose for all distances with Equation 13 and then the average dose at each distance was calculated.

Figure 4.16 A 30×30×30 cm^3 cubic water phantom from slabs of solid water phantom.

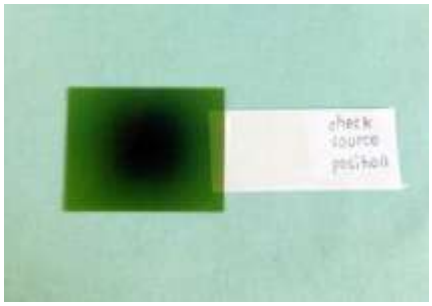

Figure4.17 The EBT2 film predetermined the source position.

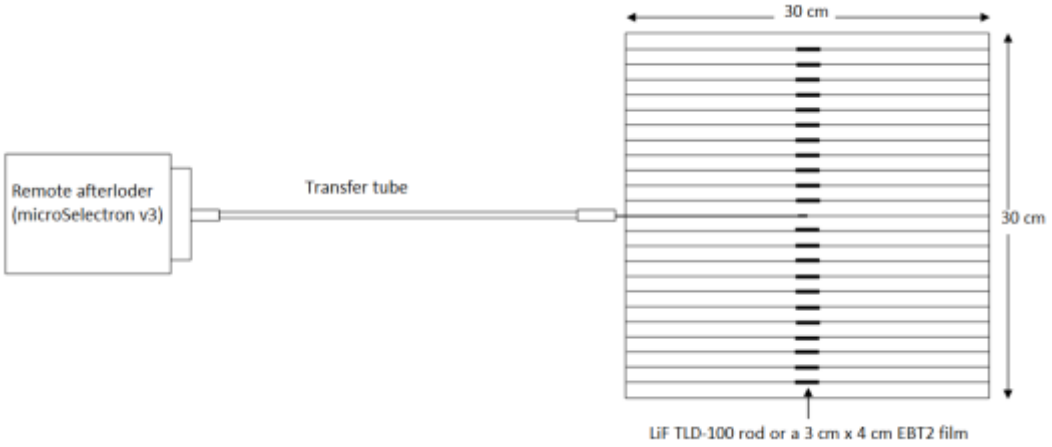

Figure 4.18 Top view of LiF TLD-100 and EBT2 film measurements. The center of a 30 cm x 30 cm x 30 cm represented Nucletron HDR ^{192}Ir source inside the flexible implant catheter connected to transfer tube.

Figure4.19 The dose measurement set up in TLD and EBT2 measurements.

4.2.5 Gafchromic EBT2 radiochromic film measurement

All EBT2 films with size of 8"×10" from the same pack (Lot number A08111102) were cut into small rectangles size of 3×4 cm2 for calibrations and measurements. These small pieces of film had the same symmetry as the original film that made them very easy to keep the orientation under control. There was a small slit at the top right corner for all original EBT2 films when the film was viewed in landscape orientation as shown in Figure 4.20. This small slit indicated that the side of the film with the polyester laminate was faced to the observer. As film orientation on scanner can affect the measurements (48), all films in this study were marked at the top right corner to indicate their orientation with respect to the original film as shown in Figure 4.21**.**

4.2.5.1 EBT2 film calibration

The EBT2 film calibration was carried out using Nucletron HDR ^{192}Ir source. First, one film was placed at 1 cm from a flexible implant catheter, in which the Nucletron HDR ^{192}Ir source was driven to predetermined position at center of a 30×30×30 cm^3 cubic water phantom as shown in Figure 4.22. Subsequently, each film was placed at 1 cm from a flexible implant catheter and then was separately exposed with dose range from 0 cGy (unexposed) to 1000 cGy as followed; 0, 25, 50, 75, 100, 150, 200, 250, 300, 350, 400, 450, 500, 600, 700, 800, 900 and 1000 cGy. Three pieces of EBT2 film were used for each dose to reduce the

uncertainty during the calibration, so the EBT2 calibration used a total of 54 film pieces.

Figure 4.20 A 8"×10" original EBT2 film with a small slit at the top right corner when EBT2 film was viewed in landscape orientation. This small slit indicated that the side of the EBT2 film with the polyester laminate was faced to the observer.

Figure 4.21 A 3×4 cm^2 EBT2 film using in the calibrations and measurements with a handle (white paper) and marker at top right corner corresponding to original film.

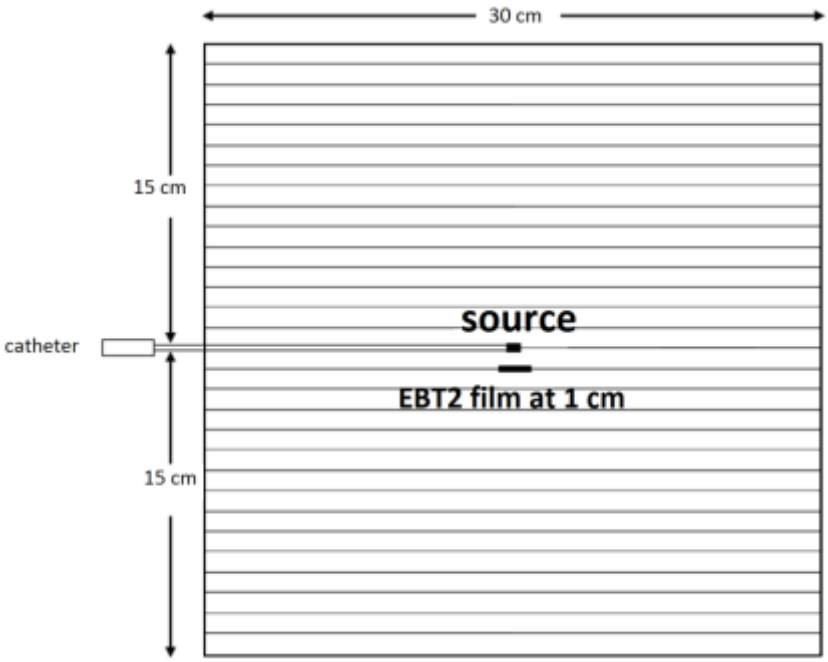

Figure 4.22 The diagram of EBT2 film calibration using Nucletron HDR ^{192}Ir source. A piece of EBT2 film was placed at reference distance (1 cm) and was separately exposed with dose range from 0 cGy (unexposed) to 1000 cGy.

4.2.5.2 EBT2 film measurement

In this study, the measurement was performed with the two set of dose; 400 cGy and 800 cGy. These two values were considered to keep pixel value in the calibrated dose range. Each set had 19 EBT2 film pieces and were placed at each 19 radial distances from 0.3 cm to 15 cm along the transverse axis from the source center as shown in Figure 4.9. Then, each distance was exposed separately. The 19 radial distances were 0.3, 0.5, 1, 1.5, 2, 2.5, 3, 4, 5, 6, 7, 8, 9, 10, 11, 12, 13, 14 and 15 cm. The same procedure was repeated twice to reduce uncertainty during measurement, thus 114 pieces of film were used for EBT2 measurement.

4.2.5.3 EBT2 analysis

All EBT2 films from calibrations and measurements in this study were scanned 24 hours after exposure using Vidar scanner with the scanning resolution of 75 dots per inch (dpi) and color depth of 16 bits per pixel (bpp). All pieces of film were placed in same position of the scanner and they were scanned in a landscape orientation, which the short side of film parallel to the scan direction,

because the landscape orientation is more uniform than the portrait orientation (49). However, each film was cut into small pieces of film, so the A4 paper congruent with the original film to keep track of the orientation were used as shown in Figure 4.23

After scanning, a digital image was produced from EBT2 film as shown in Figure 4.24 and then was evaluated with OmniPro-I'mRT and ImageJ programs. The pixel value (PV) measurements were carried out with a region of interest (ROI) corresponding to 2 mm × 2 mm in at the center of the image and these were repeated in three times to get an average PV value. The PV value from OmniPro-I'mRT and ImageJ programs were difference within 2%. Thus, ImageJ program was used to analyze all EBT2 film in this study because calibration curve was directly created.

For calibration films, the average PV value of each calibrated film with the exposed dose from 0 cGy to 1000 cGy were used to create the EBT2 calibration curve as plotted in Figure 4.25 with R^2 0.9995**.** And this curve was used to convert average PV value to dose (at 19 radial distances) for all EBT2 film measurements by using the fit equation in Equation 14.

Figure 4.23 An irradiated EBT2 film with holder for scanning.

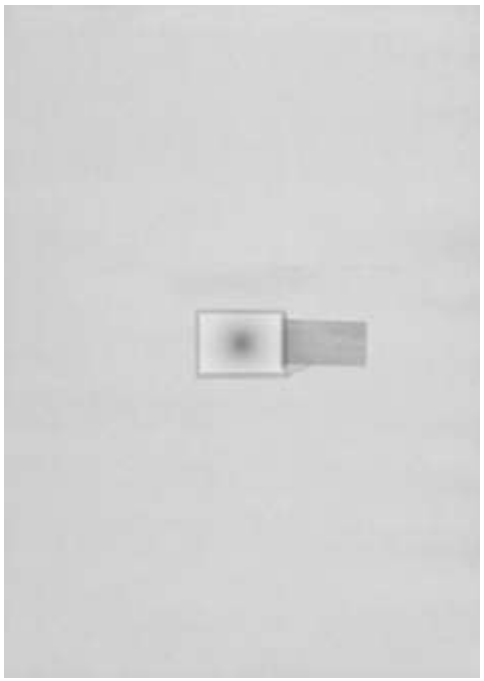

Figure 4.24 A digital image of EBT2 film after scanning. This TIFF image was the image of EBT2 film exposed with dose of 400 cGy at radial distance 0.3 cm.

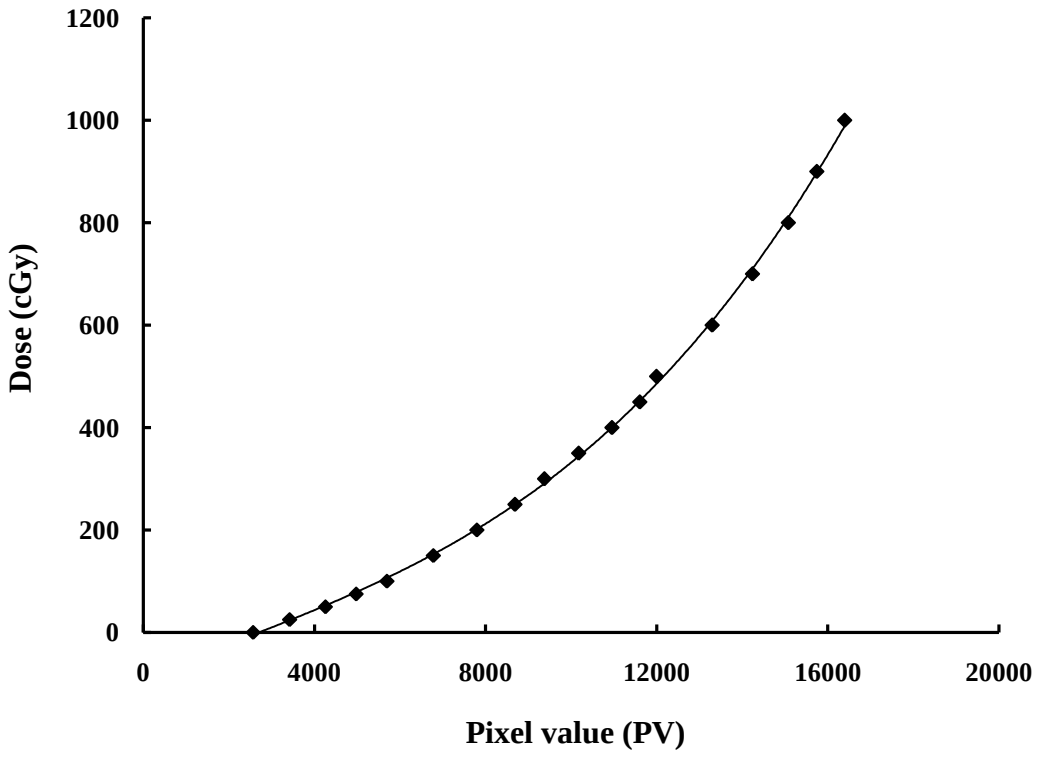

Figure 4.25 Calibration curve of Gafchromic EBT2 film using ^{192}Ir source.

$$y = (2\times10^{-10})\,x^3 - (9.975\times10^{-7})\,x^2 + (3.41557019\times10^{-2})\,x - 88.786869512 \quad (14)$$

The relative absorbed doses for all 19 radial distances along the transverse axis of source center from MC calculation were used to compare with that from TLD and EBT2 measurements. In this study, the relative absorbed dose was the absorbed dose at distance 0.3 cm to 15 cm normalized to the absorbed dose at reference point (1 cm).

4.2.6 Radial dose function

4.2.6.1 The g(r) calculations

The g(r) was calculated following Equation 7 in Chapter 3 by using relative absorbed doses obtained from MC, TLD and EBT2 methods with the geometric function, $G(r, \theta_\theta)$, of Nucletron HDR ^{192}Ir source. Due to a linear of Nucletron HDR ^{192}Ir source, the geometric function of this source was calculated according to line source approximation, $G_L(r, \theta_\theta)$, as shown in Equation 5. The θ was equal to 90 degree. The calculated $G_L(r, 90)$ values used to calculate g(r) in this study were shown in Table 4.8. Consequently, g(r) was calculated by MC and experimental methods.

Table 4.8 The. Geometry function, $G_L(r, 90)$, for Nucletron HDR ^{192}Ir source.

Distance (r)	**$G_L(r,90)$**	**Distance (r)**	**$G_L(r,90)$**
0.3	10.00776852	2.5	0.159724377
0.5	3.839506451	2.6	0.147693335
0.7	1.997539458	2.7	0.136971530
0.8	1.536905850	2.8	0.127375747
0.9	1.218491110	2.9	0.118753719
1	0.989405212	3	0.110978065
1.1	0.819186028	3.5	0.081560797
1.2	0.689305313	4	0.062457864
1.3	0.587977506	4.5	0.049356404
1.4	0.507420312	5	0.039982733
1.5	0.442329356	6	0.027769449
1.6	0.388989453	7	0.020403667
1.7	0.344736302	8	0.015622364
1.8	0.307619298	9	0.012344033
1.9	0.276184022	10	0.009998920
2	0.249328262	11	0.008263725
2.1	0.226204481	12	0.006943924
2.2	0.206152379	13	0.005916782
2.3	0.188651395	14	0.005101760
2.4	0.173286685	15	0.004444231

4.2.6.2 Correction factor (CF) calculations

Since the phantom geometry used in MC calculation and experimental measurements were different in this study. These significantly affected the g(r) values at radial distances near phantom boundaries (8). The correction factors as shown in Table 4.9 were used to transform g(r) datasets obtained with different phantom shape and size into approximate g(r) values for unbounded conditions. The calculated CF values used to transform g(r) for cylindrical and cubic phantoms into approximate g(r) values for unbounded conditions were shown in Table 4.10 and Table 4.11.

After the g(r) values from MC and experimental methods were transformed to g(r) values under unbounded conditions with the correction factors. Then, they were graphically compared to each other. In addition, the recommended range for g(r) of high-energy sources is $r \leq 10$ cm (8).

Table 4.9 Fourth-degree polynomial coefficients of correction factors (CF) used to quantitatively compare bounded to unbounded g(r) for common phantom shapes and sizes. CF was fitted as $CF = C_0 + C_1r + C_2r^2 + C_3r^3 + C_4r^4$ (8).

CF parameter	**Sphere** $CF = \frac{g(R_{sph}=40cm,r)}{g(R_{sph}=15cm,r)}$ **1cm ≤ r ≤ 15 cm**	**Cylinder** $CF = \frac{g(R_{sph}=40cm,r)}{g(R_{cyl}=20\ cm,r)}$ **1cm ≤ r ≤ 20 cm**	**Cube** $CF = \frac{g(R_{sph}=40cm,r)}{g(R_{cubc}=15cm,r)}$ **1cm ≤ r ≤ 15 cm**
C_0 [dimensionless]	1.002	1.001	1.002
C_1 [cm^{-1}]	-3.52×10^{-3}	-1.23×10^{-3}	-3.27×10^{-3}
C_2 [cm^{-2}]	2.06×10^{-3}	3.00×10^{-4}	1.31×10^{-3}
C_3 [cm^{-3}]	-2.39×10^{-4}	-2.40×10^{-5}	-2.46×10^{-4}
C_4 [cm^{-4}]	1.38×10^{-5}	1.90×10^{-6}	8.50×10^{-6}

Table 4.10 Correction factors (CF) used to transform g(r) for cubic phantom into approximate g(r) values for unbounded conditions.

Distance (cm)	CF	Distance (cm)	CF
0.1	1.0016859	2.3	0.9986537
0.2	1.0013964	2.4	0.9985789
0.3	1.0011303	2.5	0.9985008
0.4	1.0008861	2.6	0.9984183
0.5	1.0006623	2.7	0.9983306
0.6	1.0004576	2.8	0.9982367
0.7	1.0002706	2.9	0.9981356
0.8	1.0000999	3	0.9980265
0.9	0.9999443	3.5	0.9973308
1	0.9998025	4	0.996312
1.1	0.9996731	4.5	0.9948813
1.2	0.9995549	5	0.9929625
1.3	0.9994467	6	0.98742
1.4	0.9993472	7	0.9793305
1.5	0.9992553	8	0.968544
1.6	0.9991697	9	0.9551145
1.7	0.9990893	10	0.9393
1.8	0.999013	11	0.9215625
1.9	0.9989396	12	0.902568
2	0.998868	13	0.8831865
2.1	0.9987972	14	0.864492
2.2	0.9987261	15	0.8477625

Table 4.11 Correction factors (CF) used to transform g(r) for cylindrical phantom into approximate g(r) values for unbounded conditions.

Distance (cm)	CF	Distance (cm)	CF
0.1	1.00087998	2.3	0.99951916
0.2	1.00076581	2.4	0.99950726
0.3	1.00065737	2.5	0.99949922
0.4	1.00055451	2.6	0.999495
0.5	1.00045712	2.7	0.99949458
0.6	1.00036506	2.8	0.99949794
0.7	1.00027822	2.9	0.99950505
0.8	1.00019649	3	0.9995159
0.9	1.00011975	3.5	0.99962612
1	1.0000479	4	0.9998304
1.1	0.99998084	4.5	1.00013212
1.2	0.99991847	5	1.0005375
1.3	0.9998607	6	1.0016984
1.4	0.99980744	7	1.0034199
1.5	0.99975862	8	1.0058544
1.6	0.99971415	9	1.0091999
1.7	0.99967396	10	1.0137
1.8	0.99963798	11	1.0196439
1.9	0.99960614	12	1.0273664
2	0.9995784	13	1.0372479
2.1	0.99955469	14	1.0497144
2.2	0.99953496	15	1.0652375

CHAPTER V
RESULTS

5.1 Validation of DOSRZnrc

The absorbed dose distributions calculated by DOSRZnrc were validated with those calculated by Oncentra TPS in the values of relative absorbed dose on transverse axis and longitudinal axis of the source at several distances.

5.1.1 Relative absorbed dose on transverse axis of source

The relative absorbed doses obtained from Oncentra TPS and DOSRZnrc at radial distances from 0.1 cm to 15 cm along the transverse axis of source were shown in Tables 5.1 and graphically compared as shown in Figure 5.1-5.3. There were the percentage differences within 2% at radial distances from 0.2 cm to 3 cm as shown in Figure 5.4. For radial distance 0.1 cm near the source, the percentage differences were 11.85% and slightly increased up to 37% at radial distances beyond 3 cm to phantom boundaries as shown in Figure 5.5.

Table 5.1 The relative absorbed doses at radial distances from 0.1 cm to 15 cm away from the source center calculated by Oncentra TPS and DOSRZnrc.

Radial distance (cm)	Oncentra TPS	DOSRZnrc	%Differences
0.1	60.0141	67.1269	-11.85
0.2	20.7835	21.0387	-1.23
0.3	10.1866	10.2212	-0.34
0.4	5.9574	5.9665	-0.15
0.5	3.8834	3.8968	-0.34
0.6	2.7291	2.7346	-0.20
0.7	2.0198	2.0083	0.57
0.8	1.5538	1.5493	0.29
0.9	1.2317	1.2330	-0.11
1	1	1	0.00
1.1	0.8282	0.8288	-0.07
1.2	0.6972	0.6997	-0.36
1.3	0.5950	0.5993	-0.72
1.4	0.5137	0.5170	-0.64
1.5	0.4480	0.4508	-1.63
1.6	0.3942	0.3984	-1.07
1.7	0.3496	0.3519	-0.67
1.8	0.3121	0.3124	-0.09
1.9	0.2804	0.2823	-0.68
2	0.2533	0.2555	-0.87

Table 5.1 The relative absorbed doses at radial distances from 0.1 cm to 15 cm away from the source center calculated by Oncentra TPS and DOSRZnrc (Cont.).

Radial distance (cm)	Oncentra TPS	DOSRZnrc	%Differences
2.1	0.2298	0.2301	-0.09
2.2	0.2095	0.2130	-1.66
2.3	0.1917	0.1923	-0.29
2.4	0.1761	0.1779	-1.00
2.5	0.1624	0.1644	-1.24
2.6	0.1501	0.1523	-1.40
2.7	0.1392	0.1400	-0.54
2.8	0.1295	0.1306	-0.83
2.9	0.1207	0.1225	-1.44
3	0.1128	0.1138	-0.87
4	0.0632	0.0646	-2.13
5	0.0401	0.0415	-3.53
6	0.0275	0.0285	-3.69
7	0.0198	0.0210	-6.18
8	0.0148	0.0158	-6.71
9	0.0114	0.0123	-8.53
10	0.0089	0.0098	-10.20
11	0.0070	0.0079	-13.04
12	0.0056	0.0064	-14.76
13	0.0045	0.0054	-20.94
14	0.0035	0.0044	-26.06
15	0.0027	0.0038	-37.01

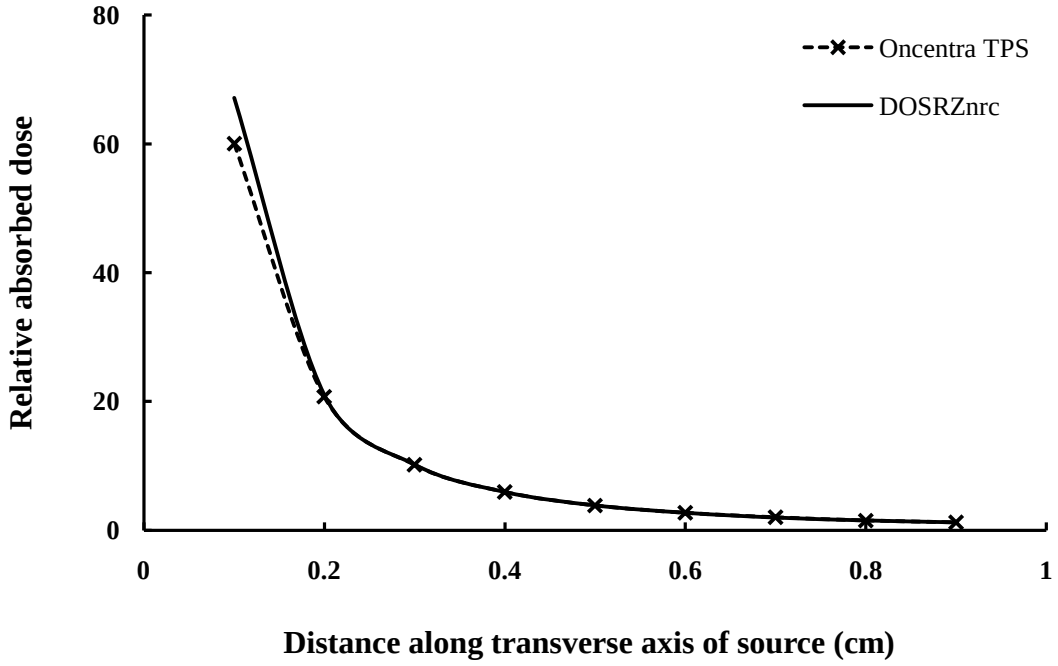

Figure 5.1 The relative absorbed dose profile curves at radial distances from 0.1 cm to 0.9 cm obtained from DOSRZnrc and Oncentra TPS.

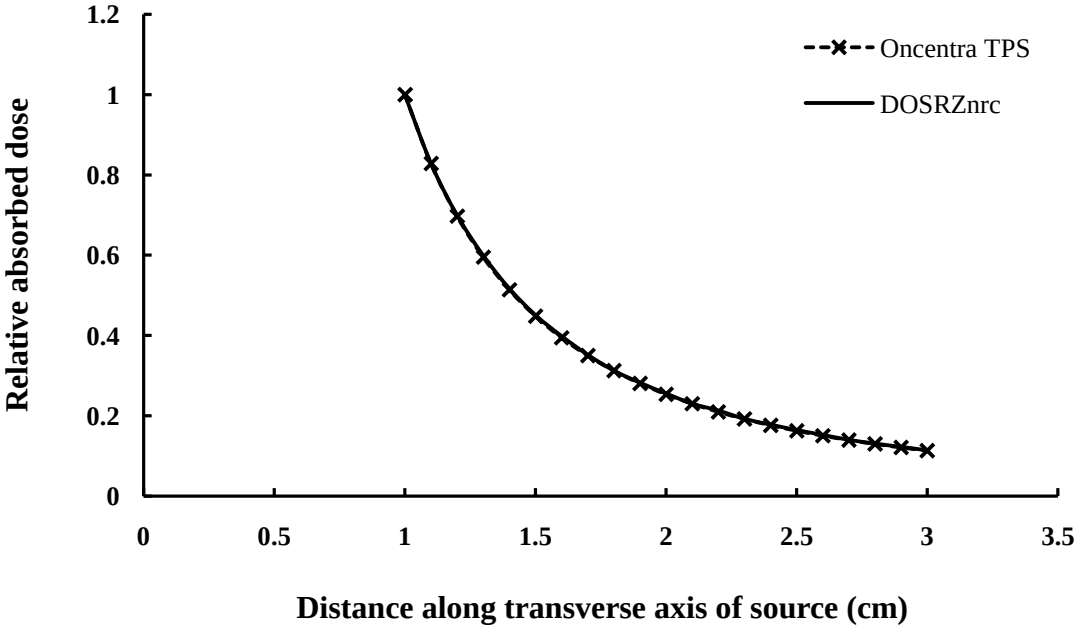

Figure 5.2 The relative absorbed dose profile curves at radial distances from 1 cm to 3 cm obtained from DOSRZnrc and Oncentra TPS.

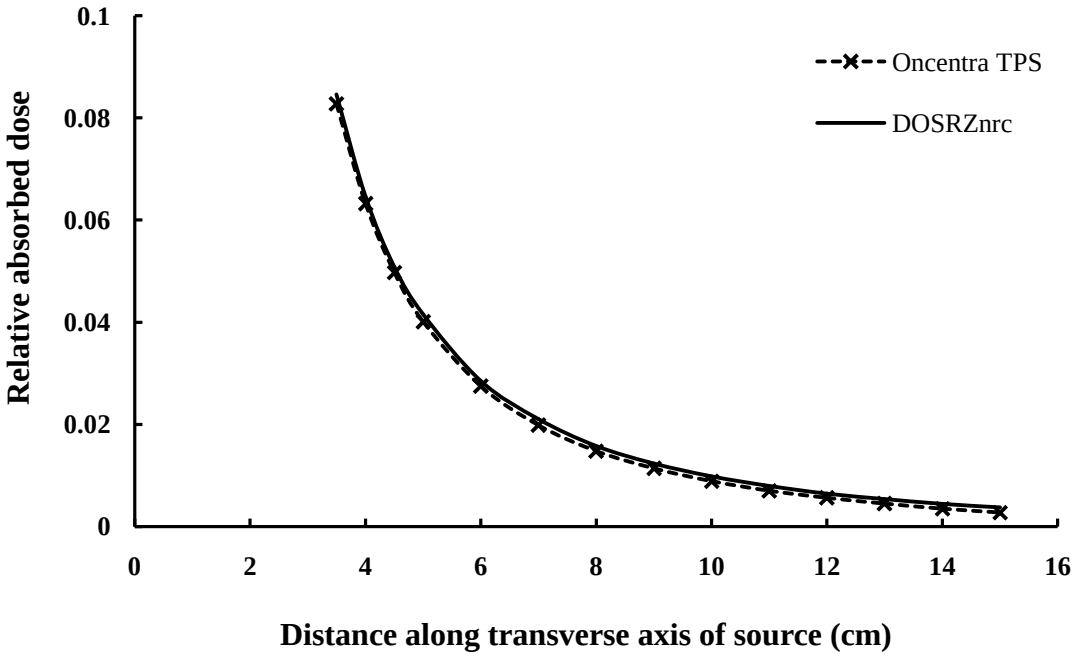

Figure 5.3 The relative absorbed dose profile curves at radial distances from 3.5 cm to 15 cm obtained from DOSRZnrc and Oncentra TPS.

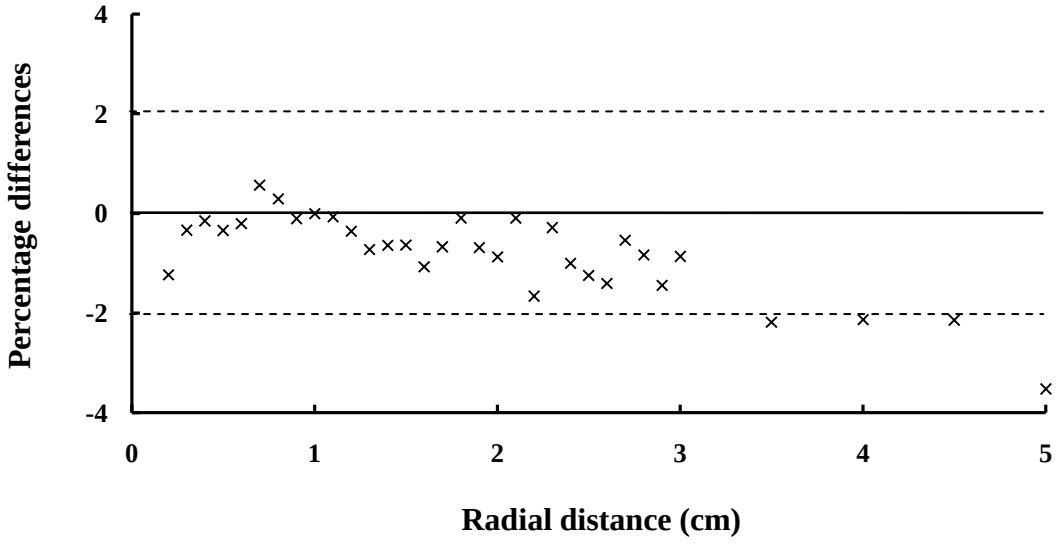

Figure 5.4 The percentage differences of relative absorbed dose obtained from DOSRZnrc and Oncentra TPS at radial distances of 0.2 cm to 5 cm along the transverse axis of the source.

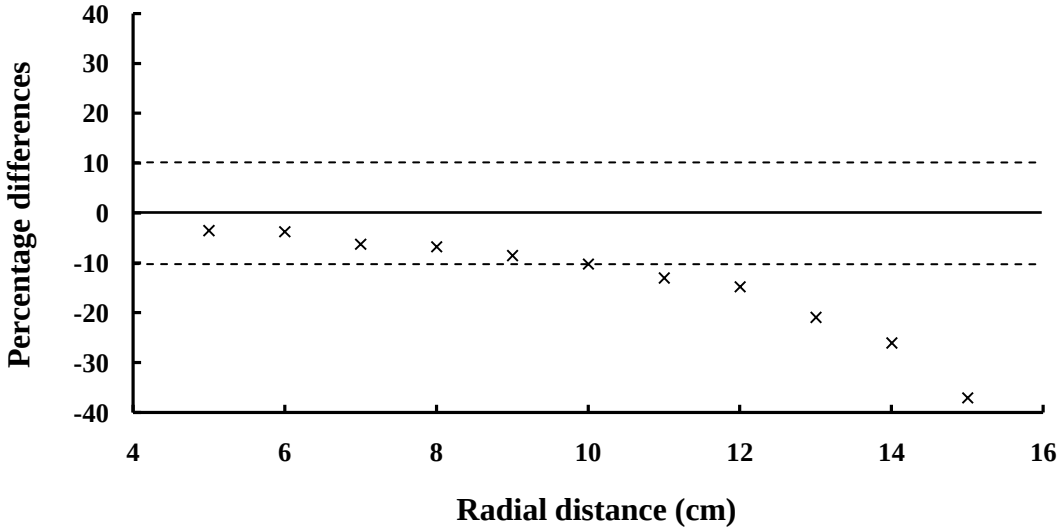

Figure 5.5 The percentage differences of relative absorbed dose obtained from DOSRZnrc and Oncentra TPS at radial distances of 5 cm to 15 cm along the transverse axis of the source.

5.1.2 Relative absorbed dose on longitudinal axis of source

The relative absorbed doses along the longitudinal axis of source (Z axis) obtained from DOSRZnrc and Oncentra TPS were graphically compared as relative absorbed dose profile curves at radial distances 0.2 cm to 5 cm from source center. For profile curves of DOSRZnrc and Oncentra TPS at radial distances 0.2 cm and 0.3 cm from source center, these profile curves were shown in Figure 5.6 with the percentage differences about 20% at radial distance 0.2 cm as shown in Figure 5.7 except for distances -0.5 cm and 0.5 cm along the longitudinal axis from the source center with the percentage differences of 26% and 36%, respectively as shown in Table 5.2 and the percentage differences about 10% at radial distance 0.3 cm as shown in Figure 5.8. Except for distances -0.5 cm and 0.5 cm along the longitudinal axis from the source center, there were percentage differences of 14% and 21%, respectively as shown in Table 5.2.

For the relative absorbed dose profile curves of DOSRZnrc and Oncentra TPS at radial distances 0.5 cm to 0.9 cm from source center as shown in Figure 5.9, there were the percentage differences about 10% for all distances as shown in Figure 5.10 - 5.12 and Table 5.2. In addition, there were the percentage differences of relative absorbed dose profile curves between DOSRZnrc and Oncentra TPS within 10% at radial distances of 1 cm to 5 cm from source center as shown in Figure 5.13 - 5.18 and Table 5.2.

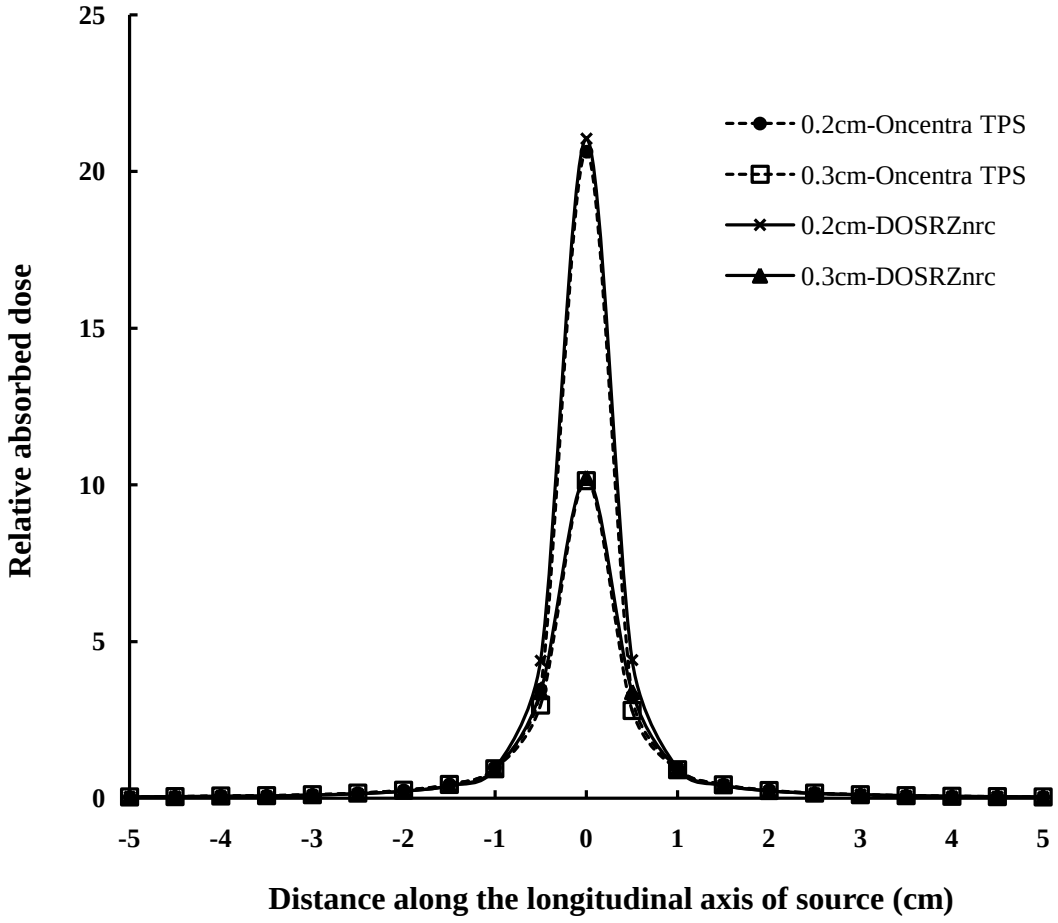

Figure 5.6 The relative absorbed dose profile curves at radial distances 0.2 cm and 0.3 cm obtained from DOSRZnrc and Oncentra TPS.

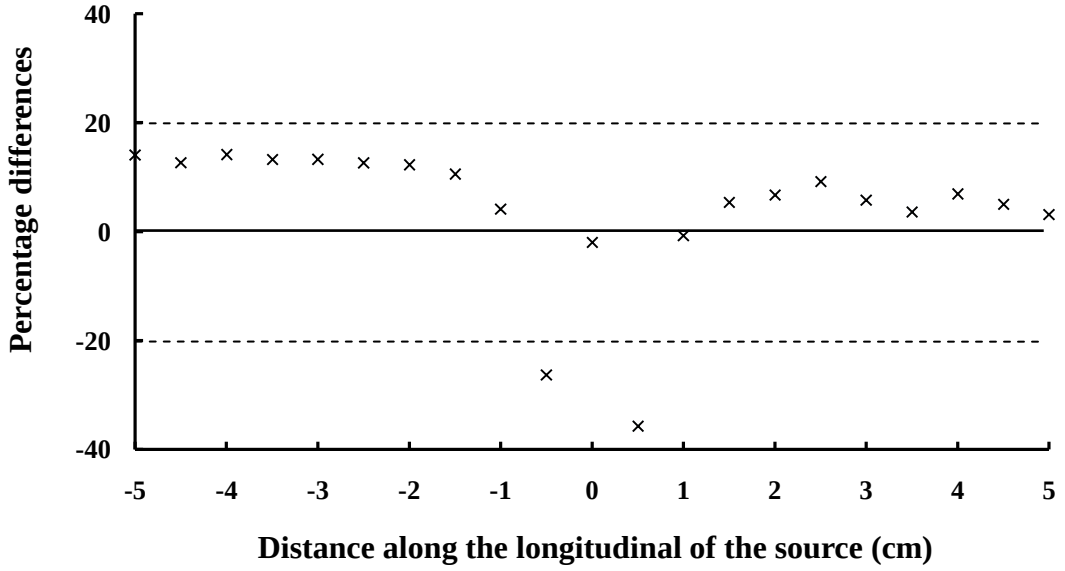

Figure 5.7 The percentage differences of relative absorbed dose at radial distance 0.2 cm obtained from DOSRZnrc and Oncentra TPS.

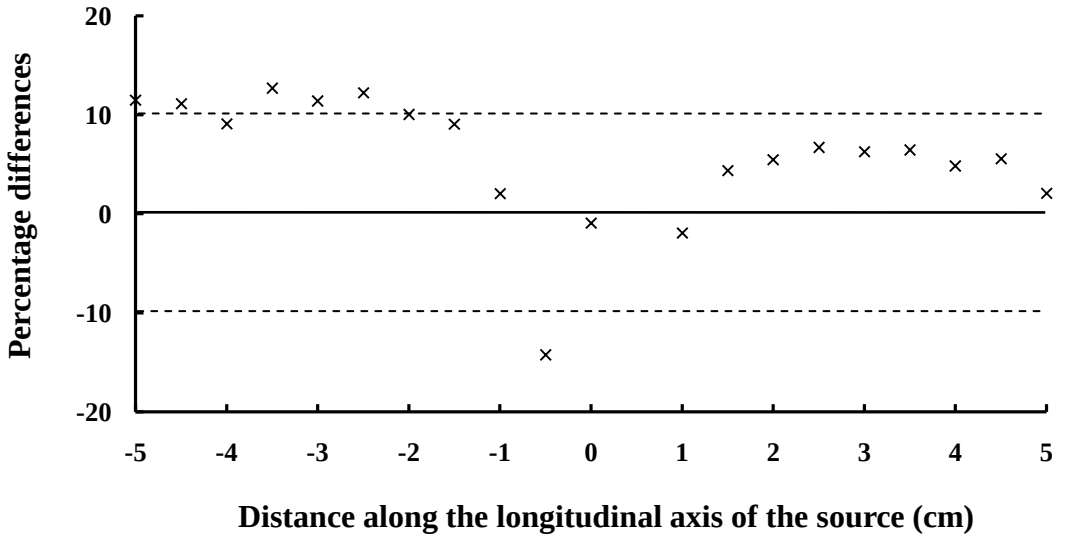

Figure 5.8 The percentage differences of relative absorbed dose at radial distance 0.3 cm obtained from DOSRZnrc and Oncentra TPS.

Table 5.2 The percentage differences of relative absorbed dose at radial distances from 0.2 cm to 5 cm away from longitudinal axis of source center obtained from DOSRZnrc and Oncentra TPS.

Z axis distance (cm)	**Radial distance (cm)**										
	0.1	**0.2**	**0.3**	**0.5**	**0.7**	**0.9**	**1**	**2**	**3**	**4**	**5**
-5.0	-	14	12	10	6	6	6	2	0	-2	-3
-4.5	-	13	11	9	8	8	6	3	0	-2	-3
-4.0	-	14	9	9	8	7	6	2	0	-2	-3
-3.5	-	13	13	10	8	6	6	2	0	-2	-3
-3.0	-	13	11	10	8	6	6	2	0	-2	-3
-2.5	-	13	12	10	8	6	4	1	0	-2	-3
-2.0	-	12	10	8	5	4	4	0	0	-2	-3
-1.5	-	11	9	5	3	3	2	0	-1	-2	-3
-1.0	-	4	2	0	0	12	1	0	-1	-2	-3
-0.5	-	-26	-14	-3	0	1	1	0	-1	-2	-3
0	-12	-2	-1	-1	0	0	0	-1	-1	-2	-3
0.5	-	-36	-21	-7	-3	-1	-1	0	-1	-2	-3
1.0	-	-1	-2	-3	-3	-2	-1	-1	-1	-2	-3
1.5	-	5	4	2	1	0	0	0	-1	-2	-3
2.0	-	7	5	5	4	2	2	-1	-1	-2	-3
2.5	-	9	7	6	4	3	3	0	-1	-2	-3
3.0	-	6	6	7	5	5	4	1	-1	-2	-4
3.5	-	4	6	6	6	5	5	0	-1	-2	-4
4.0	-	7	5	3	5	5	5	1	0	-2	-4
4.5	-	5	6	4	6	6	4	2	-2	-2	-4
5.0	-	3	2	5	5	6	4	2	-1	-3	-4

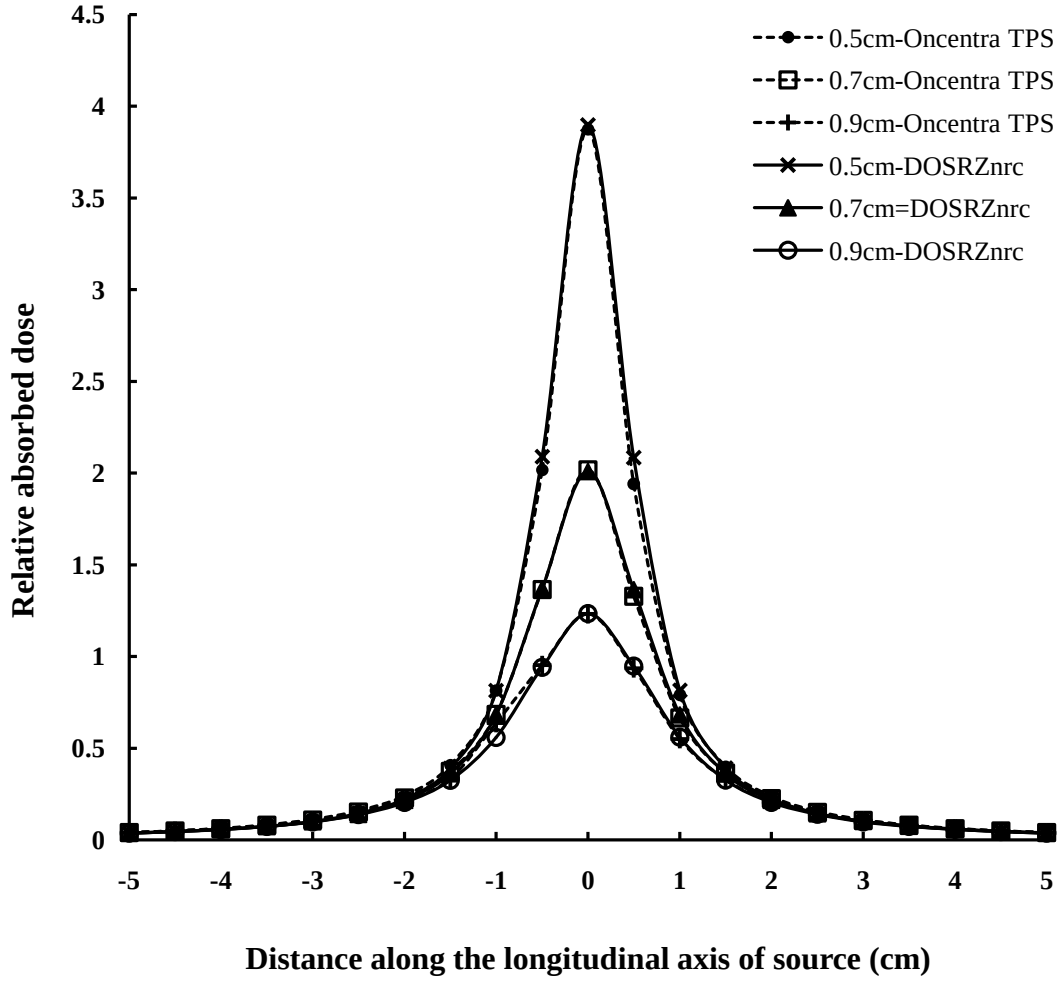

Figure 5.9 The relative absorbed dose profile curves at radial distances from 0.5 cm to 0.9 cm obtained from DOSRZnrc and Oncentra TPS.

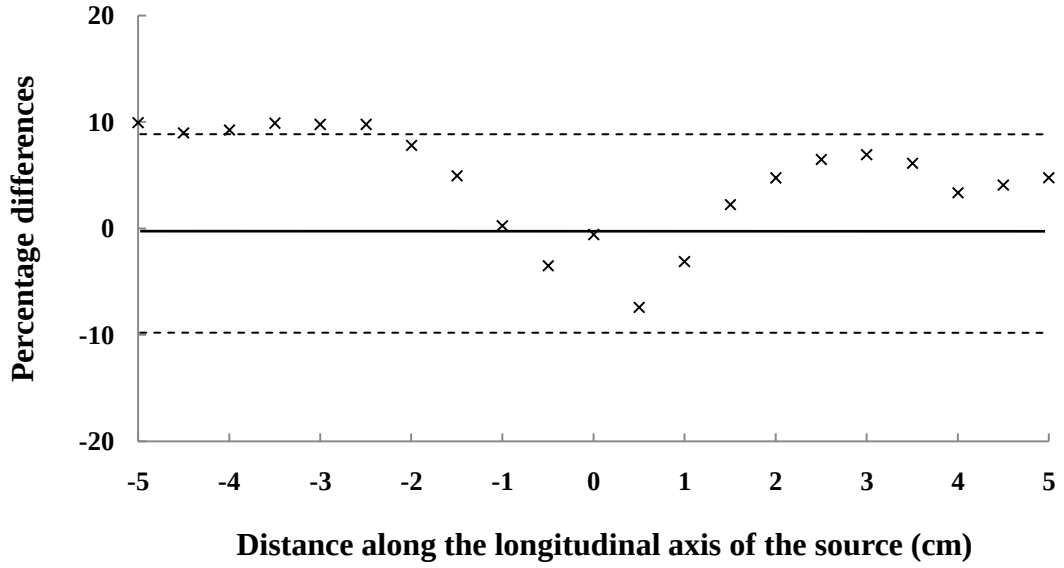

Figure 5.10 The percentage differences of relative absorbed dose at radial distance 0.5 cm obtained from DOSRZnrc and Oncentra TPS.

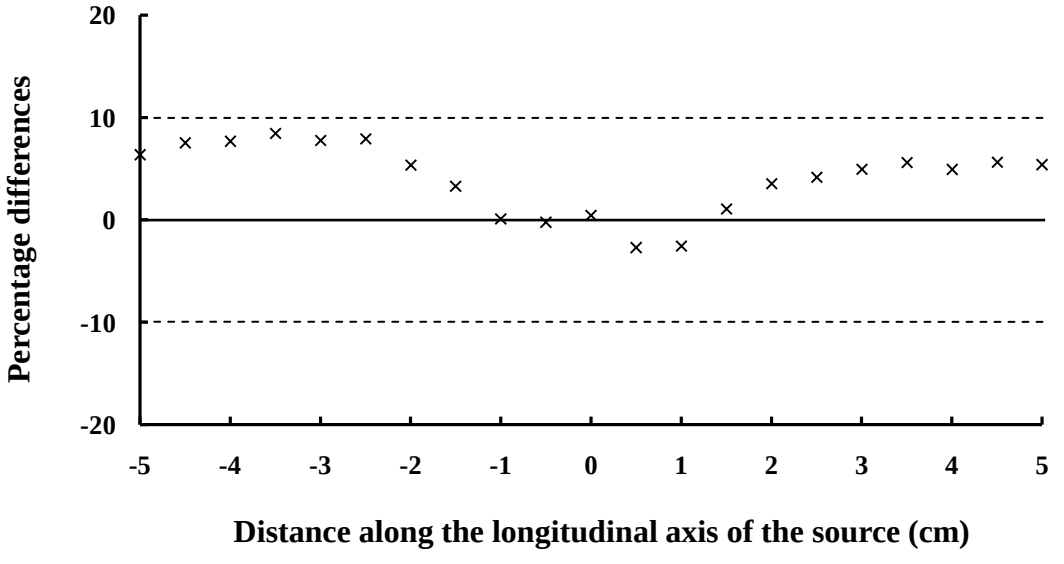

Figure 5.11 The percentage differences of relative absorbed dose at radial distance 0.7 cm obtained from DOSRZnrc and Oncentra TPS.

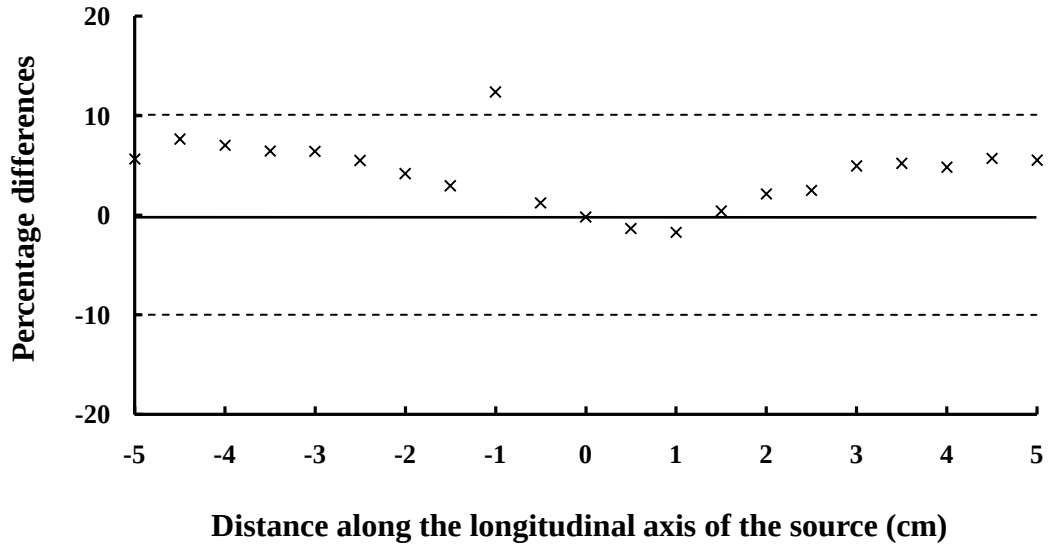

Figure 5.12 The percentage differences of relative absorbed dose at radial distance 0.9 cm obtained from DOSRZnrc and Oncentra TPS.

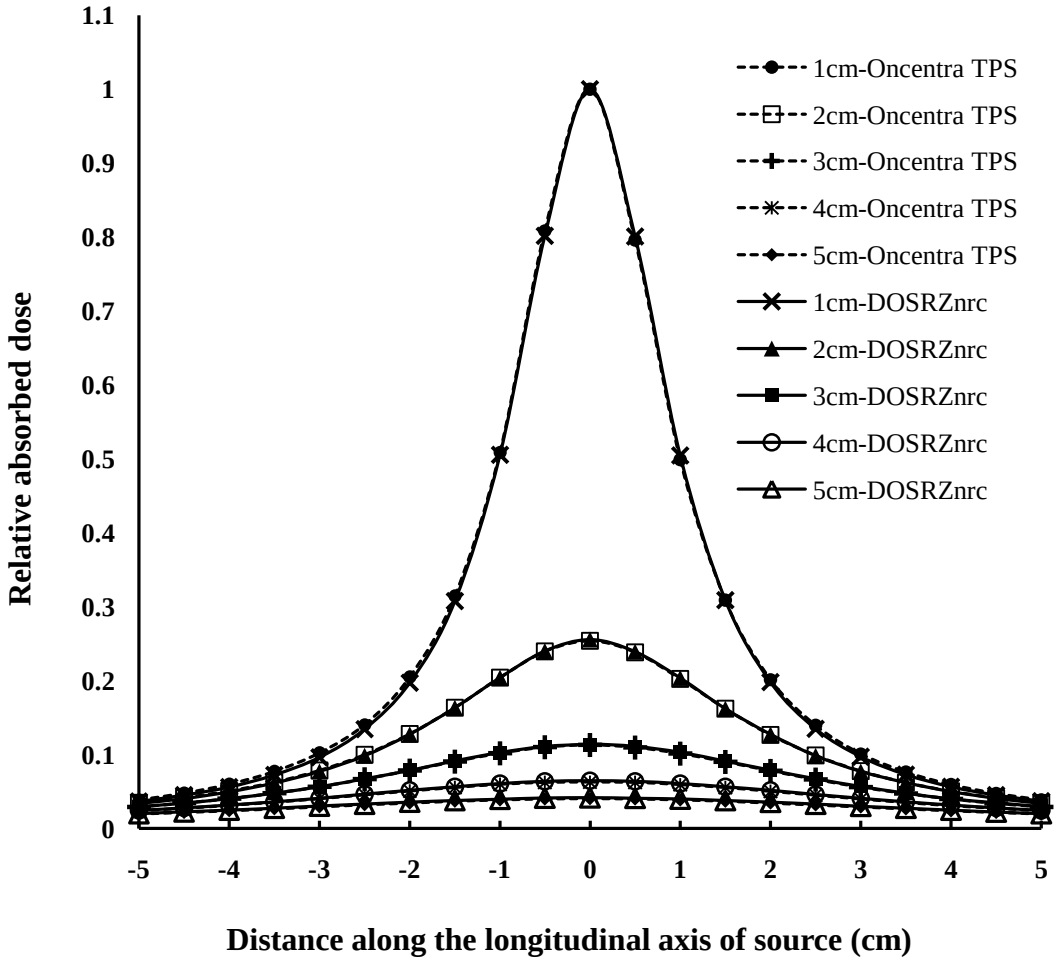

Figure 5.13 The relative absorbed dose profile curves at radial distances 1 cm to 5 cm obtained from DOSRZnrc and Oncentra TPS.

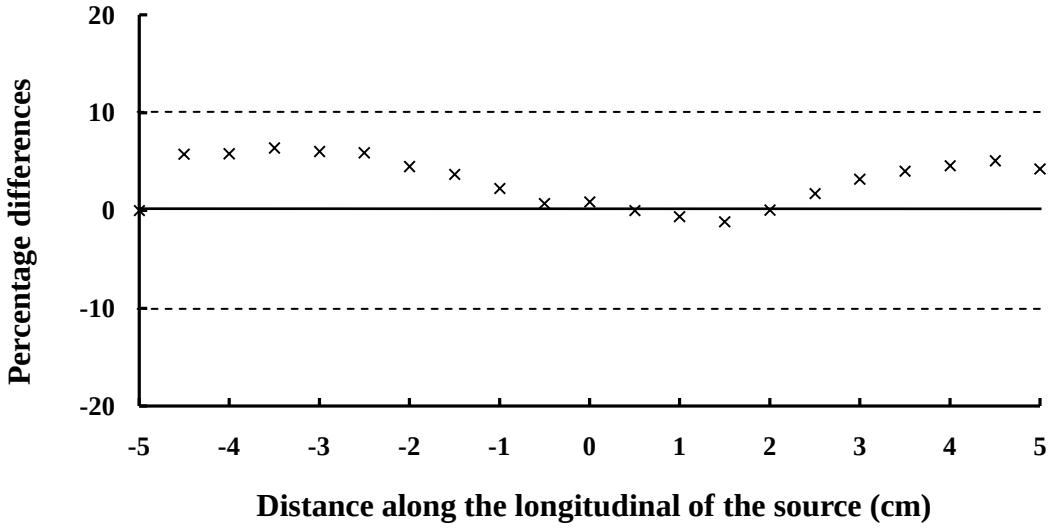

Figure 5.14 The percentage differences of relative absorbed dose at radial distance 1 cm obtained from DOSRZnrc and Oncentra TPS.

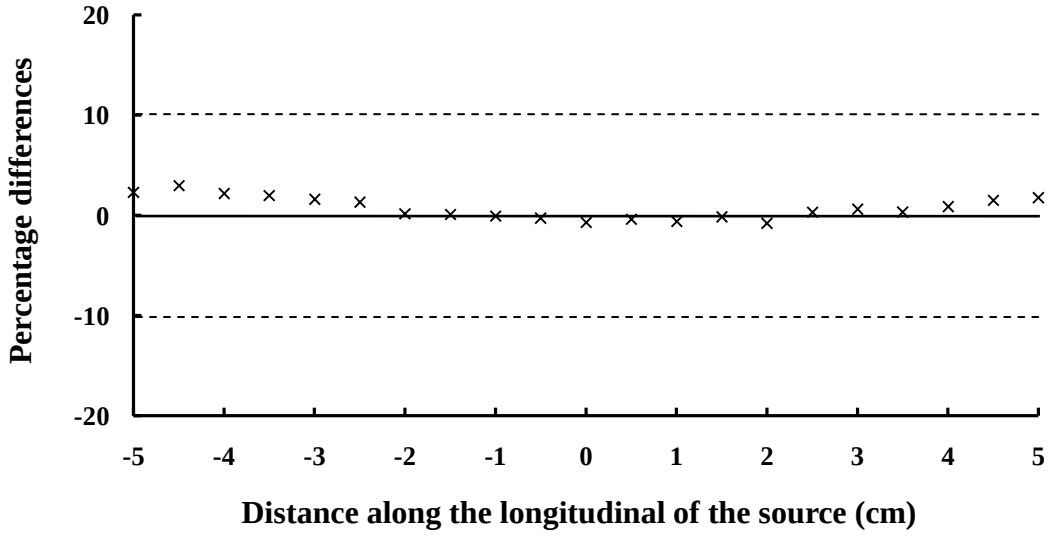

Figure 5.15 The percentage differences of relative absorbed dose at radial distance 2 cm obtained from DOSRZnrc and Oncentra TPS.

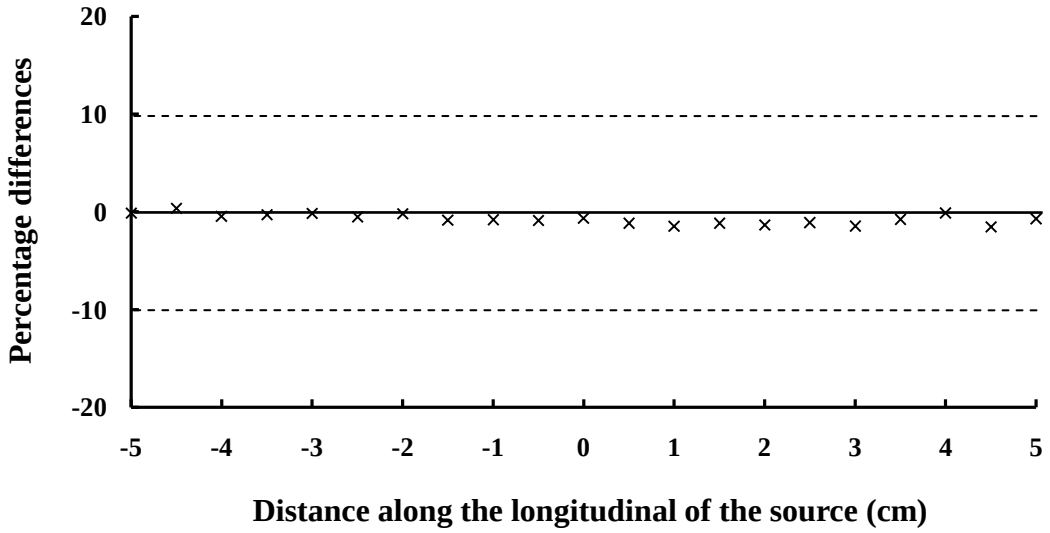

Figure 5.16 The percentage differences of relative absorbed dose at radial distance 3 cm obtained from DOSRZnrc and Oncentra TPS.

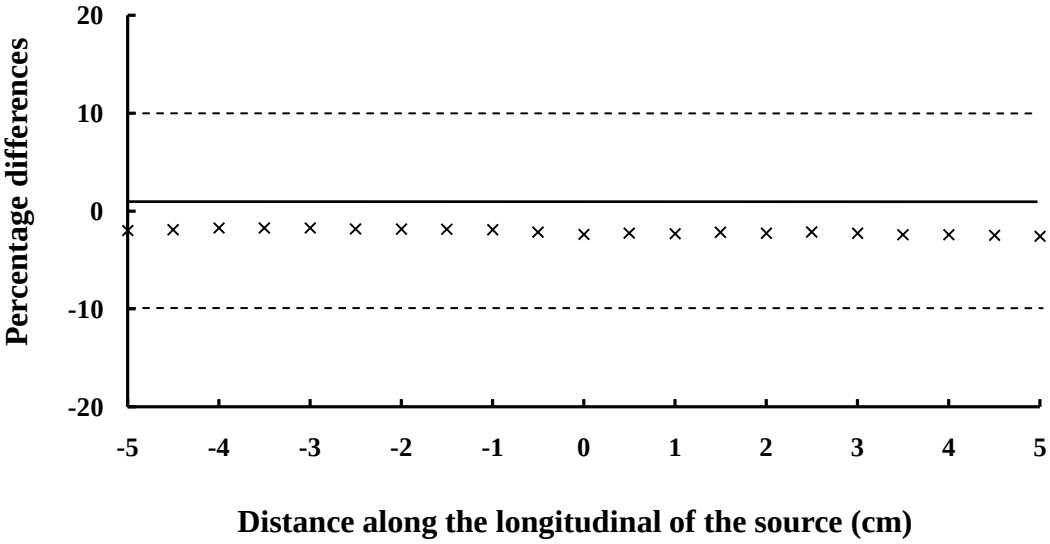

Figure 5.17 The percentage differences of relative absorbed dose at radial distance 4 cm obtained from DOSRZnrc and Oncentra TPS.

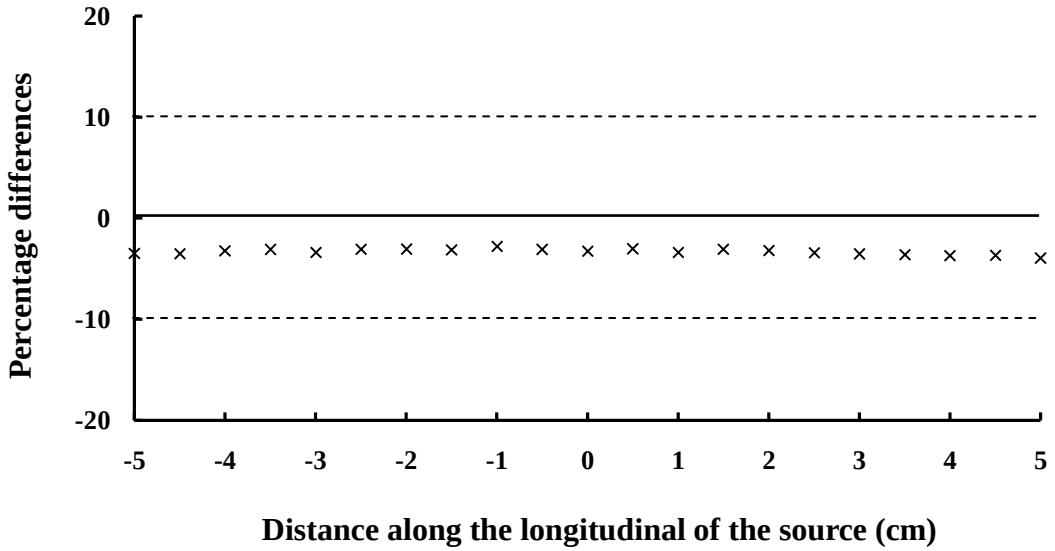

Figure 5.18 The percentage differences of relative absorbed dose at radial distance 5 cm obtained from DOSRZnrc and Oncentra TPS.

5.2 Absorbed dose calculations

The absorbed doses at radial distances from 0.1 cm to 15 cm along the transverse axis from the source calculated by DOSRZnrc were shown in Table 5.3.

Table 5.3 The absorbed doses (Gy per incident particle) at radial distances from 0.1 cm to 15 cm along the transverse axis of the source calculated by DOSRZnrc.

Radial distance (cm)	Absorbed dose (Gy/ incident particle)	Statistics
0.1	8.70E-12	1.47E-14
0.2	2.75E-12	5.78E-15
0.3	1.34E-12	3.29E-15
0.4	7.82E-13	2.17E-15
0.5	5.11E-13	1.57E-15
0.6	3.58E-13	1.20E-15
0.7	2.64E-13	9.48E-16
0.8	2.03E-13	7.75E-16
0.9	1.61E-13	6.51E-16
1	1.31E-13	5.53E-16
1.1	1.08E-13	4.80E-16
1.2	9.11E-14	4.21E-16
1.3	7.82E-14	3.75E-16
1.4	6.73E-14	3.33E-16
1.5	5.95E-14	3.03E-16
1.6	5.21E-14	2.72E-16
1.7	4.62E-14	2.49E-16
1.8	4.08E-14	2.27E-16
1.9	3.71E-14	2.10E-16
2	3.35E-14	1.94E-16

Table 5.3 The absorbed doses (Gy per incident particle) at radial distances from 0.1 cm to 15 cm along the transverse axis of the source calculated by DOSRZnrc (Cont.).

Radial distance (cm)	Absorbed dose (Gy/ incident particle)	Statistics
2.1	3.02E-14	1.33E-16
2.2	2.75E-14	1.24E-16
2.3	2.54E-14	1.16E-16
2.4	2.31E-14	1.08E-16
2.5	2.14E-14	1.01E-16
2.6	1.97E-14	9.52E-17
2.7	1.84E-14	9.04E-17
2.8	1.72E-14	8.53E-17
2.9	1.60E-14	8.09E-17
3	1.47E-14	7.60E-17
4	8.40E-15	2.26E-17
5	5.34E-15	1.57E-17
6	3.66E-15	1.17E-17
7	2.67E-15	9.08E-18
8	2.02E-15	7.28E-18
9	1.58E-15	5.96E-18
10	1.24E-15	4.94E-18
11	9.99E-16	4.19E-18
12	8.21E-16	3.59E-18
13	6.69E-16	3.08E-18
14	5.60E-16	2.71E-18
15	4.59E-16	2.34E-18

The values of absorbed dose from DOSRZnrc, LiF TLD-100 and EBT2 film measurements at radial distances from 0.3 cm to 15 cm along the transverse axis of the source were normalized with their doses at reference distance of r_0 = 1 cm and then, the values of relative absorbed dose from DOSRZnrc were used to compare with those from LiF TLD-100 and EBT2 film, respectively.

5.2.1 DOSRZnrc and LiF TLD-100

Table 5.4 showed that the relative absorbed doses obtained from DOSRZnrc were mostly less than those obtained from LiF TLD-100 with the percentage differences within 10%. Except for distance 0.3 cm near the source, there were the percentage differences of 86.88%.

Table 5.4 The relative absorbed doses obtained from DOSRZnrc and LiF TLD-100 rods at radial distances from 0.3 cm to 15 cm along the transverse axis of the source.

Radial distance (cm)	DOSRZnrc	TLD ±SD	%Differences
0.3	10.2589	19.1717 ± 1.35	-86.88
0.5	3.9154	3.7443 ± 0.21	4.37
1	1.0000	1.0000 ± 0.00	0.00
1.5	0.4556	0.4546 ± 0.01	0.21
2	0.2565	0.2622 ± 0.01	-2.24
2.5	0.1636	0.1693 ± 0.00	-3.46
3	0.1128	0.1198 ± 0.01	-6.19
4	0.0643	0.0686 ± 0.00	-6.62
5	0.0409	0.0450 ± 0.00	-9.91
6	0.0280	0.0301 ± 0.00	-7.30
7	0.0205	0.0218 ± 0.00	-6.57
8	0.0155	0.0164 ± 0.00	-6.17
9	0.0121	0.0127 ± 0.00	-5.03
10	0.0095	0.0102± 0.00	-7.52
11	0.0076	0.0080 ± 0.00	-4.86
12	0.0063	0.0064 ± 0.00	-1.29
13	0.0051	0.0053 ± 0.00	-2.66
14	0.0043	0.0042 ± 0.00	2.98
15	0.0035	0.0034 ± 0.00	4.78

5.2.2 DOSRZnrc and EBT2 film

Table 5.5 and Table 5.6 showed that the percentage differences of relative absorbed dose between DOSRZnrc and both EBT2 film measurements were about 10% at radial distances from 0.3 cm to 5 cm along the transverse axis of the source. For radial distances beyond 5 cm, the percentage differences were largely increased up to 500% in DOSRZnrc compared to EBT2 film with dose 400 cGy and up to 120% in DOSRZnrc compared to EBT2 film with dose 800 cGy.

Table 5.5 The relative absorbed dose obtained from DOSRZnrc and EBT2 film with dose of 400 cGy at radial distances from 0.3 cm to 15 cm along the transverse axis of the source.

Radial distance (cm)	DOSRZnrc	EBT2 film (400cGy) ± SD	%Differences
0.3	10.2589	9.2694 ± 2.86	9.65
0.5	3.9154	4.1223 ± 1.44	-5.29
0.7	2.0226	2.3273 ± 0.35	-15.06
0.8	1.5536	1.6691 ± 0.06	-7.43
0.9	1.2304	1.3248 ± 0.19	-7.67
1	1.0000	1.0000 ± 0.00	0.00
1.1	0.8288	0.8720 ± 0.11	-5.21
1.2	0.6974	0.6152 ± 0.25	11.79
1.3	0.5989	0.5952 ± 0.06	0.61
1.4	0.5157	0.5108 ± 0.01	0.94
1.5	0.4556	0.4789 ± 0.01	-5.12
1.6	0.3991	0.4198 ± 0.01	-5.18
1.7	0.3540	0.3679 ± 0.01	-3.91
1.8	0.3122	0.3189 ± 0.01	-2.13
1.9	0.2839	0.2860 ± 0.01	-0.76
2	0.2565	0.2669 ± 0.00	-4.08
2.1	0.2315	0.2358 ± 0.01	-1.86
2.2	0.2108	0.1883 ± 0.07	10.70
2.3	0.1944	0.1911 ± 0.01	1.70
2.4	0.1772	0.1787 ± 0.01	-0.82
2.5	0.1637	0.1761 ± 0.00	-7.62

Table 5.5 The relative absorbed dose obtained from DOSRZnrc and EBT2 film with dose of 400 cGy at radial distances from 0.3 cm to 15 cm along the transverse axis of the source (Cont.).

Radial distance (cm)	DOSRZnrc	EBT2 film (400cGy) ± SD	%Differences
2.6	0.1508	0.1511 ± 0.01	-0.2
2.7	0.1406	0.1485 ± 0.01	-5.6
2.8	0.1314	0.1327 ± 0.00	-1.0
2.9	0.1224	0.1050 ± 0.01	14.2
3	0.1128	0.1283 ± 0.01	-13.7
4	0.0643	0.0630 ± 0.00	2.1
5	0.0409	0.0405 ± 0.01	1.1
6	0.0280	0.0171 ± 0.00	39.0
7	0.0205	0.0066 ± 0.01	67.9
8	0.0155	-0.0015 ± 0.00	109.6
9	0.0121	-0.0001 ± 0.01	101.0
10	0.0095	-0.0006 ± 0.01	106.0
11	0.0076	-0.0065 ± 0.01	184.7
12	0.0063	-0.0122 ± 0.01	294.7
13	0.0051	-0.0094 ± 0.01	283.9
14	0.0043	-0.0171 ± 0.00	499.1
15	0.0035	-0.0133 ± 0.01	478.2

Table 5.6 The relative absorbed dose obtained from DOSRZnrc and EBT2 film with dose of 800 cGy at radial distances from 0.3 cm to 15 cm along the transverse axis of the source.

Radial distance (cm)	DOSRZnrc	EBT2 film (800cGy) ± SD	%Differences
0.3	10.2589	9.4638 ± 1.01	7.75
0.5	3.9154	4.4623 ± 0.41	-13.97
0.7	2.0226	2.3127 ± 0.47	-14.34
0.8	1.5536	1.7291 ± 0.09	-11.30
0.9	1.2305	1.3172 ± 0.16	-7.05
1	1.0000	1.0000 ± 0.00	0.00
1.1	0.8289	0.8783 ± 0.08	-5.97
1.2	0.6974	0.7511 ± 0.04	-7.70
1.3	0.5989	0.5286 ± 0.14	11.73
1.4	0.5157	0.5210 ± 0.02	-1.03
1.5	0.4556	0.4716 ± 0.02	-3.51
1.6	0.3991	0.3765 ± 0.12	5.68
1.7	0.3540	0.3609 ± 0.02	-1.93
1.8	0.3122	0.3175 ± 0.01	-1.68
1.9	0.2839	0.2724 ± 0.02	4.03
2	0.2565	0.2716 ± 0.01	-5.89
2.1	0.2315	0.2389 ± 0.01	-3.21
2.2	0.2108	0.2223 ± 0.01	-5.44
2.3	0.1944	0.1921 ± 0.01	1.21
2.4	0.1772	0.1778 ± 0.01	-0.33
2.5	0.1637	0.1686 ± 0.01	-2.99

Table 5.6 The relative absorbed dose obtained from DOSRZnrc and EBT2 film with dose of 800 cGy at radial distances from 0.3 cm to 15 cm along the transverse axis of the source (Cont.).

Radial distance (cm)	DOSRZnrc	EBT2 film (800cGy) ± SD	%Differences
2.6	0.1508	0.1567 ± 0.01	-3.92
2.7	0.1406	0.1434 ± 0.01	-1.98
2.8	0.1314	0.1319 ± 0.01	-0.32
2.9	0.1224	0.1215 ± 0.01	0.75
3	0.1128	0.1211 ± 0.00	-7.33
4	0.0643	0.06571 ± 0.00	-2.11
5	0.0409	0.0403 ± 0.00	1.40
6	0.0280	0.0200 ± 0.01	28.65
7	0.0205	0.0144 ± 0.00	29.62
8	0.0155	0.0085 ± 0.00	45.23
9	0.0121	0.0051 ± 0.00	57.87
10	0.0095	0.0051 ± 0.00	46.24
11	0.0076	0.0005 ± 0.00	93.24
12	0.0063	-0.0025 ± 0.00	140.53
13	0.0051	-0.0039 ± 0.00	175.81
14	0.0043	-0.00278 ± 0.00	163.67
15	0.0035	-0.0006 ± 0.00	115.95

5.3 Radial dose function, g(r)

The g(r) values obtained from DOSRZnrc, LiF TLD-100 and EBT2 film represented in $g_{MC}(r)$, $g_{TLD}(r)$ and $g_{EBT2}(r)$, respectively.

5.3.1 The g(r) values from DOSRZnrc and LiF TLD-100

Table 5.7 showed that the percentage differences of g(r) values between DOSRZnrc and LiF TLD-100 were 86.96% at radial distance 0.3 cm, within 10% at radial distances from 0.5 cm to 11 cm and slightly increased up to 25% at radial distances beyond 11 cm. Furthermore, the g(r) values between DOSRZnrc and LiF TLD-100 were graphically compared in Figure 5.19 and Figure 5.20 for radial distances from 0.3 cm to 1 cm and radial distances 1 cm to 15 cm, respectively.

Table 5.7 The radial dose functions, g(r), at radial distances from 0.3 cm to 15 cm obtained from DOSRZnrc and LiF TLD-100**.**

Radial distance (cm)	DOSRZnrc	LiF TLD-100	%Differences
0.3	1.0149	1.8975	-86.96
0.5	1.0094	0.9655	4.35
1	1.0000	0.9998	0.02
1.5	1.0188	1.0161	0.27
2	1.0174	1.0395	-2.17
2.5	1.0133	1.0474	-3.37
3	1.0054	1.0660	-6.03
4	1.0192	1.0828	-6.24
5	1.0128	1.1047	-9.07
6	1	1.0576	-5.76
7	0.9963	1.0362	-4.00
8	0.9858	1.0078	-2.23
9	0.9761	0.9702	0.60
10	0.9501	0.9465	0.38
11	0.9337	0.8849	5.23
12	0.9201	0.8187	11.02
13	0.8881	0.7763	12.59
14	0.8738	0.6982	20.10
15	0.8345	0.6324	24.22

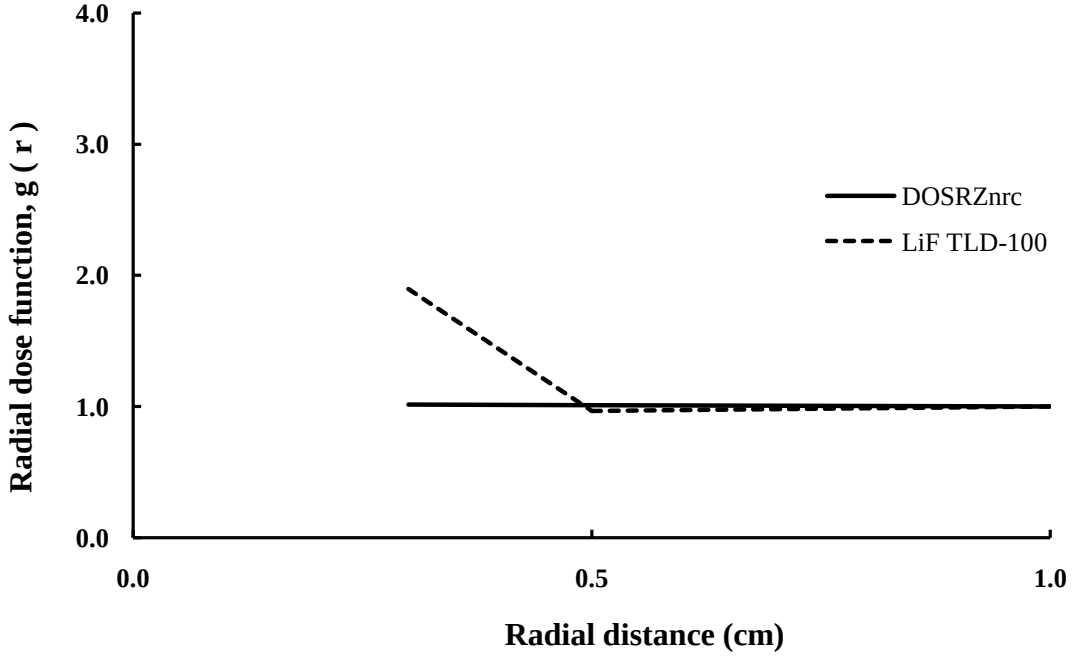

Figure 5.19 The g(r) values obtained from DOSRZnrc and TLD at radial distances from 0.3 cm to 1 cm**.**

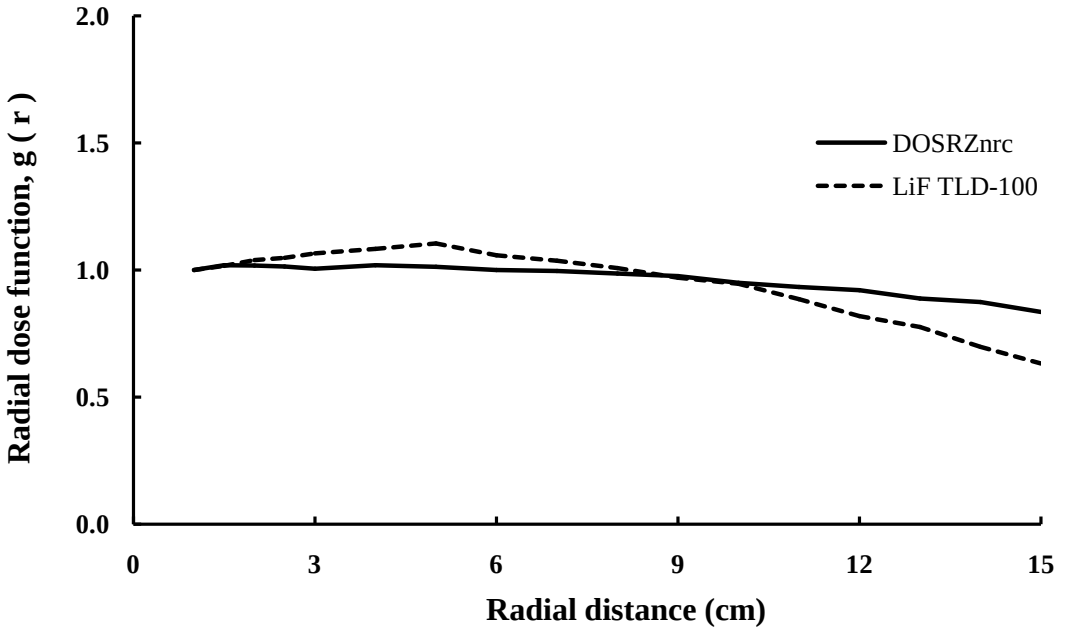

Figure 5.20 The g(r) values obtained from DOSRZnrc and TLD at radial distances from 1 cm to 15 cm.

5.3.2 The g(r) values from DOSRZnrc and EBT2 film

The percentage differences of g(r) values between DOSRZnrc and EBT2 films with doses of 400 cGy and 800 cGy were about 10% for all radial distances from 0.3 cm to 5 cm as shown in Table 5.8 and Table 5.9. Moreover, the g(r) values between DOSRZnrc and two data set of EBT2 film were graphically compared in Figure 5.21 for radial distances 0.3 cm to 5 cm.

Table 5.8 The radial dose functions, g(r), at radial distances from 0.3 cm to 5 cm obtained from DOSRZnrc and EBT2 film with doses of 400 cGy.

Radial distance (cm)	DOSRZnrc	EBT2 film (400cGy)	%Differences
0.3	1.0149	0.9174	9.60
0.5	1.0094	1.0630	-5.31
0.7	1.0021	1.1530	-15.06
0.8	1.0003	1.0746	-7.42
0.9	0.9992	1.0757	-7.65
1	1.0000	0.9998	0.02
1.1	1.0010	1.0529	-5.18
1.2	1.0010	0.8827	11.82
1.3	1.0076	1.0011	0.65
1.4	1.0053	0.9953	0.99
1.5	1.0188	1.0704	-5.06
1.6	1.0150	1.0669	-5.12
1.7	1.0158	1.0548	-3.85
1.8	1.0039	1.0246	-2.07
1.9	1.0165	1.0235	-0.69
2	1.0174	1.0581	-4.00
2.1	1.0120	1.0300	-1.78
2.2	1.0113	0.9024	10.77
2.3	1.0193	1.0010	1.79
2.4	1.0114	1.0187	-0.72
2.5	1.0133	1.0895	-7.52
2.6	1.0095	1.0104	-0.09
2.7	1.0153	1.0709	-5.48
2.8	1.0205	1.0290	-0.83
2.9	1.0194	0.8733	14.33
3	1.0054	1.1417	-13.55
4	1.0192	0.9948	2.40
5	1.0128	0.9942	1.83

Table 5.9 The radial dose functions, g(r), at radial distances from 0.3 cm to 5 cm obtained from DOSRZnrc and EBT2 film with doses of 800 cGy.

Radial distance (cm)	DOSRZnrc	EBT2 film (800cGy)	%Differences
0.3	1.0149	0.9367	7.71
0.5	1.0094	1.1507	-13.99
0.7	1.0021	1.1458	-14.34
0.8	1.0003	1.1133	-11.29
0.9	0.9992	1.0695	-7.03
1	1.0000	0.9998	0.02
1.1	1.0010	1.0604	-5.93
1.2	1.0010	1.0777	-7.66
1.3	1.0076	0.8891	11.76
1.4	1.0053	1.0151	-0.98
1.5	1.0188	1.0540	-3.46
1.6	1.0150	0.9568	5.73
1.7	1.0158	1.0348	-1.87
1.8	1.0039	1.0201	-1.62
1.9	1.0165	0.9749	4.09
2	1.0174	1.0765	-5.81
2.1	1.0120	1.0437	-3.14
2.2	1.0113	1.0655	-5.35
2.3	1.0193	1.0061	1.29
2.4	1.0114	1.0137	-0.23
2.5	1.0133	1.0426	-2.89
2.6	1.0095	1.0479	-3.81
2.7	1.0153	1.0342	-1.86
2.8	1.0205	1.0225	-0.20
2.9	1.0194	1.0104	0.88
3	1.0054	1.0775	-7.17
4	1.0192	1.0370	-1.75
5	1.0128	0.9911	2.15

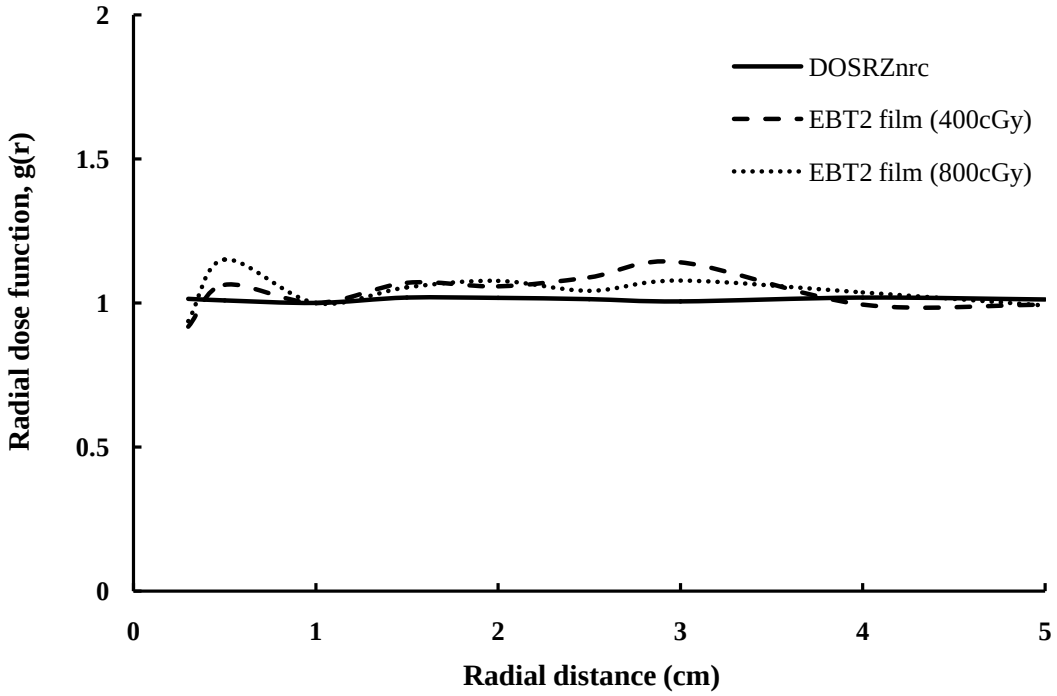

Figure 5.21 The g(r) values obtained from DOSRZnrc and EBT2 film with the dose 400 cGy and 800 cGy at radial distances 0.3 cm to 5 cm.

5.3.3 The g(r) values from DOSRZnrc and previous studies

In this study, we graphically compared our g(r) values obtained from DOSRZnrc with other studies as shown in Figure 5.22. The percentage differences between DOSRZnrc and other studies were less than 3%. The previous studies were the report of the AAPM and ESTRO 2012 (8), the database from CLRP TG-43 (6) and the study of Devan et al. (50).

In the report of the AAPM and ESTRO 2012, they provided the consensus datasets for commercially available high-energy photon sources that included the values of radial dose function for Nucletron HDR ^{192}Ir brachytherapy source using in this study as shown in Table 5.10. In the CLRP TG-43 database, these databases were belonging to the homepage of Carleton University for TG-43 brachytherapy dosimetry parameters. All parameters were calculated using EGSnrc MC user code BrachyDose (51). In addition, the g(r) values in the CLRP TG-43 database were calculated at differences ranging from 0.2 cm to 20 cm as shown in Table 5.10. In the study of Devan et al., the MC N-particle transport code system (MCNP) version 4B computer program was used to calculate the TG-43 dosimetric parameters for various commercially available brachytherapy sources that included the radial dose function for Nucletron HDR ^{192}Ir brachytherapy source as shown in Table 5.10.

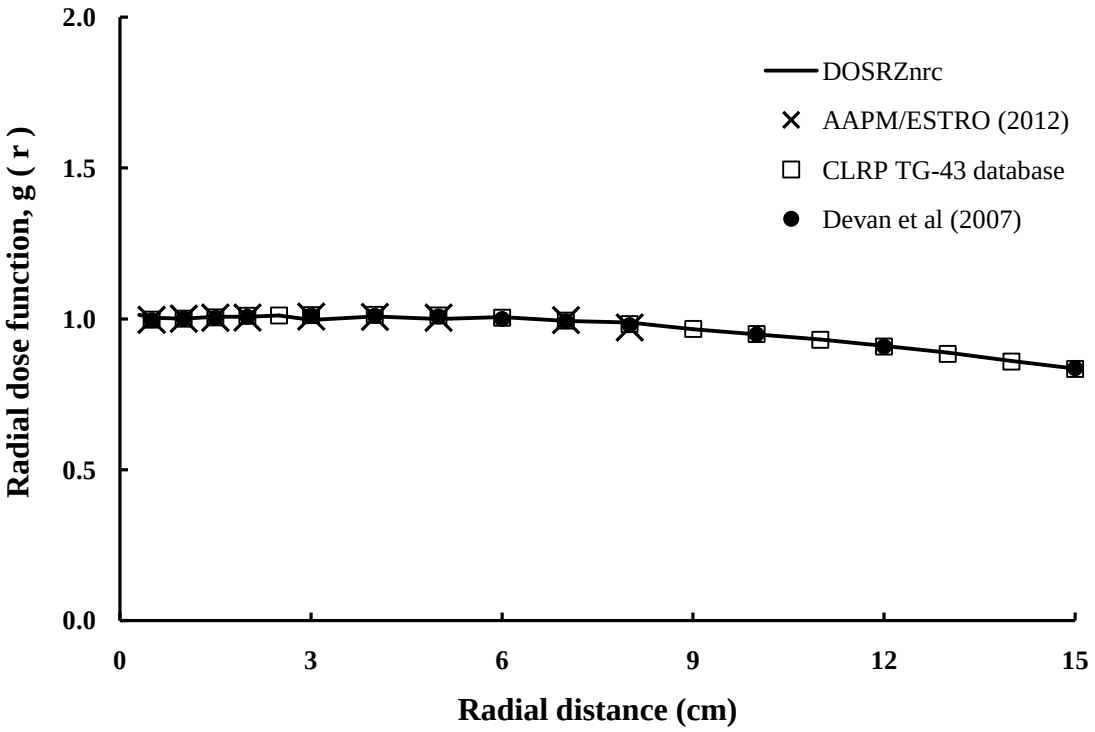

Figure 5.22 The g(r) values for Nucletron HDR ^{192}Ir source obtained from DOSRZnrc compared to other studies (6, 8, 50).

Table 5.10 The g(r) values for Nucletron HDR ^{192}Ir source obtained from DOSRZnrc, AAPM/ESTRO (2012), CLRP TG-43 database and the study of Devan et al. (2007).

Radial distance (cm)	DOSRZnrc	AAPM/ESTRO (2012)	CLRP TG-43 Database	Devan et al. (2007)
0.5	1.0094	0.997	0.997	0.995
1	1	1	1	1
1.5	1.0188	1.003	1.005	1.003
2	1.0174	1.005	1.010	1.007
2.5	1.0133	-	1.011	-
3	1.0054	1.008	1.012	1.011
4	1.0192	1.007	1.013	1.010
5	1.0128	1.003	1.011	1.008
6	1	-	1.003	0.999
7	0.9963	0.996	0.994	0.992
8	0.9858	0.972	0.982	0.979
9	0.9761	-	0.966	-
10	0.9501	0.939	0.949	0.948
11	0.9337	-	0.93	-
12	0.9201	-	0.908	0.908
13	0.8881	-	0.884	-
14	0.8738	-	0.858	-
15	0.8345	-	0.834	0.836

CHAPTER VI
DISCUSSION

In this study, the MC method was used to calculate the absorbed dose distribution around the Nucletron HDR ^{192}Ir brachytherapy source by using DOSRZnrc MC code. In addition, these results must be compared with the experimental measurements as recommendation from AAPM TG-43 reports (2, 20). This chapter will summarize and discuss the results from the study.

6.1 Validation of DOSRZnrc

The validation of DOSRZnrc calculation by Oncentra TPS showed that there was a good agreement within 2% at radial distances from 0.2 cm to 3 cm and within 5% at radial distances from 4 cm to 6 cm along the transverse axis from the source. A high difference presented at radial distances near the source (≤ 0.1 cm) and the phantom boundaries (≥ 6 cm) along the transverse axis of the source. At the distances along the longitudinal axis from the source center, the results of relative absorbed dose between DOSRZnrc and Oncentra TPS showed that there was a good agreement within 10% for radial distances 5 cm along the transverse axis from the source center except at radial distances near the source (≤ 0.3 cm) with high differences up to 36% as shown in Table 5.2.

A high difference at distances near the source was the weak point of Oncentra TPS based on TG-43 dose calculation formalism due to not account the heterogeneity effects, radiation attenuation and scattering of the source. As shown in Table 5.2, the radial distances of 0.2 cm to 0.3 cm along the transverse axis from the source center were close to the source (source outer diameter of 0.09 cm) and the distances of 0.2 cm to 0.3 cm along the longitudinal axis from the source center were near the distal and proximal ends of the source (source length of 0.45 cm). These could cause the high differences between DOSRZnrc and Oncentra TPS at distances

near the source. Moreover, the variation of source tip modeling between DOSRZnrc and Oncentra TPS due to the limitation of DOSRZnrc can also cause high differences at distances of 0.2 cm to 0.3 cm along the longitudinal axis from the source center. In addition, a high difference between DOSRZnrc and Oncentra TPS at radial distances larger than 6 cm from the source center to the phantom boundaries caused by the limitation of Oncentra TPS based on TG-43 dose calculation formalism for not accounting radiation scattering effects near the phantom boundaries.

Our results, which the difference between the relative absorbed dose calculated from Oncentra TPS and DOSRZnrc less than 2% at radial distances from 0.2 cm to 3 cm and within 5% at radial distances from 4 cm to 6 cm along the transverse axis from the source, were in accordance with the study of Aliresa Naseri and Asghar Mesbahi (9). They validated the accuracy of TPS calculations for three ^{60}Co sources using MCNP4C Monte Carlo code and their result demonstrated a good agreement (< 2%) between TPS and MC except for distances less than 1 cm and beyond the tip of the source. They mentioned that there was a small difference at point beyond the tip of the source because the algorithm in TPS cannot consider the photon attenuation.

In the study of Uniyal et al. (52), they used Gafchromic EBT2 film to verify the accuracy of TPS in homogeneous and heterogeneous mediums. Their study showed that the relative depth doses obtained by EBT2 film and TPS were good agreement with each other at distances up to 2 cm with the differences within 3% in case of homogeneous medium. Because the values of relative depth doses were defined as the ratio of dose rate at the given radial distance to dose rate at the reference distance of 1 cm along the transverse axis from the source center that similar to the values of relative absorbed dose in our study so these results were similar to our study Moreover, our results were good agreement with the criteria of IAEA-TRS 430 report with the differences less than 5% between Oncentra TPS and DOSRZnrc dose calculation (53).

For all of these criteria, DOSRZnrc calculations of absorbed dose around Nucletron HDR ^{192}Ir source in this study were acceptable at radial distances from 0.2 cm to 6 cm along the transverse axis of the source and these distances were clinical distances in brachytherapy treatment.

6.2 Experimental measurements

The results of absorbed dose distribution calculated by DOSRZnrc were used to compare with LiF TLD-100 and EBT2 measurements.

6.2.1 LiF TLD-100 measurements

Our results of relative absorbed dose were slightly high differences within 10% between DOSRZnrc and LiF TLD-100 for all radial distances from 0.5 cm to 15 cm. And very high differences for radial distances near the source ($\leq$ 0.3 cm) were noticed that might be caused by the physical size of LiF TLD-100 rod that can significantly affect the accuracy of dose measurement due to the combination of high dose gradients and source self-attenuation. For the slightly high differences about 10% for all radial distances from 0.5 cm to 15 cm along the transverse axis of the source center might be caused by the combination of the uncertainties of TLD measurements such as the uncertainties in TLD calibration, annealing, reading and the limitation of our dedicated phantom during measurements.

6.2.2 EBT2 film measurements

The comparison of relative absorbed doses from DOSRZnrc and EBT2 film showed that there were differences about 10% for radial distances from 0.3 cm to 5 cm along the transverse axis from the source center. For radial distances beyond 6 cm, there was an incorrect of dose measurement using EBT2 film with a very high difference as shown in Table 5.5 and Table 5.6 in Chapter 5. The reason for a very high difference could be the low doses at the distances further away from the source and the limitation of EBT2 film response to these doses, which were less than 20 cGy and 40 cGy for exposed doses of 400 cGy and 800 cGy, respectively as shown in Appendix Table A.4 and Table A.5. For the slightly high differences about 10% at radial distances from 0.3 cm to 5 cm along the transverse axis of the source center might be caused by the uncertainties during EBT2 film measurements such as film preparation, film placements, film orientation dependence and film scanning included the post exposure density growth time.

Our results were in accordance with the study of Uniyal et al. (54). This study quantified the effect of heterogeneities in HDR brachytherapy treatment using

the Gafchromic EBT2 film dosimeter compared with TPS calculation. They compared the values of relative depth dose obtained from EBT2 film and TPS in phantom and the relative depth dose was defined as the ratio of dose rate at the given radial distance to dose rate at the reference distance of 1 cm along the transverse axis from the source center. They mentioned that there was a limitation of the Gafchromic EBT2 film for distances larger than 3 cm from the source center because of the lower doses and these doses were equal to 0.109 in values of relative depth dose at distance 3 cm.

In our study, the relative absorbed dose which was the relative depth dose in the study of Uniyal et al. was less than 0.109 at radial distance beyond 3 cm as shown in Table 5.5 and Table 5.6 in Chapter 5. For this reason, the suitability of the EBT2 measurements in clinical brachytherapy should be done at radial distance less than 3 cm. Moreover, the EBT2 film was more suitable than TLD for dose measurements at distances close to the source because of its high spatial resolution with small detecting volume for high dose gradient area.

6.3 Radial dose function calculations

In this study, our g(r) values for Nucletron HDR ^{192}Ir source obtained from DOSRZnrc, TLD, and EBT2 film were calculated under unbounded condition with correction factor for the different phantom geometry represented as $g_{MC}(r)$, $g_{TLD}(r)$ and $g_{EBT2}(r)$, respectively. Because the phantom geometry significantly affected the g(r) values at radial distances near the phantom boundaries (8). For the comparison of the $g_{MC}(r)$ values with $g_{TLD}(r)$ and $g_{EBT2}(r)$ values, the differences were slightly high for radial distances from 0.5 cm to 15 cm in TLD measurements and for radial distances from 0.3 cm to 5 cm in EBT2 measurements. Furthermore, there was a very high difference between $g_{MC}(r)$ and $g_{TLD}(r)$ values at distance close to the source. All these differences were higher than 3% as recommended by the report of AAPM and ESTRO (8). These might be caused by numbers of uncertainties in TLD and EBT2 film measurements

In this study, the uncertainties of TLD measurement might be caused by the finite size of TLD rods and the positioning error of the source to TLD distances (3). For distance near the source, there was a very high uncertainty in TLD

measurements due to the combination of the high dose gradients near the source and the numbers of uncertainties in TLD measurements. Some other factors such as the process of TLD calibration, annealing and reading were also taken to account. For EBT2 film measurement, the uncertainties increased during the procedure of the EBT2 measurement from film preparation such as film cutting, film marking and film storage, film calibration curve, film measurement such as the positioning of the source and film, time for post-exposure density growth and the film scanning.

6.4 Calibration of dosimeters

6.4.1 TLD

In this study, we calibrated TLD using ^{60}Co because the average energy of ^{60}Co (1.25 MeV) was closer to ^{192}Ir source. And we calculated the absorbed dose from TL reading using Equation 13 in Chapter 4. Our study was similar to the study of Uniyal et al. (55) that they calibrated TLD rods in a ^{60}Co gamma ray beam. But they used Equation 15 to calculate the dose with accounted the correction factor for the energy dependence of TLD response between ^{60}Co beam and ^{192}Ir source. As we compared our TLD results calculated by Equation 13 in Chapter 4 and calculated by Equation 15 from the study of Uniyal et al. (55). The results showed that there was a difference of absorbed dose between two equations less than 3% for all radial distances as shown in Appendix (Table A.6).

$$D(r,\theta) = \frac{f\, R_{(r,\theta)} F_1}{CF_i\, dt\, E_r} \quad (15)$$

And the relative absorbed dose normalized with the dose at reference point of 1 cm from two equations were compared and no difference between them as shown in Appendix (Table A.7). Thus, the correction factor for the energy dependence of TLD response between ^{60}Co beam and ^{192}Ir source might not be required in our study for TLD measurements.

For the most studies of HDR brachytherapy, TLD used in ^{192}Ir brachytherapy was calibrated with ^{60}Co or megavoltage source (5, 55, 56) because these sources can readily accessed and can precisely deliver a prescribed dose of radiation. It is possible to produce a uniform radiation field on a flat surface that made several TLD irradiated the same dose in a single irradiation. Some studies calibrated TLD by using ^{192}Ir source and they mentioned that a careful measurement setup was required because of the high dose gradients around the source.

Previously, the study of Meigooni et al. (57) mentioned that there was a shift of photon spectrum of ^{192}Ir source toward lower photon energies with increasing depths in phantom, thus the TLD sensitivity correction factor should be applied in TLD dose measurements. They demonstrated that the uncertainties in dose measurements would be in range of about 10% in TLD measurements when TLD sensitivity correction factor was not account. However, Ambika et al. (52) studied the response of LiF TLD-100 rod at various depths in phantom to photons from an ^{192}Ir HDR source. They mentioned that the over-response of LiF TLD-100 due to the shift of photon spectrum toward lower photon energies with increasing depths in phantom did not exceed 2.5% at a depth up to 10 cm compared to the value at depth 1 cm. Thus, the TLD sensitivity correction factor due to ^{192}Ir spectra change with depth might not be required in TLD measurements.

6.4.2 Gafchromic EBT2 film

According to the manufacturer, the EBT2 film response was nearly energy independent in the range of photon energy 50 keV to 6 MV that included photon energies emitted from ^{192}Ir source and we calibrated EBT2 film with Nucletron HDR ^{192}Ir source. For the several studies of radiochromic film dosimetry of HDR ^{192}Ir source, they calibrated film with ^{60}CO gamma ray beam, 6 MV linear accelerator and ^{192}Ir source.

From the study of Sellakuma et al. (58), they have evaluated the dosimetric paramenters for Nucletron HDR ^{192}Ir source such as dose rate constant, geometry function, anisotropy function and radial dose function using Gafchromic EBT film base on TG-43 formalism. They calibrated film with ^{192}Ir source in a 30 cm x 30 cm x 30 cm solid water phantom that was similar to our study. To compare our EBT2 film

calibration curve with the study of Sellakuma et al., we used the values of radial dose function, which were calculated in both studies, as shown in Appendix (Table A.8). The results showed that there were differences about 10% for almost radial distances between two studies. However, there was a good agreement (<3%) of radial dose function between the study of Sellakuma et al. and our MC results recommended by the report of AAPM and ESTRO (8) as shown in Appendix (Table A.9).These can be noted that there was slightly differences of the results calculated between two EBT2 film calibration curves, which calibrated with the same ^{192}Ir source. The uncertainties of EBT2 film measurements in our study might affectted these differences.

Furthermore, we compared our EBT2 film calibration curve with the two studies of Uniyal et al. (52, 54) that used 6 MV photon beams for film calibration as shown in Appendix (Table A.10 and Table A.12). The results showed that there were high differences for all radial distances from 1 cm to 5 cm along the transverse axis between the values of radial dose function calculated from our calibration curve and from the two studies of Uniyal et al. In Appendix (Table A.11 and Table A.13), there were high differences between the two studies of Uniyal et al. and our MC results. Therefore, the use of ^{192}Ir source and 6 MV photon beam for film calibration was not similar to each other. As we compared the values of radial dose function from the two studies of Uniyal et al.(52, 54), there was a good agreement (<3%) at radial distances from 1 cm to 3 cm as shown in Appendix (Table A.14) because these two studies had the same condition for doing film calibration curve.

Moreover, absorbed dose distribution around Nucletron HDR ^{192}Ir source was done in DOSRZnrc MC code without detector modeling in phantom, it was an ideal simulation as direct measurement. Thus, these might be increased the differences between MC and experimental measurements in this study. For MC calculation, the accuracy of result depended on the accurate input data such as the source geometry, photon spectrum and photon cross sections to describe the actual source. According to AAPM TG-138 report (3), they mentioned that MC simulations contain the uncertainties in their results. There were the uncertainties in any model of physical system in the simulation such as source geometry, internal component locations and material composition.

CHAPTER VII
CONCLUSION

In this study, DOSRZnrc MC code can calculate the absorbed dose around the Nucletron HDR ^{192}Ir source in brachytherapy for all radial distances from the source center to phantom boundaries. The results showed the significant variations at radial distances close to the source due to the high dose gradients and DOSRZnrc MC calculations were acceptable for these distances (0.2 - 6 cm) as compared with Oncentra Brachy TPS. Furthermore, the absorbed dose calculations from DOSRZnrc were in accordance with LiF TLD-100 and EBT2 film measurements for radial distances from 0.3 cm to 15 cm. The slightly high differences between simulation and measurements were caused by the uncertainties of LiF TLD-100 and EBT2 film during the measurements. The accurate specification of source and experiment geometry details was required in MC simulation (59). The LiF TLD-100 rods can use to measure the absorbed dose for radial distances more than 0.5 cm up to 15 cm from the source. The finite size of LiF TLD-100 rods was a potential problem for dose measurements at the radial distances near the source (< 0.5 cm). For the EBT2 film measurements, it was found to be a suitable dosimeter at distances near the source (0.3 – 5 cm) due to its very high resolution.

Furthermore, due to the weak point of TPS based on TG-43 dose calculation formalism for not accounting the radiation attenuation and scattering, MC method was an alternative way to calculate the TG-43 dosimetric parameters such as radial dose function in this study. The values of radial dose function can be used as input data for TPS to study the effects of tissue inhomogeneity in patients. However, other dosimetric parameters such as anisotropy function, geometry function and dose rate constant can be calculated by MC method.

In conclusion, EGSnrc/DOSRZnrc MC code can calculate the absorbed dose in brachytherapy for all radial distances especially at radial distances close to the source. The dosimetric paramenter based on TG-43, radial dose function, was calculated by DOSRZnrc. The absorbed doses using LiF TLD-100 rods were

acceptable for radial distances from 0.5 cm to 15 cm. While those measured by EBT2-film were acceptable from 0.3 cm to 5 cm. The experimental measurement required the repetition and meticulous cares to reduce the uncertainties during measurements.

REFERENCES

1. Yue NJ. Principle and practice of brachytherapy dosimetry. Radiat Meas 2007;41: S22-27.
2. Rivard MJ, Coursey BM, DeWerd LA, Hanson WF, Hug MS, Ibbott GS, et al. Update of AAPM Task Group No. 43 Report: A revised AAPM protocol for brachytherapy dose calculations. Med Phys 2004;31(3):633-74.
3. DeWerd LA, Ibbott GS, Meigooni AS, Mitch MG, Rivard MJ, Stump KE, et al. A dosimetric uncertainty analysis for photon-emitting brachytherapy sources: Report of AAPM Task Group No.138 and GEC-ESTRO. Med Phys 2011;38(2):782-801.
4. Niroomand-Rad A, Blackwell CR, Coursey BM, Gall KP, Galvin JM, McLaughlin WL, et al. Radiochromic film dosimetry: recommendations of AAPM radiation therapy committee Task Group 55. Med Phys 1998; 25(11):2093-115.
5. Anctil JC, Clark BG, Arsenault CF. Experimental determination of dosimetry functions of Ir-192 sources. Med Phys 1998;25(12):2279-87.
6. Carleton Laboratory. Monte carlo simulations for brachytherapy [document on the internet]. 2007 [cited 2011 Nov 16]. Available from: http://physics.carleton.ca/~drogers/talks/trieste07/IV_brachy_Rogers_Trieste07_colour.pdf.
7. Williamson JF, Rivard MJ. Quantitative dosimetry methods for brachytherapy. AAPM [Homepage on the internet]. 2005 [cited 2012 Sep 2]. Available from: www.aapm.org/meetings/05SS/program/AAPM_quant_dosimetry.pdf.
8. Pérez-Calatayud J, Ballester F, Das RK, DeWard LA, Ibbott GS, Meigooni AS, et al. Dose calculation for photon-emitting brachytherapy sources with average energy higher than 50 keV: Report of the AAPM and ESTRO 2012;39(5):2904-29.

9. Naseri A, Mesbahi A. Application of Monte Carlo calculations for validation of a treatment planning system in high dose rate brachytherapy. Rep Prac Oncol Radiother 2010;I4:200-04.
10. Daskalov GM, Löffler E, Williamson JF. Monte Carlo-aided dosimetry of a new high dose-rate brachytherapy source. Med Phys 1998;25(11):2200-08.
11. Angelopoulos A, Baras P, Sakelliou L, Karaiskos P, Sandilos P. Monte Carlo dosimetry of a new ^{192}Ir high dose rate brachytherapy source. Med Phys 2000;27(11):2521-27.
12. Rivard MJ, Venselaar JFM, Beaulieu L. The evaluation of brachythepy treatment planning. Med Phys 2009;36(6):2136-53.
13. Beaulieu L, Tedgren AC, Carrier JF, Davis SD, Mourtada F, Rivard MJ, et al. Report of the Task Group 186 on model-based dose calculation methods in brachytherapy beyond the TG-43 formalism: Current status are recommendations for clinical implementation. Med Phys 2012;39(10): 6208-36.
14. Mayles P, Nahum A, Rosenwald JC. Handbook of radiotherapy physics: theory and practice. New York: Taylor & Francis; 2007.
15. Khan FM. The physics of radiation therapy. 3rd ed. Minneapolis: Lippincott William & Wilkins; 2003.
16. Radiation Oncology. ICRU [online]. 2010 [cited 12 Feb 2014]. Available from: http://en.wikibooks.org/wiki/Radiation_Oncology/Physics/ICRU.
17. Podgorsak EB. Radiation oncology physics: a handbook for teachers and students. Veinna: IAEA; 2005.
18. Williamson JF. Brachytherapy technology and physics practice since 1950: a half-century of progress. Phys Med Biol 2006;51:R303-25.
19. Levitt SH, Purdy JA, Perez CA, Vijayakumar S. Technical basis of radiation therapy: practical clinical applications. 5th ed. Heidelberg: Springer; 2012.
20. Nath R, Anderson L, Luxton G, Weaver KA, Williamson JF, Meigooni AS, et al. Dosimetry of interstitial brachytherapy sources: Recommendations of the AAPM Radiation Therapy Committee Task Group No. 43. Med Phys 1995;22:209-34.

21. Baltas D, Sakelliou L, Zamboglou N. Series in medical physics and biomedical engineering: the physics of modern brachytherapy for oncology. Florida: Taylor & Francis; 2006.
22. Palmer A, Bradley D, Nisbet A. Physic-aspects of dose accuracy in high dose rate (HDR) brachytherapy: source dosimetry, treatment planning, equipment performance and in vivo verification techniques. J Contemp Brachytherapy 2012;4(2):81-91.
23. Perez-Calatayud J, Cabañero DG, Pallarés FB. Monte carlo application in brachytherapy dosimetry. In: Lemoigne Y, Caner A, editors. Radiotherapy and Brachytherapy. Dordrecht: Springer; 2009. p. 239-50.
24. Thermoluminescence basics theory and applications [online]. [cited 2013 Aug 15]. Available from: http://www.nucleonix.com/manuals/tld%exp%20man.pdf.
25. Carrasco MA, Perucha M, Luis FJ, Baeza M, Herrador M. A comparison between radiographic EBT2 film model and its predecessor for EBT film model. Phys Med 2013;29(4):412-22.
26. Aldelaijan S, Mohammed H, Tomic N, Liang LH, DeBlois F, Sarfehnia A, et al. Radiochromic film dosimetry of HDR ^{192}Ir source radiation fields. Med Phys 2011;38(11):6074-83.
27. Gafchromic®EBT2 self-developing film for radiotherapy dosimetry. International specialty products [Online]. 2009 [cited 2013 Feb 20]. Available from: http://www.fimecorp.com/docs/GAFCHROMIC%20EBT2%20Technical%20Brief%20-%20Rev.%201.pdf.
28. Matney JE, Parker BC, Neck DW, Henkelmann G, Rosen II. Evaluation of a commercial flatbed document scanner and radiographic film scanner for radiochromic EBT film dosimetry. J Appl Chin Med Phys 2010;11(2): 98-208.
29. Alnawaf H, Yu PK, Butson M. Comparison of Epson scanner quality for radiochromic film evaluation. J Appl Chin Med Phys 2012;13(5):314-21.

30. Lewis DF. Performance of the Vidar® Red LED Dosimetry Pro Advantage™: A scanner optimized for use with GAFCHROMIC® EBT Dosimetry Film. International Specialty Products [Homepage on internet]. [cited 2013 Feb 20]. Available from: http://www.vidar.com/film/images/stories/PDFs/products/dosimetrypro/pdf/vidarredled.pdf.
31. OmniPro I'mRT. Iba dosimetry [online]. [cited 2013 July 16]. Available from: http://www.iba-dosimetry.com.
32. ImageJ [online]. [cited 2013 July 16] Available from: http://rsbweb.nih.gov/ij/.
33. Chetty IJ, Curran B, DeMarco JJ, Ezzell G, Faddegon BA, Kawrakow I, et al. Report of the AAPM Task Group No. 105: Issue associated with clinical implementation of Monte carlo-based photon and electron external beam treatment planning. Med Phys 2007;34(12):4818-53.
34. Harrison RL. Introduction to monte carlo simulation. AIP Conf Proc 2010; 1240:17-21.
35. Rollett AD, Manohar P. The monte carlo method. In: Raabe D, Roters F, Barlat F, Chen LQ, editors. Continuum scale simulation of engineering materials: fundamentals-microstructures-process applications; 2005. p. 76-113.
36. Rogers DWO, Bielajew AF. Monte carlo techniques of electron and photon transport for radiation dosimetry. Carleton Laboratory [Homepage on internet]. 1990 [cited 2012 Mar 13]. Available from: http://people.physics.carleton.ca/~drogers/pubs/papers/RB90.pdf.
37. Rogers DWO. Monte carlo technique in radiotherapy. Med Phys 2002;58(2): 63-70.
38. Kawrakow I, Mainegra-Hing E, Rogers DWO, Tessier F, Walters BRB. The EGSnrc code system: Monte carlo simulation of electron and photon transport. NRCC Technical Report PIRS–701. [Homepage on internet]. 2011 [cited 2012 Mar 13]. Available from: www.irs.inms.nrc.ca/inms/irs/EGSnrc/pirs701/.
39. Mainegra-Hing E. User Manual for egs_inprz, a GUI for the NRC RZ user codes. NRCC Technical Report PIRS–801. [Homepage on internet]. 2011 [cited 2012 Mar 13]. Available from: www.irs.inms.nrc.ca/inms/irs/EGSnrc/pirs801/.

40. Kawrakow I, Mainegra-Hing E, Rogers DWO. EGSnrcMP: the multi-platform environment for EGSnrc. NRCC Technical Report PIRS–877. [Homepage on internet]. 2011 [cited 2012 Mar 13]. Available from: www.irs.inms.nrc.ca/inms/ irs/EGSnrc/pirs877/.
41. Rogers DWO, Kawrakow I, Seuntjens JP, Walters BRB, Mainegra-Hing E. NRC User Codes for EGSnrc. NRCC Technical Report PIRS–702. [Homepage on internet]. 2011 [cited 2012 Mar 13]. Available from: www.irs.inms.nrc.ca/inms/irs/EGSnrc/pirs702/.
42. Dries WJF. Monte Carlo calculated dose distribution for endovascular HDR brachytherapy with Ir-192. Radiother Oncol 1997;45:77-82.
43. Borg J, Rogers DWO. Monte Carlo calculations of photon spectra in air from ^{192}Ir source: NRC Report PIRS-629r. Carleton Laboratory [Homepage on internet]. 1999 [cited 2012 Mar 13]. Available from: http://people.physics.carleton.ca/~drogers/pubs/papers/pirs629r.pdf
44. Taylor REP, Rogers DWO. EGSnrc Monte Carlo calculated dosimetry parameters for ^{192}Ir and ^{169}Yb brachytherapy sources. Med Phys 2008;35(11):4933-44.
45. Borg J, Rogers DWO. Spectra and air-kerma strength for encapsulated ^{192}Ir sources. Med Phys 1999;26(11):2441-4.
46. Ballester F, Hernández C, Perez-Calatayud J, Lliso F. Monte Carlo calculation of dose rate distributions around 192Ir wires. Med Phys 1997;24(8):1221-28.
47. Wang R, Li XA. Dose characterization in the near-source region for two high dose rate brachytherapy sources. Med Phys 2002;29(8):1678-86.
48. Huet C, Dagois S, Derreumaux S, Trompier F, Chenaf F. Robbes I. Characterization and optimization of EBT2 radiochromic films dosimetry system for precise measurements of output factors in small fields used in radiotherapy. Radiat Meas 2012;47:40-49.
49. Mayers S. Characterisation of gafchromic EBT2 film for use in radiation therapy dosimetry. Univesity of Wollongong Research online [Homepage on the internet]. 2011 [cited 2011 Dec 21]. Available from: http://ro.uow.edu.au/cgi/viewcontent.cgi?article=4282&context=theses.

50. Devan K, Aruna P, Manigandan D, Bharanidharan G, Subbaiah KV, Sunny CS, et al. Evaluation of dosimetric parameters for various ^{192}Ir brachytherapy source under unbound phantom geometry by Monte Carlo simulation. Med Dosim 2007;32(4):305-15.
51. Taylor RFP, Yegin G, Rogers DWO. Benchmarking BrachyDose: Voxel based EGSnrc Monte Carlo calculations of TG-43 dosimetry parameters. Med Phys 2007;34(2),445-57.
52. Uniyal SC, Sharma SD, Naithani UC. . Dosimetric verification of high dose rate brachytherapy treatment planning system in homogeneous and heterogeneous media. Phys Medica 2012;1-7.
53. IAEA. Technical Reports Series No.430: Commissioning and quality assurance of computerized planning systems for radiation treatment of cancer [document on internet] .2004 [cited 2013 May 28]. Available from: http://www-pub.iaea.org/mtcd/publications/pdf/trs430_web.pdf**.**
54. Uniyal SC, Naithani, Sharma SD, Srivastava AK. Radiochromic film dosimetry of rectal inhomogeneity and applicator attenuation in high dose rate brachytherapy of uterine cervix. J Appl Clin Med Phys 2012;13(1):66-75.
55. Uniyal SC, Sharma SD, Naithani UC. A dosimetry method in the transverse plane of HDR Ir-192 brachytherapy source using gafchromic EBT2 film. Phys Med 2012;28(2):129-33.
56. Haworth A, Butler DJ, Wilfert L, Ebert MA, Todd SP, Hayton AJ, et al. Comparison of TLD calibration methods for ^{192}Ir dosimetry. J Appl Clin Med Phys 2013;14(1):258-72.
57. Meigooni AS, Meli JA, Nath R. Influence of the variation of energy spectra with depth in the dosimetry of ^{192}Ir using LiF TLD. Med Phys Biol 1988;33(10):1159-70.
58. Sellakuma P, Kumar AS, Supe SS, Anand MD, Nithra K, Sajitha S. Evaluation of dosimetric functions for Ir-192 source using radiochromic film. Nucl Instrum Methods 2009;B267:1862-2866.
59. Williamson JF, Li Z. Monte Carlo aids dosimetry of the microSelectron pulsed and high dose-rate ^{192}Ir sources. Med Phys 1995;22(6):809-19.

APPENDIX

Results

Table A.1 The values of individual TL reading (Q_i) from three measurements.

Radial distance (cm)	1st Measurement 21 May 2013		2nd Measurement 6 July 2013		3rd Measurement 7 July 2013		SD
	$Q_{i,1}$	$Q_{i,2}$	$Q_{i,1}$	$Q_{i,2}$	$Q_{i,1}$	$Q_{i,2}$	
0.3	54533.813	34450.672	53008.988	33508.781	42886.793	44126.305	8879.94
0.5	9399.994	8552.454	10300.107	8695.612	8674.546	9895.56	730.34
1	2446.632	2697.67	2418.679	2349.122	2324.373	2706.871	169.94
1.5	1175.753	1097.833	1125.491	1096.901	1150.493	1117.766	30.89
2	635.626	672.396	611.833	686.744	651.684	672.67	27.83
2.5	442.136	422.207	440.553	413.339	435.55	422.239	11.71
3	320.293	311.934	318.096	318.307	296.947	320.528	9.08
4	185.428	178.241	186.248	166.982	183.882	163.348	9.91
5	118.729	119.827	121.829	113.001	120.481	113.408	3.76
6	75.879	66.934	73.79	65.216	71.662	63.782	4.93
7	58.635	52.051	57.922	49.697	57.881	49.423	4.35
8	41.258	40.062	40.602	39.379	32.397	39.328	3.24
9	31.75	31.822	32.653	32.675	25.164	32.53	2.94
10	25.14	26.133	25.02	26.081	20.828	26.547	2.11
11	20.935	20.626	20.457	20.494	16.907	20.69	1.53
12	17.073	15.918	16.703	15.537	13.181	15.874	1.37
13	13.085	13.407	13.122	13.283	-	13.339	5.41
14	10.987	10.877	10.802	10.732	10.82	10.827	0.09
15	8.768	8.54	8.471	8.136	8.376	8.129	0.25

Table A.2 The pixel value (PV) from EBT2 film measurements with exposed dose 400 cGy.

Radial distance (cm)	Average PV			SD
	1st Measurement	2nd Measurement	3rd Measurement	
0.3	29215.543	28127.404	23427.062	3076.36
0.5	20847.301	21733.4	17093.037	2463.49
0.7	16266.828	16496.827	15353.628	604.67
0.8	14562.153	13225.576	14211.332	692.97
0.9	12796.739	12963.884	12101.689	457.24
1	11473.876	10675.105	11287.052	417.82
1.1	11035.109	10428.081	9837.1856	598.98
1.2	9980.3987	6256.3837	9994.622	2154.18
1.3	9161.6343	8583.1673	8334.5673	424.36
1.4	8254.8253	7740.8697	8227.01	289.04
1.5	8019.5097	7513.9587	7931.622	270.11
1.6	7522.9187	6953.157	7521.276	328.48
1.7	7039.449	6546.1647	7030.954	282.38
1.8	6531.055	6182.9523	6517.041	197.06
1.9	6160.0547	5910.5733	6183.969	151.41
2	6015.034	5673.707	5990.679	190.42
2.1	5643.825	5441.934	5604.622	107.05
2.2	5517.7647	5365.004	4147.0487	751.18
2.3	5134.379	4965.49	5121.908	94.11
2.4	4970.3807	4855.597	4968.378	65.70
2.5	4973.228	4766.6017	4975.719	120.02

Table A.2 The pixel value (PV) from EBT2 film measurements with exposed dose 400 cGy (Cont.).

Radial distance (cm)	Average PV			SD
	1st Measurement	2nd Measurement	3rd Measurement	
2.6	4661.5807	4522.168	4653.061	78.15
2.7	4631.7213	4478.852	4637.342	89.93
2.8	4448.0623	4285.75	4451.148	94.61
2.9	4266.262	3956.954	3952.8817	179.77
3.	4467.3317	4109.4637	4464.556	205.82
3.5	3884.9617	3715.5867	3880.333	96.48
4	3592.8473	3407.1277	3589.372	106.24
4.5	3300.1007	3256.988	3302.281	25.54
5	3321.3183	3085.6693	3310.281	132.98
6	2960.9157	2889.7037	2928.617	35.66
7	2836.0027	2696.055	2834.673	80.42
8	2705.652	2632.296	2699.337	40.65
9	2737.2563	2621.6	2737.847	66.95
10	2743.8047	2596.1927	2741.189	84.48
11	2646.7127	2516.225	2680.1037	86.60
12	2470.653	2474.0697	2657.976	107.18
13	2593.3733	2492.9927	2635.8483	73.36
14	2432.01	2467.655	2498.9342	33.49
15	2636.1243	2362.02	2579.784	144.76

Table A.3 The pixel value (PV) from EBT2 film measurements with exposed dose 800 cGy.

Radial distance (cm)	Average PV			SD
	1st Measurement	2nd Measurement	3rd Measurement	
0.3	34628.209	35096.52	34912.459	235.93
0.5	26704.816	26787.25	26857.286	76.32
0.7	19764.48	21601.633	21485.332	1028.75
0.8	19508.39	17780.244	19214.02	924.56
0.9	17282.327	17150.115	16205.399	587.33
1	15649.94	14546.81	15121.064	551.72
1.1	14964.79	14229.027	13663.293	652.60
1.2	13744.695	12605.854	13754.566	660.38
1.3	12428.744	9216.6253	12431.561	1855.33
1.4	11548.106	10951.822	11546.862	343.91
1.5	11110.512	10275.694	11133.745	488.83
1.6	7533.4557	9660.0637	7520.301	1231.61
1.7	9794.732	9056.173	9802.158	428.57
1.8	9136.2157	8742.7677	9042.587	205.53
1.9	8414.6483	8153.1483	8405.474	148.40
2	8480.667	7985.0443	8482.49	286.68
2.1	7896.9963	7632.857	7881.577	148.25
2.2	7637.368	7330.439	7629.087	174.86
2.3	7070.2233	6883.898	7071.597	107.97
2.4	6836.1213	6574.352	6841.852	152.81
2.5	6704.5793	6327.742	6709.99	219.15

Table A.3 The pixel value (PV) from EBT2 film measurements with exposed dose 800 cGy (Cont.).

Radial distance (cm)	Average PV			SD
	1st Measurement	2nd Measurement	3rd Measurement	
2.6	6426.152	6184.587	6440.724	143.86
2.7	6186.8073	5897.602	6185.372	166.56
2.8	5917.978	5724.352	5917.439	111.63
2.9	5691.947	5518.541	5698.765	102.14
3.	5878.2773	5433.5677	5590.099	225.58
3.5	5082.456	4740.871	5025.622	183.03
4	4461.058	4306.6117	4362.952	78.16
4.5	4015.521	3966.6847	3953.061	32.84
5	3938.7413	3670.338	3654.5473	159.72
6	2959.3603	3340.9583	3340.5322	220.19
7	3166.6827	3033.0487	3048.5893	73.08
8	2955.677	2941.5687	2870.855	45.45
9	2884.8903	2809.6517	2809.061	43.61
10	2922.5877	2704.2683	2890	117.77
11	2738.2007	2634.3213	2768.9353	70.54
12	2684.9257	2592.08	2616.9303	48.06
13	2631.6507	2556.692	2596.865	37.51
14	-	2546.209	2641.1012	67.10
15	2676.597	-	2685.3373	6.18

Table A.4 The predicted dose from EBT2 film measurements using Equation 14 with exposed dose 400 cGy.

Radial distance (cm)	Predicted Dose (cGy)			SD
	1st Measurement	2nd Measurement	3rd Measurement	
0.3	5045.1081	4533.4116	2735.4545	1213.05
0.5	2001.8744	2235.5301	1202.4516	541.74
0.7	1063.7745	1101.1487	924.3873	93.16
0.8	814.6959	651.1624	769.2122	84.41
0.9	604.0831	622.1355	532.9548	47.15
1	473.9204	405.4797	457.2624	35.69
1.1	435.4350	385.7395	341.0898	47.20
1.2	351.5875	134.8502	352.6412	125.44
1.3	294.2252	257.3735	242.4036	26.67
1.4	237.7075	208.6204	236.0813	16.34
1.5	224.1404	196.4012	219.1824	14.79
1.6	196.8768	167.7235	196.7896	16.81
1.7	172.0009	148.1735	171.5777	13.64
1.8	147.4669	131.5487	146.8128	9.01
1.9	130.5253	119.5542	131.5942	6.66
2	124.1082	109.4319	123.0414	8.18
2.1	108.1744	99.7887	106.5311	4.44
2.2	102.9162	96.6425	49.9760	28.92
2.3	87.3661	80.7143	86.8709	3.71
2.4	80.9053	76.4472	80.8271	2.55
2.5	81.0166	73.0255	81.1139	4.64

Table A.4 The predicted dose from EBT2 film measurements using Equation 14 with exposed dose 400 cGy (Cont.).

Radial distance (cm)	Predicted Dose (cGy)			SD
	1st Measurement	2nd Measurement	3rd Measurement	
2.6	69.0255	63.7768	68.7028	2.94
2.7	67.8956	62.1597	68.1081	3.37
2.8	61.0141	55.0266	61.1288	3.49
2.9	54.3134	43.1464	43.0012	6.49
3.	61.7307	48.6174	61.6274	7.54
3.5	40.5864	34.6171	40.4223	3.40
4	30.3359	23.9236	30.2152	3.67
4.5	20.2616	18.7929	20.3360	0.87
5	20.9858	12.9909	20.6089	4.51
6	8.7978	6.4153	7.7162	1.19
7	4.6236	-0.0270	4.5793	2.67
8	0.2911	-2.1375	0.0818	1.35
9	1.3395	-2.4911	1.3591	2.22
10	1.5569	-3.3305	1.4700	2.80
11	-1.6607	-5.9677	-0.5555	2.86
12	-7.4677	-7.3553	-1.2881	3.54
13	-3.4236	-6.7326	-2.0201	2.42
14	-8.7380	-7.5663	-6.5371	1.10
15	-2.0109	-11.0353	-3.8722	4.76

Table A.5 The predicted dose from EBT2 film measurements using Equation 14 with exposed dose 800 cGy.

Radial distance (cm)	Predicted Dose (cGy)			SD
	1st Measurement	2nd Measurement	3rd Measurement	
0.3	8202.5442	8527.4813	8398.7281	163.63
0.5	3920.9169	3954.7156	3983.5920	31.37
0.7	1740.8025	2199.6077	2168.2469	256.32
0.8	1682.8391	1327.3976	1617.9451	189.28
0.9	1235.9787	1212.4910	1053.9499	99.01
1	968.0695	812.6673	891.1148	77.70
1.1	869.2486	771.4615	701.8489	84.09
1.2	711.5763	583.9229	712.7624	74.05
1.3	565.6457	297.8815	565.9332	154.68
1.4	480.6528	428.3773	480.5394	30.15
1.5	441.8919	373.8832	443.8943	39.86
1.6	286.2236	417.1713	285.5247	75.81
1.7	338.0167	287.2890	338.5530	29.44
1.8	292.5443	267.2535	286.4027	13.19
1.9	247.1709	231.7925	246.6221	8.72
2	251.1401	222.1891	251.2502	16.75
2.1	217.2451	202.7580	216.3853	8.13
2.2	203.0011	186.7838	202.5549	9.24
2.3	173.5380	164.3246	173.6067	5.34
2.4	161.9975	149.4953	162.2759	7.30
2.5	155.6632	138.0870	155.9216	10.22

Table A.5 The predicted dose from EBT2 film measurements using Equation 14 with exposed dose 800 cGy (Cont.).

Radial distance (cm)	Predicted Dose (cGy)			SD
	1st Measurement	2nd Measurement	3rd Measurement	
2.6	142.5977	131.6219	143.2703	6.54
2.7	131.7213	118.9926	131.6571	7.33
2.8	119.8752	111.5729	119.8518	4.79
2.9	110.2015	102.9483	110.4896	4.27
3.	118.1576	99.4452	105.9242	9.50
3.5	85.3087	72.0417	83.0694	7.10
4	61.4973	55.7914	57.8638	2.89
4.5	45.2396	43.4935	43.0076	1.17
5	42.4975	33.0346	32.4836	5.63
6	8.7457	21.6568	21.6423	7.45
7	15.7279	11.2192	11.7419	2.47
8	8.6223	8.1497	5.7859	1.52
9	6.2545	3.7459	3.7263	1.45
10	7.5145	0.2452	6.4252	3.92
11	1.3708	-2.0706	2.3916	2.34
12	-0.3958	-3.4663	-2.6454	1.59
13	-2.1589	-4.6340	-3.3083	1.24
14	-	-4.9797	-1.8463	2.22
15	-0.6716	-	-0.3821	0.20

Table A.6 The absorbed dose calculated from TLD reading using the two different equations from this study and the study of Uniyal et al. (2012) (55).

Radial distance (cm)	1st Measurement 21 May 2013 TLD 1			1st Measurement 21 May 2013 TLD 2		
	This study	The study of Uniyal et al. (2012)	% Differences	This study	The study of Uniyal et al. (2012)	% Differences
0.3	6983.8748	7186.2048	-2.90	4397.8168	4525.2261	-2.90
0.5	1211.8333	1246.9414	-2.90	1083.9705	1115.3742	-2.90
1	317.9520	327.1634	-2.90	324.7741	334.1831	-2.90
1.5	148.0722	152.3620	-2.90	136.4530	140.4062	-2.90
2	80.3433	82.6709	-2.90	84.1964	86.6357	-2.90
2.5	55.9533	57.5743	-2.90	51.7041	53.2021	-2.90
3	39.6195	40.7673	-2.90	38.9824	40.1117	-2.90
4	22.7302	23.3887	-2.90	22.4069	23.0561	-2.90
5	15.1332	15.5717	-2.90	14.6235	15.0472	-2.90
6	10.0419	10.3328	-2.90	9.1157	9.3798	-2.90
7	7.2681	7.4787	-2.90	6.8805	7.0799	-2.90
8	5.2524	5.4046	-2.90	5.1062	5.2542	-2.90
9	3.9138	4.0271	-2.90	4.0229	4.1395	-2.90
10	3.2899	3.3852	-2.90	3.2698	3.3646	-2.90
11	2.6816	2.7593	-2.90	2.4956	2.5679	-2.90
12	2.0897	2.1503	-2.90	1.9253	1.9811	-2.90
13	1.6786	1.7273	-2.90	1.7335	1.7837	-2.90
14	1.3648	1.4043	-2.90	1.2976	1.3352	-2.90
15	1.0752	1.1064	-2.90	1.1105	1.1427	-2.90

Table A.7 The relative absorbed dose calculated from TLD reading using the two different equations from this study and the study of Uniyal et al. (2012)(55).

Radial distance (cm)	1st Measurement 21 May 2013		
	This study	The study of Uniyal et al.(2012)	%Differences
0.3	17.7085	17.7085	
0.5	3.5720	3.5720	
1	1.0000	1.0000	
1.5	0.4427	0.4427	
2	0.2560	0.2560	
2.5	0.1675	0.1675	
3	0.1223	0.1223	
4	0.0702	0.0702	
5	0.0463	0.0463	
6	0.0298	0.0298	0 %
7	0.0220	0.0220	
8	0.0161	0.0161	
9	0.0123	0.0123	
10	0.0102	0.0102	
11	0.0081	0.0081	
12	0.0062	0.0062	
13	0.0053	0.0053	
14	0.0041	0.0041	
15	0.0034	0.0034	

Table A.8 The radial dose function under unbounded condition calculated from EBT2 film in this study compared with the study of Sellakuma et al (2009) (58).

Radial distance (cm)	The study of Sellakuma et al. (2009)	EBT2 film with dose 400 cGy	% Difference	EBT2 film with dose 800 cGy	% Difference
0.3	0.9859	0.9174	6.94	0.9367	4.99
0.5	0.9915	1.0630	-7.21	1.1507	-16.05
0.7	0.9956	1.1530	-15.82	1.1458	-15.09
0.8	0.9971	1.0746	-7.77	1.1133	-11.64
0.9	0.9985	1.0757	-7.73	1.0695	-7.11
1	0.9996	0.9998	-0.02	0.9998	-0.02
1.1	1.0006	1.0529	-5.23	1.0604	-5.98
1.2	1.0014	0.8827	11.85	1.0777	-7.62
1.3	1.0020	1.0011	0.10	0.8891	11.27
1.4	1.0026	0.9953	0.73	1.0151	-1.25
1.5	1.0031	1.0704	-6.70	1.0540	-5.07
1.6	1.0036	1.0669	-6.31	0.9568	4.66
1.7	1.0040	1.0548	-5.07	1.0348	-3.07
1.8	1.0043	1.0246	-2.02	1.0201	-1.58
1.9	1.0046	1.0235	-1.89	0.9749	2.95
2	1.0049	1.0581	-5.30	1.0765	-7.13
2.1	1.0051	1.0300	-2.48	1.0437	-3.84
2.2	1.0053	0.9024	10.24	1.0655	-5.98
2.3	1.0055	1.0010	0.44	1.0061	-0.06
2.4	1.0056	1.0187	-1.30	1.0137	-0.81
2.5	1.0057	1.0895	-8.33	1.0426	-3.67
2.6	1.0058	1.0104	-0.46	1.0479	-4.19
2.7	1.0058	1.0709	-6.47	1.0342	-2.82
2.8	1.0058	1.0290	-2.31	1.0225	-1.66
2.9	1.0057	0.8733	13.16	1.0104	-0.47
3	1.0056	1.1417	-13.53	1.0775	-7.15
4	1.0015	0.9948	0.67	1.0370	-3.54
5	0.9995	0.9942	0.53	0.9911	0.85

Table A.9 The radial dose function under unbounded condition calculated from DOSRZnrc in this study compared with the study of Sellakuma et al. (2009) (58).

Radial distance (cm)	The study of Sellakuma et al. (2009)	DOSRZnrc	% Difference
0.3	0.9859	1.0149	-2.94
0.5	0.9915	1.0094	-1.81
0.7	0.9956	1.0021	-0.66
0.8	0.9971	1.0003	-0.32
0.9	0.9985	0.9992	-0.08
1	0.9996	1.0000	-0.04
1.1	1.0006	1.0010	-0.05
1.2	1.0014	1.0010	0.03
1.3	1.0020	1.0076	-0.56
1.4	1.0026	1.0053	-0.26
1.5	1.0031	1.0188	-1.56
1.6	1.0036	1.0150	-1.13
1.7	1.0040	1.0158	-1.17
1.8	1.0043	1.0039	0.04
1.9	1.0046	1.0165	-1.19
2	1.0049	1.0174	-1.25
2.1	1.0051	1.0120	-0.69
2.2	1.0053	1.0113	-0.60
2.3	1.0055	1.0193	-1.37
2.4	1.0056	1.0114	-0.57
2.5	1.0057	1.0133	-0.76
2.6	1.0058	1.0095	-0.37
2.7	1.0058	1.0153	-0.94
2.8	1.0058	1.0205	-1.46
2.9	1.0057	1.0194	-1.36
3	1.0056	1.0054	0.02
4	1.0015	1.0192	-1.77
5	0.9995	1.0128	-1.33

Table A.10 The radial dose function under unbounded condition calculated from EBT2 film in this study compared with the study of Uniyal et al. (2012) (52).

Radial distance (cm)	The study of Uniyal et al. (2012)	EBT2 film with dose 400 cGy	% Difference	EBT2 film with dose 800 cGy	% Difference
1	0.9998	0.9998	0.00	0.9998	0.00
2	0.9592	1.0581	-9.87	1.0765	-12.65
3	0.9610	1.1417	-10.94	1.0775	-13.16
4	0.8681	0.9948	-7.79	1.0370	-20.16
5	0.8109	0.9942	-15.64	0.9911	-28.10

Table A.11 The radial dose function under unbounded condition calculated from DOSRZnrc in this study compared with the study of of Uniyal et al. (2012) (52).

Radial distance (cm)	The study of Uniyal et al. (2012)	DOSRZnrc	% Difference
1	0.9998	1.0000	-0.02
2	0.9592	1.0174	-6.06
3	0.9610	1.0054	-4.63
4	0.8681	1.0192	-17.41
5	0.8109	1.0128	-24.91

Tble A.12 The radial dose function under unbounded condition calculated from EBT2 film in this study compared with the study of Uniyal et al. (2012) (54).

Radial distance (cm)	The study of Uniyal et al. (2012)	EBT2 film with dose 400 cGy	% Difference	EBT2 film with dose 800 cGy	% Difference
1	0.9998	0.9998	0.00	0.9998	0.00
1.5	0.9678	1.0704	-10.60	1.0540	-8.90
2	0.9672	1.0581	-9.40	1.0765	-11.31
2.5	0.9649	1.0895	-12.91	1.0426	-8.05
3	0.9699	1.1417	-17.72	1.0775	-11.10
3.5	0.9558	1.0462	-9.46	1.0888	-13.92
4	0.8996	0.9948	-10.58	1.0370	-15.27
4.5	0.9972	0.8880	10.95	0.9873	0.99
5	0.8600	0.9942	-15.61	0.9911	-15.24

Table A.13 The radial dose function under unbounded condition calculated from DOSRZnrc in this study compared with the study of of Uniyal et al. (2012) (54).

Radial distance (cm)	The study of Uniyal et al. (2012)	DOSRZnrc	% Difference
1	0.9998	1.0000	-0.02
1.5	0.9678	1.0188	-5.27
2	0.9672	1.0174	-5.19
2.5	0.9649	1.0133	-5.02
3	0.9699	1.0054	-3.67
3.5	0.9558	1.0189	-6.60
4	0.8996	1.0192	-13.29
4.5	0.9972	1.0147	-1.75
5	0.8600	1.0128	-17.77

Table A.14 The radial dose function under unbounded condition calculated from EBT2 film in this study compared with the study of Uniyal et al. (2012) (52, 54).

Radial distance (cm)	The study of Uniyal et al. (2012) (52)	The study of Uniyal et al. (2012) (54)	% Difference
1	0.9998	0.9998	0.00
1.5	0.9678	-	-
2	0.9672	0.9592	0.82
2.5	0.9649	-	-
3	0.9699	0.9610	0.92
3.5	0.9558	-	-
4	0.8996	0.8681	3.51
4.5	0.9972	0.8109	-
5	0.8600	0.8109	5.71

BIOGRAPHY

NAME	Miss. Viyada Sanoesan
DATE OF BIRTH	21 March 1984
PLACE OF BIRTH	Rayong, Thailand
INSTITUTIONS ATTENDED	Mahidol University, 2007: Bachelor of Science (Radiological Technology) Mahidol University, 2014: Master of Science (Radiological Technology)
RESEARCH GRANTS	This thesis is partially supported by Graduate studies of Mahidol University Alumni Association
HOME ADDRESS	96 Moo 3 Soonthornwohan Rd. Songsalueng, Klaeng, Rayong, Thailand 21110 Tel. 086-321-9073 Email: tu_jaba@hotmail.com
PUBLICATION/ PRESENTATION	13th Asia-Oceania Congress of Medical Physics & 11th South-East Asia Congress of Medical Physics